# The LPM effect in sequential bremsstrahlung: analytic results for sub-leading (single) logarithms

**Peter Arnold,**[a] **Tyler Gorda**[b,c] **and Shahin Iqbal**[d,e]

[a]*Department of Physics, University of Virginia,*
*P.O. Box 400714, Charlottesville, VA 22904, U.S.A.*

[b]*Technische Universität Darmstadt, Department of Physics,*
*D-64289 Darmstadt, Germany*

[c]*Helmholtz Research Academy for FAIR, D-64289 Darmstadt, Germany*

[d]*National Centre for Physics, Quaid-i-Azam University,*
*Islamabad, Pakistan*

[e]*Institute of Particle Physics, Central China Normal University,*
*Wuhan, 430079, China*

*E-mail:* parnold@virginia.edu, tyler.gorda@physik.tu-darmstadt.de,
smi6nd@virginia.edu

ABSTRACT: Consider the in-medium splitting $g \to gg$ of a very high-energy gluon traversing a QCD medium, accounting for the Landau-Pomeranchuk-Migdal (LPM) effect. It has been known for some time that soft radiative corrections to that splitting generate a double-log correction to the splitting rate, whose effects can be absorbed into running of the medium parameter $\hat{q}$ describing the rate of transverse momentum kicks to high-energy particles due to small-angle scattering from the medium. Less has been known about sub-leading, *single* logarithms in this context. In this paper, we find analytic formulas for those single logs (with various caveats and clarifications).

# Contents

# 1  Introduction

## 1.1  Background and motivation

When passing through matter, high energy particles lose energy by showering, via the splitting processes of hard bremsstrahlung and pair production. At very high energy, the quantum mechanical duration of each splitting process, known as the formation time, exceeds the mean free time for collisions with the medium, leading to a significant reduction in the splitting rate known as the Landau-Pomeranchuk-Migdal (LPM) effect [1–3].[1] The generalization of the LPM effect from QED to QCD was originally carried out by Baier, Dokshitzer, Mueller, Peigne, and Schiff [5–7] and by Zakharov [8, 9] (BDMPS-Z). A long-standing problem in field theory has been to understand how to implement this effect in cases where the formation times of two consecutive splittings overlap. Several authors [10–12] have previously analyzed this issue for QCD at leading-log order. They found that (i) soft gluon bremsstrahlung produces a double-log enhancement of overlap effects and that (ii) this enhancement can be absorbed into a previously-discovered running [13] of the medium parameter $\hat{q}$ (sometimes called the "jet quenching parameter") describing transverse momentum diffusion of a high-energy particle moving through the medium. In a series of papers [14–20], we and collaborators have worked on a program to evaluate the effects of overlapping formation times without leading-log or soft bremsstrahlung approximations.

---

[1]The papers of Landau and Pomeranchuk [1, 2] are also available in English translation [4].

We have verified [20] that our results contain the previously known double logarithm. That double logarithm is accompanied by a sub-leading single logarithm, which was extracted numerically in ref. [20]. The purpose of the current paper is to now extract an analytic result for the single logarithm.

The overarching goal of the program [14–20], including the contribution of this paper, is to ultimately provide a theoretical calculation that will determine whether or not in-medium jets can be treated as the evolution of a collection of individual high-energy partons, or whether formation times overlap so drastically that the number distribution of high-energy partons in the shower at any moment is not even approximately a sensible concept.[2] This is a problem whose answer, for a first pass, would be interesting even in the simplest, idealized situation. So, though the framework developed in refs. [14–20] can in principle be used to study overlapping formation times in a variety of situations relevant to high-energy parton splitting in medium, explicit calculations so far have studied the simplest theoretical case, as we do here. We study the case of an infinite, static, homogeneous medium, which in practice means that we assume that the medium properties are constant over the length and time scales of the relevant formation time. We also work in the $\hat{q}$ approximation (sometimes referred to as the multiple scattering approximation). We work in the large-$N_c$ limit, where $N_c$ is the number of quark colors. We will also only consider quantities that have been integrated over the transverse momenta of all the daughters of each splitting. Throughout, we focus on gluon splitting, generated by $g \rightarrow gg$. Overlap effects arise in double gluon splitting $g \rightarrow gg \rightarrow ggg$ and in corresponding virtual corrections to single gluon splitting. As one example of a useful thought experiment for evaluating the significance of overlap effects, ref. [19] proposed computing their effect on the *shape* of the distribution $\langle \epsilon(z) \rangle$ of where the energy of the shower is deposited along the direction $z$ of the high-energy parton that initiated the in-medium shower.[3] The "shape" of the distribution means the features you see if you ignore the overall scale of the $z$ axis. The motivation for studying the shape was to find characteristics of shower development that are independent of the size of $\hat{q}$ (so that they do not depend on effects that can be absorbed into $\hat{q}$) and which are infrared (IR) safe. As a warm-up for a future QCD calculation, ref. [19] explicitly computed aspects of the shape for large-$N_f$ QED in the $\hat{q}$ approximation. However, ref. [19] also noted that there are potential issues with this proposal for QCD — technical issues that are associated with the soft, sub-leading single logarithms that are the subject of this paper.

Our motivation for finding analytic expressions for single logs are several-fold. Within the context of the $\hat{q}$ approximation, the double log enhancements, and the sub-leading single logs, will appear as double-log and single-log infrared (IR) divergences in computations of energy loss and shower development. (i) We hope that having analytic expressions

---

[2]For more discussion of the motivations and current state of this program, see sections 1 of refs. [19, 20].

[3]$\epsilon(z)$ refers to the energy deposited per unit length in the $z$ direction. Here "deposited" does not simply mean "energy loss" from a leading parton. For a quark-gluon plasma, it refers to where some subset of particles in the cascade have split in energy down to $E \sim T$, so that they thermalize with the plasma at that location $z$. In our notation, $\epsilon(z)$ represents the distribution of deposited energy for a single example of a random shower created by a single initial gluon of a given energy $E_0$ in our simplified case of an infinite, uniform medium. $\langle \epsilon(z) \rangle$ represents the statistical average over all such showers.

will aid in understanding and resolving potential issues in finding IR-safe $\hat{q}$-independent measures of the importance of overlap corrections. (ii) In order to go beyond leading (or even sub-leading) log analysis of overlap effects in calculations of shower development, one will need to subtract out these IR divergences and handle them separately. But it's difficult and expensive to accurately extract the single logs numerically [20], and so this subtraction will be much simpler with analytic results in hand for the single logs. (iii) The extracted double-log and single-log effects may then need to be resummed, as was originally done for double logs in ref. [13]. Having analytic expressions (as opposed to numerics) for single logs at first order may facilitate developing the resummation at next-to-leading-log order. (iv) It's useful to understand whether single logs arise only from the boundaries of integration regions that produce double logs, or whether there is an additional, independent source of IR divergences. (v) With analytic expressions, one may attempt to investigate whether there is a simple, natural way to absorb single logs (and not just double logs) into a redefinition [10–13] of the medium parameter $\hat{q}$. In this paper, we will focus just on deriving the analytic expressions for single logs. We leave application to IR-safe $\hat{q}$-independent characteristics of shower development (i), implementation of the subtractions (ii), and exploration of resummation (iii) to later work. We will resolve the question (iv) of whether there are any single IR logs that are independent from double logs. The question (v) of whether the single logs can be naturally absorbed into a redefinition of $\hat{q}$ is addressed in a companion paper [21].

## 1.2 Infrared cut-offs

Our claim to have calculated IR logarithms has an important technical caveat. The caveat was originally discussed in section 3.2 of ref. [20], but we review it here. A schematic of the integration region that gives rise to the IR double log is shown in figure 1. Here, $y$ is the energy fraction[4] of the softest daughter gluon in a double splitting process $g \to ggg$ (with energies $E \to xE, yE, (1-x-y)E$) or else the softest virtual gluon in a virtual correction to a single splitting process $g \to gg$ (with energies $E \to xE, (1-x)E$). $\Delta t$ is the time scale associated with the emission of that softest gluon. (Specifically, rates equal the product of the amplitude and conjugate amplitude for a process, and $\Delta t$ is the time separation between emission of the $y$ gluon in the amplitude and emission of the $y$ gluon in the conjugate amplitude.) The shaded region in figure 1(a) shows the full region that gives rise to the double-log IR divergence in a strict $\hat{q}$ approximation (here specialized to the case of an infinite medium). This region corresponds to

$$\frac{yE}{\hat{q}L} \ll \Delta t \ll t_{\text{form}}(y) , \tag{1.1a}$$

where $t_{\text{form}}(y) \sim \sqrt{yE/\hat{q}}$ is the formation time associated with the soft emission and

$$L \equiv t_{\text{form}}(x) \tag{1.1b}$$

---

[4]Technically, calculations are carried out in Light Cone Perturbation Theory (LCPT) and $y$ is the longitudinal light-cone momentum fraction of the softest daughter compared to the particle that initiates the double splitting. However, since the parents and daughters have high energy and are nearly collinear, we can for most purposes think of $y$ as the energy fraction.
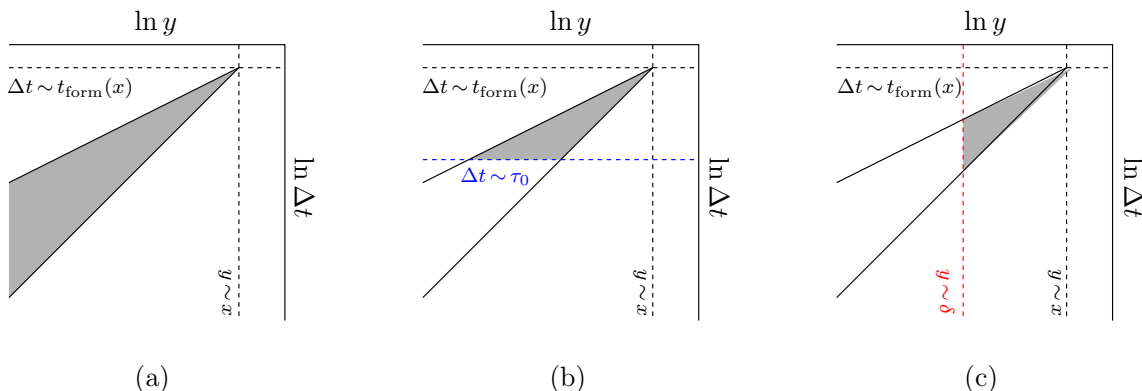
**Figure 1**. The region of integration (1.1) giving rise to a double log in the $\hat{q}$ approximation with (a) no cut-off, (b) the cut-off $\Delta t \sim \tau_0$ used in earlier literature, and (c) the IR regulator $y \sim \delta$ used in our calculations. See text for discussion. Above, $t_{\text{form}}(x) \sim \sqrt{xE/\hat{q}}$ is the formation time associated with a single splitting $E \to x, (1-x)E$.

is the formation length scale of the underlying single splitting process.[5] The second inequality just says that the time of the $y$ emission must fit within the $y$ formation time $t_{\text{form}}(y)$. These inequalities (1.1a) can be equivalently expressed as a range on $y$:

$$\frac{\hat{q}(\Delta t)^2}{E} \ll y \ll \frac{\hat{q}L\,\Delta t}{E}\,. \tag{1.1c}$$

The $\hat{q}$ approximation is an approximation that assumes multiple scattering from the medium. A calculation in the original work of Liou, Mueller, and Wu [13] on double-log contributions to $\hat{q}$ may be interpreted as the observation that the $\hat{q}$ approximation therefore breaks down for time scales $\lesssim$ the characteristic mean-free-time $\tau_0$ for the high-energy partons to elastically scatter from the medium. The actual region that contributes to the double logarithms would then be cut off as shown in figure 1(b).[6] (We more explicitly identify some of the scales in this figure, for the case of a weakly-coupled thermalized quark-gluon plasma, in figure 2. For a strongly-coupled quark-gluon plasma, simply erase the explicit factors of $g$.)

---

[5]The original work [13] on double log corrections to $\hat{q}$ directly studied transverse momentum diffusion of a high-energy particle traversing a medium of some length $L$ and studied the effect of a soft radiation on that transverse momentum. In contrast, the IR double logs in our application (like the IR double logs in refs. [10–12]) correspond to the effect of a soft radiation occurring on top of an underlying hard single splitting process $g \to gg$. In that case, the relevant analog of the medium size $L$ is the relevant scale of the formation length for the underlying splitting process. For a medium that is thin enough, that scale also turns out to be $L$, but for the infinite-medium case that we treat in our work, the relevant formation time is parametrically of order $t_{\text{form}}(x) \sim \sqrt{xE/\hat{q}}$, where $xE$ is the least-energetic daughter of the underlying single-splitting process $E \to xE, (1-x)E$.

[6]Our characterization of the double log region in figure 1(b) can be translated to the corresponding region $A=A_1+A_2$ of figure 2 of ref. [13] as follows: their medium size $L$ plays the role of our formation time $L \equiv t_{\text{form}}(x)$ (see our footnote 5), and their variables $\omega, t, l_0$ are our $yE, \Delta t, \tau_0$. The reason that one of the region boundaries in their figure 2 is curved and ours are all straight is because our axes are logarithmic, as indicated in our figure.

JHEP04(2022)085
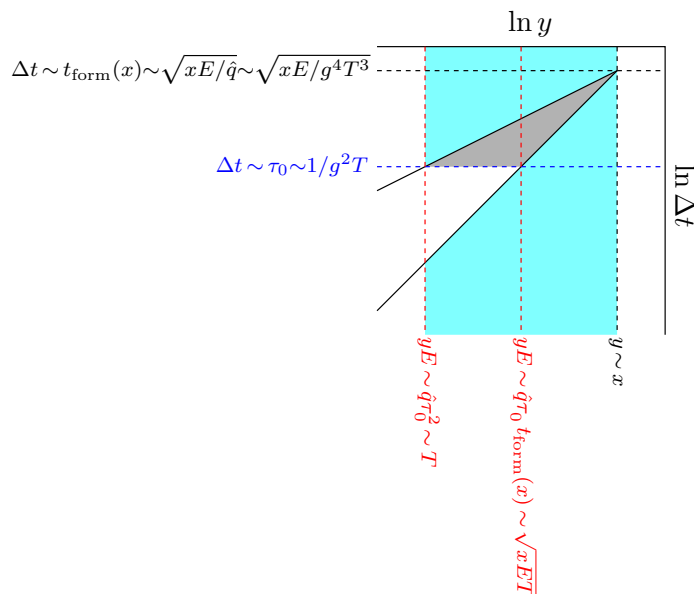
**Figure 2**. Parametric scales associated with various features of figure 1(b). The light blue region, combined with the gray region, shows where the $\hat{q}$ approximation is useful in our (theoretically idealized) application. In the lower light-blue region, $\hat{q}$-approximation propagators over the short time of the $y$ emission are approximately vacuum propagators. We have only shown $y < x$ above because, in our discussion here, $y$ represents the softest gluon.

For technical reasons, our previous work [20] has implemented a different type of IR regularization: an IR cut-off $(p^+)^{\min} = (P^+)^{\text{initial}}\delta$ on longitudinal light-cone momenta (equivalent, given our high-energy approximations, to an IR cut-off $E\delta$ on energy), where $\delta$ is a small number. This cut-off is depicted in figure 1(c). One motivation for this cut-off is that it seemed technically the easiest to implement. Unlike, for example, a sharp cut-off on time, there is also less question about consistency of the regulator when adding together different diagrams. Another motivation is that our regulator allowed our calculations to correctly reproduce the renormalization and running of the QCD coupling constant, arising from UV divergences as $\Delta t \to 0$. This is possible because the $\hat{q}$ approximation is valid somewhat more generally than just $\Delta t \gg \tau_0$ because propagators in the $\hat{q}$ approximation correctly reproduce simple vacuum propagators as $\Delta t \to 0$. Because of this, the actual range of usefulness of the $\hat{q}$ approximation in our application is depicted by the combination of the gray and light blue regions in figure 2.[7]

Our strategy for now is to use the simple IR cut-off of figure 1(c), with the intention of later finding IR-safe applications to energy loss. To do better, and handle the full physics of figure 2, one would need to go beyond the $\hat{q}$ approximation to handle the transition between the gray-shaded region of figure 2 and the unshaded region beneath it. As mentioned earlier, the underlying framework of our formalism can in principle be applied without making the $\hat{q}$ approximation, but that would require a leap in calculational complexity.

---

[7]This statement about the validity of the $\hat{q}$ approximation is a theoretical idealization, applicable to the theoretical limit of extremely high energies in the theorists' limit of a medium wide enough to completely contain the corresponding formation time.
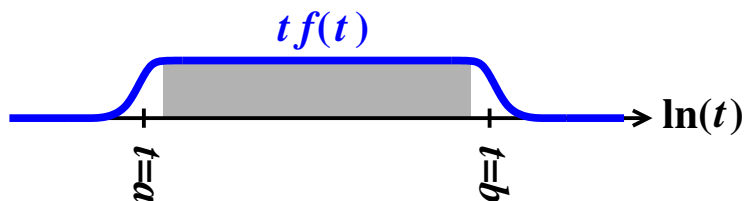
**Figure 3**. A simple calculus example of an integrand $f(t)$ that gives rise to a leading logarithm $\ln(b/a)$ from the shaded region, plus a sub-leading additive constant $c$ determined by the details of the behavior at the boundaries of that region. Note that this qualitative plot is of $t\,f(t)$ vs. $\ln t$, and so the logarithmic region corresponds to a flat plateau.
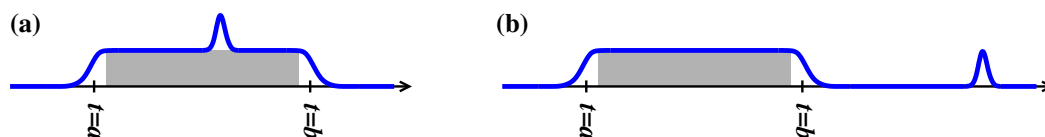


**Figure 4**. Like figure 3 but showing cases where there are additional contributions to the sub-leading additive constant $c$ that do not correspond to the boundaries of the logarithmic contribution.

In our case we have a two-dimensional integral (over $y$ and $\Delta t$) that gives a double log, and we are interested in determining a sub-leading single log. To set the stage, let's instead first review what would happen in a simple calculus example of a *one*-dimensional integral that gives a *single* log, and imagine that we were interested in determining a sub-leading additive constant. Consider a function $f(t)$ that is approximately proportional to $1/t$ over a range $(a, b)$ that spans several orders of magnitude, and suppose that $f$ falls off quickly outside of this region. This is depicted in figure 3 by a qualitative plot of $t \times f(t)$ vs. $\ln t$. At leading log order, $\int_0^\infty dt\, f(t) \approx \ln(b/a)$, coming from the shaded region of figure 3. Beyond that approximation, we have $\int_0^\infty dt\, f(t) \simeq \ln(b/a) + c$, where the additive constant $c$ is determined by exactly how $f(t)$ falls off at $t \sim a$ and at $t \sim b$ — that is, by how it falls off at the boundary of the logarithmic region $(a, b)$. Note that, though the boundaries of the region that give rise to the logarithm will contribute to $c$, there could be *other* contributions to $c$ that have nothing to do with the logarithm. For instance, a function $f(t)$ might look like figures 4(a) or (b), where the extra hump would give an additional contribution to $c$.

A similar situation applies to the case of leading double logarithms, which arise from integrals proportional to

$$\iint \frac{dy\, d(\Delta t)}{y\, \Delta t} \tag{1.2}$$

over the shaded regions of figure 1. Sub-leading single logarithms then arise from the details of how the integrand falls off at the *boundaries* of the shaded integration region. (And one must check whether there are any additional contributions to sub-leading logs that are not associated with that boundary.)

We can now see how the choice of IR regulator impacts the interpretation of results for single logs by comparing our IR regulator of figure 1(c) with the situation of figure 1(b). For the boundaries that are in common between the two figures, the contributions to single

logarithms will be the same; for boundaries that differ, the contributions to single logarithms will also differ. So, though parts of the calculation are common to any analysis, the full result for our single logarithm will depend on our particular choice (figure 1(c)) of IR regulator. (If an IR-regulated expression is not good enough for a particular application, and one needs a truly complete result for single logarithms, then one would have to go beyond the $\hat{q}$ approximation in order to compute the single log contribution from the $\Delta t \sim \tau_0$ boundary in figure 1(b).)

## 1.3 Reproducing the known double log result

In ref. [20], we found numerically that, with our IR regularization, the double logarithm arising from a single splitting overlapping a second, softer splitting could be absorbed into the usual BDMPS-Z single splitting rate by replacing

$$\hat{q}_{\mathrm{A}} \longrightarrow \hat{q}_{\mathrm{A}}^{\mathrm{eff}}(\delta) = \left[1 + \frac{C_{\mathrm{A}}\alpha_{\mathrm{s}}}{4\pi}\ln^2\delta\right]\hat{q}_{\mathrm{A}}. \tag{1.3}$$

Ref. [20] discusses how, after accounting for our different choice of IR regularization, this is equivalent to earlier (analytic) results from the literature [10–13] that

$$\hat{q}^{\mathrm{eff}}(L) = \left[1 + \frac{C_{\mathrm{A}}\alpha_{\mathrm{s}}}{2\pi}\ln^2\!\left(\frac{L}{\tau_0}\right)\right]\hat{q}. \tag{1.4}$$

We'll present here a somewhat simpler way to summarize the equivalence. The leading-log results (1.3) and (1.4) have the same form:

$$\hat{q}^{\mathrm{eff}} = \left[1 + \frac{C_{\mathrm{A}}\alpha_{\mathrm{s}}}{\pi}\mathcal{L}\right]\hat{q}, \tag{1.5}$$

where $\mathcal{L}$ is the *area* of the shaded double-log region $\mathcal{R}$ plotted on log-log plots such as figure 1. Specifically, $\mathcal{L}$ is given by the integral (1.2), which can be rewritten as[8]

$$\mathcal{L} \equiv \iint_{\mathcal{R}} \frac{dy\,d(\Delta t)}{y\,\Delta t} = \iint_{\mathcal{R}} d(\ln y)\,d(\ln(\Delta t)) = \text{area on log-log plot.} \tag{1.6}$$

With this rewriting, the coefficient $C_{\mathrm{A}}\alpha_{\mathrm{s}}/\pi$ of the double log $\mathcal{L}$ in (1.5) is universal, and the difference in the double log due to our choice of IR regulator can be understood as packaged into the area (1.6).

---

[8]To be more specific, the area of the triangular shaded region in figure 1(c) can be found by calling the left-hand boundary $y \sim \delta$ the "base" of the triangle. Using (1.1a), this base has (logarithmic) length $\ln t_{\mathrm{form}}(\delta) - \ln(E\delta/\hat{q}L) \simeq -\frac{1}{2}\ln\delta + \log\!\left(t_{\mathrm{form}}(x)/(E/\hat{q})^{1/2}\right)$, which, at leading-log level for small $\delta$ but fixed $x$ is just $-\frac{1}{2}\ln\delta$. The corresponding "height" of the triangle perpendicular to the base is $\ln x - \ln \delta \approx -\ln\delta$, and so $\mathcal{L} \approx \frac{1}{4}\ln^2\delta$ at leading log, so that (1.5) gives (1.3). Similarly, for the area of the triangular shaded region in figure 1(b), take the base to be the horizontal boundary $\Delta t \sim \tau_0$, with length given by (1.1c) as $\ln(\hat{q}L\tau_0/E) - \ln(\hat{q}\tau_0^2/E) = \ln(L/\tau_0)$. The height is $\ln L - \ln\tau_0 = \ln(L/\tau_0)$, and so $\mathcal{L} \approx \frac{1}{2}\ln^2(L/\tau_0)$, so that (1.5) gives (1.4).

## 1.4 Results for single log

We find that the only IR single logarithms are those that are associated with the boundaries of the double-log region.[9] On a related note, the IR single logarithms arise (on net) only from the time-ordered diagrams that contributed to double logarithms in the leading-log work of refs. [10–12], which are but a subset of the full set of diagrams [20] needed for a more general calculation that avoids large-logarithm approximations. (This conclusion required finding and correcting a phase error in our earlier work [20], which is explained in appendix A.)

The simplest (though slightly misleading) way to express our final result for IR single logs is to simply generalize (1.3) to include single logarithms. Our result is

$$\hat{q}_{\mathrm{A}} \longrightarrow \hat{q}_{\mathrm{A}}^{\mathrm{eff}}(\delta, x) = \left[1 + \frac{C_{\mathrm{A}}\alpha_{\mathrm{s}}}{2\pi}\left(\tfrac{1}{2}\ln^2\delta + \bar{s}(x)\,\ln\delta\right)\right]\hat{q}_{\mathrm{A}} \tag{1.7}$$

for our application, where[10]

$$\bar{s}(x) = -\ln\bigl(16\,x(1{-}x)(1{-}x{+}x^2)\bigr) + 2\,\frac{\left[x^2\bigl(\ln x - \tfrac{\pi}{8}\bigr) + (1{-}x)^2\bigl(\ln(1{-}x) - \tfrac{\pi}{8}\bigr)\right]}{(1 - x + x^2)}\,. \tag{1.8}$$

$x$ and $1{-}x$ are the energy fractions of the two daughters in the underlying single splitting process. The appearance of the factors $1{-}x{+}x^2$ above is related to the fact that the formation time for the underlying single-splitting process is[11]

$$\left[\frac{\hat{q}_{\mathrm{A}}}{2E}\left(-1 + \frac{1}{x} + \frac{1}{1{-}x}\right)\right]^{-1/2} = \sqrt{\frac{2x(1{-}x)E}{(1{-}x{+}x^2)\hat{q}_{\mathrm{A}}}}\,. \tag{1.9}$$

We have extracted the single log coefficient (1.8) from the $y{\to}0$ limit of the generic-$y$ formulas of ref. [20]. Those generic-$y$ formulas were derived in the large-$N_{\mathrm{c}}$ limit. Since the result [10–13] for double logs does not depend on the large-$N_{\mathrm{c}}$ limit, one might reasonably hope that the same is true for single logs.

We gave a caveat above that expressing the final answer in the form (1.7) is slightly misleading. That's because our single log has complicated $x$ dependence, whose form depends specifically on our application of $\hat{q}$ to overlap effects on jet quenching in the infinite-medium limit. Because of this, it does not clearly have as "universal" a form as the double log result (1.5). The question of universality will be addressed in ref. [21].

Figure 5 shows a test of our (corrected) numerical extraction of the single log coefficient in ref. [20] vs. our new analytic result (1.8) above. They are in full agreement.

---

[9]Though there are no other IR single logarithms (where IR means associated with soft emission), there is an additional non-IR logarithm — namely the UV logarithm associated with renormalization of the coupling constant [20].

[10]The notation $\bar{s}(x)$ for the single-log coefficient is inherited from ref. [20]. You may think of $s$ as standing for "single" log. For our present purpose, the bar is merely a vestige of earlier notational choices.

[11]More precisely, (1.9) is $|\Omega_0|^{-1}$, where $\Omega_0$ is the complex harmonic oscillator frequency (2.4) associated with making the $\hat{q}$ approximation to the LPM effect in single $g{\to}gg$ splitting. The phrase "formation time" by itself is often used to refer parametrically to this time scale and does not, as far as we know, have a universally established convention for what factors of 2 to include in (1.9).
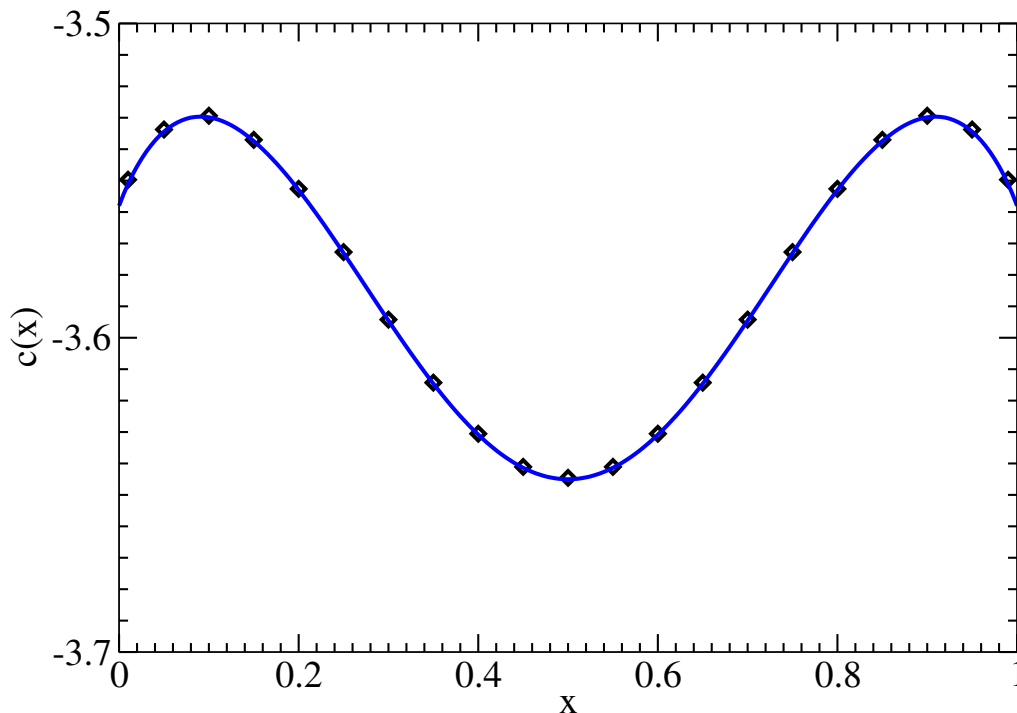
**Figure 5**. A test of numerical vs. analytic extraction of the single log coefficient $\bar{s}(x)$. The plot is of $c(x) \equiv \bar{s}(x) - \ln\left(-1 + \frac{1}{x} + \frac{1}{1-x}\right)$ vs. $x$, where the subtraction of the logarithm (based on the "educated guess" for $\bar{s}(x)$ in ref. [20]) makes the fine details more visible by removing the logarithmic divergence of $\bar{s}(x)$ as $x \to 0$ or 1. The numerical extraction of $c(x)$ is shown by the diamonds and is the same as figure 20 of ref. [20] except corrected by a $4\pi$ downward shift, as explained in appendices A and E.7 of this paper. (We have also very slightly improved the accuracy.) The solid curve is our analytic result, based on (1.8).

## 1.5 Outline

In the next section, we review the diagrams that produce double logarithmic IR behavior, which we call the ABC diagrams. These are the same diagrams which (on net) produce the IR single logarithms. We also summarize the result for each ABC diagram's individual contribution to the single log coefficient $\bar{s}(x)$. In section 3, we discuss how *other* (non-ABC) diagrams, which contribute to overlapping gluon splitting in more general situations, do not contribute to the IR logarithms that arise when one of the splittings is soft.

There are two qualitatively different types of ABC diagrams, named A3 and A1, to which other ABC diagrams can be related (with some caveats). In section 4, we give an overview of the extraction of the small-$y$ behavior of the A3 diagram from the complicated, general-$y$ formulas of refs. [14, 20]. In section 5, we discuss the almost-symmetry that allows us to relate the result for that diagram to a sub-class of other ABC diagrams. In sections 6 and 7, we repeat that procedure for the A1 diagram and relate it to the remaining ABC diagrams. A large variety of details are left for appendices.

Our conclusion, such as it is, is given in section 8.
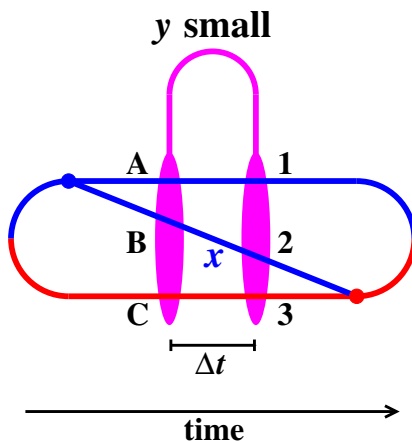
**Figure 6**. The nine time-ordered rate diagrams which (together with their complex conjugates) produce the double logarithm. In our analysis, all of the lines are gluons. The labeling A, B, C, 1, 2, and 3 is our naming convention for where the relatively-soft $y$ gluon may connect the three harder gluon lines. The magenta color of the $y$ gluon is used to indicate that the line could be either blue or red depending on how it is connected (see figure 7).

## 2 Diagrams

### 2.1 Relevant diagrams and total rate

The nine time-ordered diagrams which (on net) produce the double logarithm [10–12] are collectively depicted by figure 6. Three particular examples are shown in figure 7 and are drawn in the style of refs. [14, 20]. The blue part represents a contribution to the amplitude for the process (either double splitting $g{\to}ggg$ or a virtual correction to single splitting $g{\to}gg$); the red part represents a contribution to the conjugate amplitude; and the entire diagram represents a contribution to the rate. Only high-energy parton lines are shown: each line implicitly interacts multiple times with the medium, and there is implicit averaging of the rate over the randomness of the medium. Following ref. [10], we name the diagrams A1, A2, . . . , C3. We'll refer to them collectively as the "ABC diagrams." The double log arises from the case where the $y$ gluon is soft compared to the other daughters of the double splitting. But the $y$ gluon should be understood to still be high energy, with energy large compared to the energy scales of the QCD medium (e.g. large compared to the temperature $T$ for a quark-gluon plasma). The ABC diagrams are the diagrams where emission of the soft $y$ gluon is completely contained within the time interval spanned by the underlying single-splitting process that creates the $x$ gluon.

Generically, differential rates from individual ABC diagrams have small-$y$ expansions of the form [14, 20]

$$\frac{d\Gamma}{dx\,dy} = \frac{\#\ln y + \#}{y^{3/2}} + \frac{\#\ln y + \#}{y} + O(y^{-1/2}), \tag{2.1}$$

where "#" represents various $x$-dependent coefficients specific to the diagram. These rates have already been integrated over the "$\Delta t$" of figure 1(a). The $O(y^{-3/2})$ terms above generate IR power-law divergences when integrated over $y$. The $y^{-1}\ln y$ and $y^{-1}$ terms
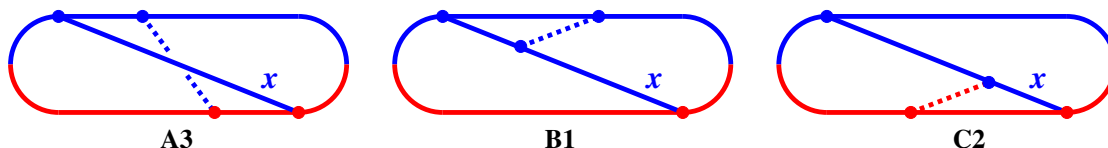
**Figure 7**. Three examples of figure 6. The soft $y$ gluon is denoted by the dashed line. A3 and C2 contribute to the rate for double splitting $g \to ggg$, whereas B1 is an example of a virtual (i.e. loop) correction to single splitting $g \to gg$. In the nomenclature of ref. [20], A3 is called $xy\bar{y}\bar{x}$, B1 is $yxy\bar{x}$ with renaming $y \leftrightarrow z \equiv 1-x-y$ of the loop momentum fraction variable, and C2 is $z\bar{y}y\bar{z}$ (the $x \leftrightarrow z$ permutation of $x\bar{y}y\bar{x}$).

respectively generate double and single logs, and the $O(y^{-1/2})$ terms are IR finite. When one adds all of the ABC diagrams together, the power-law divergences cancel [20], leaving just the terms that generate logs.

Specifically, in this paper, we will find that the rate corresponding to the sum of all ABC diagrams has the small-$y$ expansion

$$\left[\frac{d\Gamma}{dx\,dy}\right]_{\text{ABC}} \simeq -\frac{C_{\text{A}}\alpha_{\text{s}}}{4\pi y} \left[\frac{d\Gamma}{dx}\right]_{\text{LO}} (\ln y + \bar{s}(x)), \tag{2.2}$$

where $\bar{s}(x)$ is our result (1.8) for the single-log coefficient, and where[12]

$$\left[\frac{d\Gamma}{dx}\right]_{\text{LO}} = \frac{\alpha_{\text{s}}}{\pi} P(x)\,\text{Re}(i\Omega_0) \tag{2.3}$$

is the leading-order BDMPS-Z result for single splitting $g \to gg$ in the $\hat{q}$ approximation. Above,

$$\Omega_0 \equiv \sqrt{\frac{-i\hat{q}_{\text{A}}}{2E}\left(-1 + \frac{1}{x} + \frac{1}{1-x}\right)} = \sqrt{\frac{-i\hat{q}_{\text{A}}(1-x+x^2)}{2x(1-x)E}} \tag{2.4}$$

gives the complex harmonic oscillator frequency associated with the single splitting process, and $P(x)$ is the DGLAP $g \to gg$ splitting function[13]

$$P(x) = C_{\text{A}}\frac{1 + x^4 + (1-x)^4}{x(1-x)} = C_{\text{A}}\frac{2(1-x+x^2)^2}{x(1-x)}. \tag{2.5}$$

To first order in the $\alpha_{\text{s}}$ associated with high-energy splitting, the IR log corrections (2.2) can be absorbed into the leading-order single splitting rate (2.3) by the redefinition

$$\hat{q}_{\text{A}} \longrightarrow \left[1 - \frac{C_{\text{A}}\alpha_{\text{s}}}{2\pi}\int_\delta dy\,\frac{\ln y + \bar{s}(x)}{y}\right]\hat{q}_{\text{A}}, \tag{2.6}$$

since $\Omega_0 \propto \sqrt{\hat{q}_{\text{A}}}$. As discussed earlier, we have chosen to regulate the IR with a sharp lower cut-off $\delta$ on $y$. The $\delta$ dependence of the above integral gives our previously quoted result (1.7) for $\hat{q}_{\text{A}}^{\text{eff}}$.

---

[12](2.3) is written here in the form used in appendix A.1 of ref. [20].

[13]For technical clarification concerning (2.5), see comments after eq. (A.5) in ref. [20]. In particular, $P(x)$ should be defined as the absolute value of the right-hand side in cases where one intends to "front-end" transform the diagram in a way that $x$ or $1-x$ might become negative.

## 2.2 Results for individual ABC diagrams

It will be useful to break down our results diagram by diagram, which is how we attacked finding the small-$y$ expansion.

The results have an appealing symmetry that allows one to cover all nine diagrams with just two equations. We refer to each specific ABC diagram with a pair of integers $p, q$ where $p = 1, 2, 3$ represents A,B,C and $q = 1, 2, 3$ represents $1, 2, 3$. So, for example, the B3 diagram corresponds to $p, q = 2, 3$. We consider here the labels A1, A2, ..., C3 to be short-hand for the corresponding diagram of figure 6 *plus* its complex conjugate. We also use the notation[14]

$$(\mathfrak{x}_1, \mathfrak{x}_2, \mathfrak{x}_3) \equiv (1-x, x, -1) \tag{2.7}$$

for the longitudinal momentum fractions, in the $y \to 0$ limit, of the three hard lines corresponding to A,B,C or 1,2,3 in figure 6.

We will need the complex harmonic oscillator frequencies $\Omega_0$ and $\Omega_y$ associated, in the $y \to 0$ limit, with (i) the underlying $x$ emission process and (ii) the soft $y$ emission process. $\Omega_0$ was given already in (2.4), but here it will be useful to note that it can be written symmetrically in terms of the momentum fractions (2.7) as

$$\Omega_0 \equiv \sqrt{\frac{-i\hat{q}_{\rm A}}{2E} \left( \frac{1}{\mathfrak{x}_1} + \frac{1}{\mathfrak{x}_2} + \frac{1}{\mathfrak{x}_3} \right)} = \sqrt{\frac{-i\hat{q}_{\rm A}(\mathfrak{x}_1^2 + \mathfrak{x}_2^2 + \mathfrak{x}_3^2)}{4|\mathfrak{x}_1\mathfrak{x}_2\mathfrak{x}_3|E}}. \tag{2.8}$$

The other frequency is

$$\Omega_y \equiv \sqrt{\frac{-i\hat{q}_{\rm A}}{2yE}}. \tag{2.9}$$

It can be useful to note that

$$\mathfrak{x}_1^2 + \mathfrak{x}_2^2 + \mathfrak{x}_3^2 = 2(1 - x + x^2). \tag{2.10}$$

With this notation, our results for the differential rates associated with the ABC diagrams split into two cases. For $p \neq q$ diagrams,

$$\begin{aligned}
\left[ \frac{d\Gamma}{dx\, dy} \right]_{pq} &\simeq \frac{C_{\rm A} \alpha_{\rm s}^2 \, P(x)}{2\pi^2 y} \,{\rm Re}\Bigg[ i\Omega_y \Big\{ -\ln\big(\tfrac{\Omega_y}{2\pi\Omega_0}\big) - \gamma_{\rm E} - \tfrac{i\pi}{2}\delta_{p3} \Big\} \\
&\quad + i\Omega_0 \Big\{ 2\left[ \tfrac{1}{\epsilon} + \ln\left( \tfrac{\pi\mu^2}{\Omega_0 E} \right) \right] - \left( 1 + \tfrac{\mathfrak{x}_r^2}{2(\mathfrak{x}_1^2 + \mathfrak{x}_2^2 + \mathfrak{x}_3^2)} \right) \left[ \ln\left( \tfrac{|\mathfrak{x}_1\mathfrak{x}_2\mathfrak{x}_3|y\Omega_y}{\Omega_0} \right) + \tfrac{i\pi}{2}\delta_{p3} \right] \\
&\quad + \tfrac{\mathfrak{x}_r^2}{2(\mathfrak{x}_1^2 + \mathfrak{x}_2^2 + \mathfrak{x}_3^2)} \big[ 1 - \ln 2 + 2\ln(2|\mathfrak{x}_p\mathfrak{x}_q|) \big] \Big\} \Bigg],
\end{aligned} \tag{2.11a}$$

where $\mathfrak{x}_r$ above represents the longitudinal momentum fraction in (2.7) that is not $\mathfrak{x}_p$ or $\mathfrak{x}_q$,[15] and $\delta_{ij}$ is a Kronecker delta.

---

[14] For readers wondering at our unusual choice of font for $(\mathfrak{x}_1, \mathfrak{x}_2, \mathfrak{x}_3)$: we've used this to avoid confusion with the 4-particle values of $(x_1, x_2, x_3, x_4)$ used later (and also because, even for purely 3-particle situations, the particular ordering of $(\mathfrak{x}_1, \mathfrak{x}_2, \mathfrak{x}_3)$ is different from the convention $(x_1, x_2, x_3)$ used in past work, such as section 4.2 of ref. [14]).

[15] If one prefers $\mathfrak{x}_r$ defined by an equation: $|\mathfrak{x}_r| = |\epsilon_{pqs}\mathfrak{x}_s|$.

For the diagrams A1, B2, and C3, which involve gluon self-energy loops,

$$\left[\frac{d\Gamma}{dx\,dy}\right]_{pp} \simeq -2 \times \frac{C_A \alpha_s^2\, P(x)}{2\pi^2 y}\, \mathrm{Re}\bigg[i\Omega_y\Big\{-\ln\big(\tfrac{\Omega_y}{2\pi\Omega_0}\big) - \gamma_E - \tfrac{i\pi}{2}\delta_{p3}\Big\}$$
$$+ i\Omega_0\bigg\{2\Big[\tfrac{1}{\epsilon} + \ln\big(\tfrac{\pi\mu^2}{\Omega_0 E}\big)\Big] - \Big[\ln\big(\tfrac{|\mathfrak{r}_1 \mathfrak{r}_2 \mathfrak{r}_3| y\Omega_y}{\Omega_0}\big) + \tfrac{i\pi}{2}\delta_{p3}\Big]$$
$$+ \tfrac{\mathfrak{r}_q^2 + \mathfrak{r}_r^2}{4(\mathfrak{r}_1^2 + \mathfrak{r}_2^2 + \mathfrak{r}_3^2)}(1 - \ln 2)\bigg\}\bigg] \quad (2.11\text{b})$$

(no sum on $p$), where in this formula $\mathfrak{r}_q$ and $\mathfrak{r}_r$ represent the two longitudinal momenta in (2.7) that are not $\mathfrak{r}_p$.[16]

Above, we've used the color red to indicate the leading terms in the small-$y$ expansion. These are the $O(y^{-3/2})$ terms of (2.1), which generate IR power-law divergences. The color blue indicates the sub-leading $O(y^{-1})$ terms, which generate the IR double and single logarithms.

We use dimensional regularization, and the IR log-divergent terms in (2.11) contain a UV-divergent piece $1/\epsilon$. The appearance of such mixed UV-IR divergences in individual diagrams is a well-known annoyance of Light-Cone Perturbation Theory (LCPT), which was used to calculate our original generic-$y$ results in ref. [20]. These mixed divergences must cancel when one sums all the ABC diagrams. And they do indeed cancel, as does the dependence of the IR logs on the UV-renormalization scale $\mu$.

Note that the permutation symmetry between results for different $p \neq q$ diagrams in (2.11a) is slightly spoiled by the $\tfrac{i\pi}{2}\delta_{p3}$ terms, and similarly for permutation symmetry of the diagrams of (2.11b). These additional terms appear only in the C1, C2, and C3 diagrams. They originate from the fact that the $y$ gluon propagator in time-ordered ABC diagrams (such as the explicit examples in figure 7) are colored red (conjugate amplitude) for the three C diagrams, as opposed to blue (amplitude) for the A and B diagrams. As a result, the complex phases that appear in the calculation are different, leading to $i\pi$ terms in the formula. (For more discussion of $i\pi$ terms, see ref. [21].)

The sum of the small-$y$ rates (2.11) is

$$\left[\frac{d\Gamma}{dx\,dy}\right]_{\mathrm{ABC}} \simeq \frac{C_A \alpha_s^2\, P(x)}{2\pi^2 y}\, \mathrm{Re}\bigg[i\Omega_0\Big\{-\Big[\ln\big(\tfrac{|\mathfrak{r}_i \mathfrak{r}_j \mathfrak{r}_k| y\Omega_y}{\Omega_0}\big) + \tfrac{i\pi(\mathfrak{r}_1^2 + \mathfrak{r}_2^2)}{4(\mathfrak{r}_1^2 + \mathfrak{r}_2^2 + \mathfrak{r}_3^2)}\Big]$$
$$+ \tfrac{2[\mathfrak{r}_1^2 \ln(2|\mathfrak{r}_2 \mathfrak{r}_3|) + \mathfrak{r}_2^2 \ln(2|\mathfrak{r}_3 \mathfrak{r}_1|) + \mathfrak{r}_3^2 \ln(2|\mathfrak{r}_1 \mathfrak{r}_2|)]}{(\mathfrak{r}_1^2 + \mathfrak{r}_2^2 + \mathfrak{r}_3^2)}\Big\}\bigg], \quad (2.12)$$

which is

$$\left[\frac{d\Gamma}{dx\,dy}\right]_{\mathrm{ABC}} \simeq \frac{C_A \alpha_s^2\, P(x)}{2\pi^2 y}\, \mathrm{Re}\bigg[i\Omega_0\Big\{-\ln\big(\tfrac{x(1-x)y\Omega_y}{4\Omega_0}\big)$$
$$+ \tfrac{\big[(1-x)^2\big(\ln x - \tfrac{i\pi}{8}\big) + x^2\big(\ln(1-x) - \tfrac{i\pi}{8}\big) + \ln\big(x(1-x)\big)\big]}{(1 - x + x^2)}\Big\}\bigg]. \quad (2.13)$$

---

[16]If one prefers the right-hand side of (2.11b) to be written solely in terms of the index $p$: $\mathfrak{r}_q^2 + \mathfrak{r}_r^2 = (\mathfrak{r}_1^2 + \mathfrak{r}_2^2 + \mathfrak{r}_3^2) - \mathfrak{r}_p^2$.

Note that the IR power-law divergences have canceled.[17] Eq. (2.13) can be massaged into our final result (1.8) using (i) the formulas for $\Omega_y$ and $\Omega_0$ and (ii) the fact that $\Omega_0$ has phase $e^{-i\pi/4}$ implies $\mathrm{Re}(i\Omega_0 \times i) = -\mathrm{Re}(i\Omega_0)$.

## 3 Non-ABC diagrams

### 3.1 Overview

On net, our single logs will come from the same diagrams as figure 6, from the boundaries of the double-log integration regions. However, there are many other diagrams that *individually* contribute to single and even to double logs. The IR-log contributions from those other diagrams, however, cancel in groups, as summarized in table 1 (to be explained shortly).[18] The fact that various individual diagrams might have canceling IR-log contributions is not surprising because individual diagrams also have canceling IR *power-law* divergences in the $\hat{q}$ approximation. These power-law divergences were first noted in ref. [14], and their explicit cancellation among all diagrams was verified in ref. [20].[19]

The simplest demonstration of the cancellation of single IR logs for diagrams *other* than the ABC diagrams of figure 6 is the comparison in figure 5 of the total numerical result (extracted from the sum of *all* diagrams) to our analytic result (1.8), which we will derive by only considering the ABC diagrams. However, we may also discuss diagrammatically why the IR logs of the non-ABC diagrams cancel.

Throughout this paper, the longitudinal momentum fractions of the three daughters of a double splitting process $g \to ggg$ will be referred to as $(x, y, z)$, where

$$z \equiv 1 - x - y. \tag{3.1}$$

### 3.2 Cancellation of IR logs for non-ABC diagrams

First, let's summarize the form of the $y \to 0$ expansion of individual diagrams (in the $\hat{q}$ approximation). Generically, differential rates from individual diagrams have small-$y$ expansions of the same form (2.1) as the ABC diagrams:

$$\frac{d\Gamma}{dx\,dy} = \frac{\# \ln y + \#}{y^{3/2}} + \frac{\# \ln y + \#}{y} + O(y^{-1/2}). \tag{3.2}$$

Some individual diagrams additionally have more singular $O(y^{-5/2})$ behavior, but this will not be relevant: those diagrams appear in combinations where the $O(y^{-5/2})$ terms cancel in a way that will not affect the arguments below. (Specifically, the $y^{-5/2}$ terms cancel for the pair of entries in table 1 marked "$*$", and similarly for the pairs marked $*'$, $\dagger$, and $\dagger'$.)

We now argue that the two darker-blue rectangles in table 1 (the two rectangles labeled $\alpha$) give canceling contributions to IR logs. The real ($g \to ggg$) double splitting

---

[17]See the discussion in appendix E.3 of ref. [20].

[18]Table 1 in this paper, describing the cancellation of IR logs of non-ABC diagrams, has a form that is somewhat related to table 1 of ref. [20], which summarized the cancellation of power-law IR divergences. Readers interested in both can find a description of how they are related in appendix B.

[19]See in particular appendix E of ref. [20].

| Real | $(x,y)$ | $(x,z)$ | $(z,y)$ | $(z,x)$ | $(y,x)$ | $(y,z)$ |
|---|---|---|---|---|---|---|
| $2\operatorname{Re}(yx\bar{x}\bar{y})$ | $\alpha$ | | $\alpha'$ | | A3 | B3 |
| $2\operatorname{Re}(y\bar{x}x\bar{y})$ | $*$ | | $*'$ | | C1 | C2 |
| $2\operatorname{Re}(x\bar{y}\bar{x}y)$ | $*$ | | $*'$ | | $\beta$ | $\beta'$ |
| $\mathcal{A}_{\text{seq}}(x,y)$ | | | | | | |

| Virtual Class I | | | $[x\to 1-x$ cousins$]$ | |
|---|---|---|---|---|
| | $(x,y)$ | $(x,z)^{\bullet}$ | $(1-x,y)$ | $(1-x,x-y)^{\bullet}$ |
| $2\operatorname{Re}(yx\bar{x}y)$ | $\alpha$ | | $\alpha'$ | |
| $2\operatorname{Re}(y\bar{x}xy)$ | $\dagger$ | | $\dagger'$ | |
| $2\operatorname{Re}(\bar{x}yxy)$ | $\dagger$ | | $\dagger'$ | |
| $\text{bkEnd}(\mathcal{A}_{\text{seq}}(x,y))$ | | | | |
| $2\operatorname{Re}(yxy\bar{x})$ | $\beta$ | B1 | $\beta'$ | A2 |
| $2\operatorname{Re}(xyy\bar{x})$ | $\longleftarrow$ A1 $\longrightarrow$ | | $\longleftarrow$ B2 $\longrightarrow$ | |

| Virtual Class II | $(x,y)$ | $(1-x,y)^{\bullet}$ |
|---|---|---|
| $\text{frEnd}(\mathcal{A}_{\text{seq}}(y,x))$ | $\beta$ | $\beta'$ |
| $2\operatorname{Re}(x\bar{y}\bar{y}x)$ | $\longleftarrow$ C3 $\longrightarrow$ | |

**Table 1**. The shaded regions (labeled $\alpha$, $\alpha'$, $\beta$, and $\beta'$) depict groups of cancellations among IR single and double logs from real ($g \to ggg$) and virtual (next-to-leading-order $g \to gg$) processes as $y \to 0$. The unshaded entries do not cancel and are labeled according to figure 6. The fist column gives the names of diagrams, in the convention of ref. [20]. For the real diagrams, each row covers six distinct diagrams given by permutations of the daughters $(x,y,z)$ of the $g\to ggg$ process, where the column headers denote what $(x,y)$ is permuted into relative to the diagram name in the first column, and where $z \equiv 1-x-y$. A column header $(\xi,\chi)$ means to replace $(x,y) \to (\xi,\chi)$ in the diagram listed in the first column. Column headers with bullet superscripts ($\bullet$) do not represent different diagrams but instead represent a different labeling of the internal lines of the un-bulleted header to the left, corresponding to a different soft limit ($y\to 0$) of that diagram. For each Class I virtual diagram, another distinct diagram can be generated by substituting $x \to 1-x$ (see ref. [20]), as also indicated by the column headers $(\xi,\chi)$. $\mathcal{A}_{\text{seq}}$ represents only one of the two large-$N_{\text{c}}$ color routings of "sequential" diagrams (see ref. [15] for details). bkEnd and frEnd refer to back-end and front-end transformations, as described in refs. [18, 20]. The notations $*$, $*'$, $\dagger$ and $\dagger'$ on certain pairs of table entries are explained in the text. The labels A1, A2, . . . , C3 above are shorthand for the corresponding diagrams of figure 6 *plus* their complex conjugates. The meaning of the double-sized boxes for A1, B2, and C3 is explained in appendix B.

diagrams corresponding to the $(x, y)$ column of the top rectangle in table 1 are shown in figure 8. The $\mathcal{A}_{\text{seq}}(x, y)$ entry of the table corresponds to the sum of the entire bottom row of the figure, with the caveat [15][20] that $\mathcal{A}_{\text{seq}}(x, y)$ includes only one of the two large-$N_{\text{c}}$ color routings of those bottom diagrams. [The other color routing is represented by the $(x, z)$ column entry for $\mathcal{A}_{\text{seq}}$.] The virtual diagrams for $g{\to}gg$ corresponding to the lower darker-blue ($\alpha$) rectangle in table 1 are shown in figure 9. These diagrams are "back-end" transformations of the diagrams in figure 8, which means that the drawings of the diagrams are related by sliding the latest-time (right-most) vertex around the back of the diagram from the amplitude to the conjugate amplitude, or vice versa.[21] As discussed in refs. [18, 20], the differential rates for such a pair of diagrams have identical magnitudes but opposite signs. This does not mean that their effects exactly cancel, however, because rates for $g{\to}ggg$ processes and rates for virtual corrections to $g{\to}gg$ processes appear differently in applications. However, in applications to shower development and energy loss (see examples in ref. [20][22]), the differential $g{\to}ggg$ rates and $g{\to}gg$ rates are integrated against functions that become the same in the soft limit $y{\to}0$, reflecting the fact that if one of the daughters of $g{\to}ggg$ becomes arbitrarily soft, then effects of $g{\to}ggg$ become physically indistinguishable from those of $g{\to}gg$. Generically, then, the effects of two back-end related diagrams should cancel at leading order in $y{\to}0$, and the corrections to that cancellation should be suppressed by an additional factor of $y$ (coming from the Taylor expansion in $y$ of whatever functions that $g{\to}ggg$ and virtual $g{\to}gg$ processes are multiplied by in the application of interest). Since the sum of diagrams in figure 8 and the sum of diagrams in figure 9 each behave like (2.1) and so are $O(y^{-3/2})$, that means that their combined effect in applications will be order $y \times y^{-3/2} = y^{-1/2}$, which is not singular enough to contribute to IR logarithms.

A similar argument applies to the sum of diagrams in the $(x, z)$ column of the same two darker-blue rectangles ($\alpha$) in table 1. However, the $(x, z)$ column for the *virtual* entries does not represent a different diagram than the $(x, y)$ entries but instead represents different IR limits of the same diagrams. An example is shown by the diagram on the right-hand side of figure 10. This figure also shows the distinct $g{\to}ggg$ diagram that is the back-end partner.

So, in total, the darker-blue ($\alpha$) rectangles do not contribute to IR logs.

The cancellation between the lighter-blue ($\alpha'$) rectangles is somewhat similar, but an additional argument is needed. As an example, consider the IR cancellation of (a) the $(z, y)$ column entry of the $2\,\text{Re}(yx\bar{x}\bar{y})$ row of table 1 with (c) the $(1{-}x, y)$ column entry of the $2\,\text{Re}(yx\bar{x}y)$ row. Figure 11 shows, correspondingly, the diagrams (a) $yz\bar{z}\bar{y}$, (b) its back-end transform, and (c) $yx\bar{x}y$ with $x \to 1{-}x$. If we were adding (a) and its back-end transformation (b) for a given $y$, they would cancel just like in our previous discussion. But in the case of $g{\to}gg$ processes, the variables we use to specify the momentum fractions of the two daughters should be fixed ($x$ and $1{-}x$) and should not change when we later

---

[20]Specifically, see sections 2.2.1 and 3.1 of ref. [15].

[21]See in particular section 4.1 of ref. [18] and section 2.2 of ref. [20]. Since we take $2\,\text{Re}(\cdots)$ of these diagrams at the end of the day, it doesn't matter that the back-end transformation of $x\bar{y}\bar{x}y$ is the complex conjugate of $\bar{x}yxy$ and is not $\bar{x}yxy$ itself.

[22]Specifically, see ref. [20] sections 1.2 and 3.1 and appendix F.
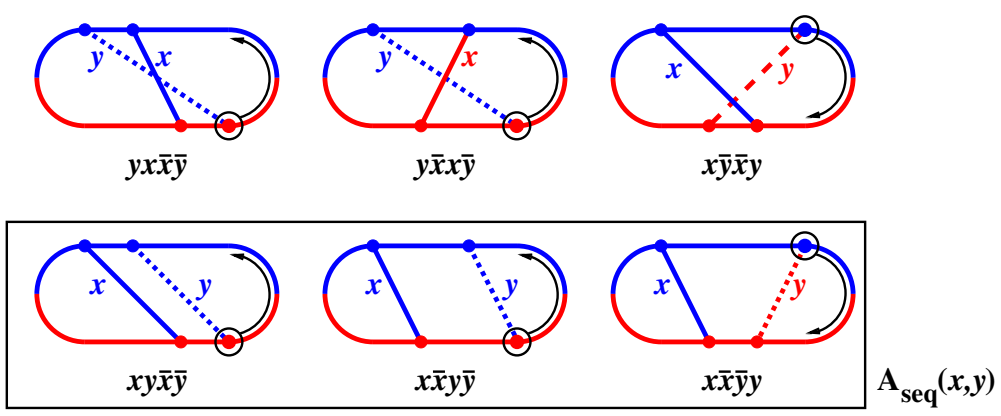
**Figure 8**. The $g \to ggg$ diagrams corresponding to the $(x, y)$ column of the upper darker-blue $(\alpha)$ rectangle of table 1. The black circles and arrows depict the action of a back-end transformation on these diagrams.
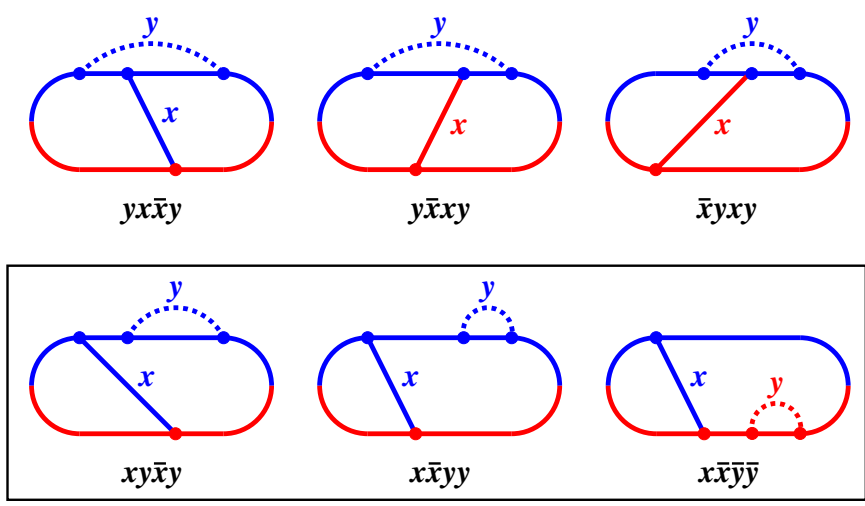


**Figure 9**. The virtual $g \to gg$ diagrams corresponding to the $(x, y)$ column of the lower darker-blue $(\alpha)$ rectangle of table 1.
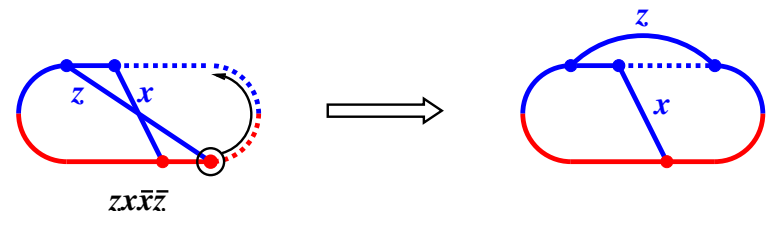


**Figure 10**. The back-end transformation of the $y \leftrightarrow z$ permutation of $yx\bar{x}\bar{y}$. The dotted lines indicate the soft gluon $(y \to 0)$. The virtual diagram on the right is the *same* diagram as the $yx\bar{x}y$ diagram of figure 9 (since $y$ is just a loop variable and not a fixed, external momentum fraction), but a different virtual gluon line is soft in the diagram here.
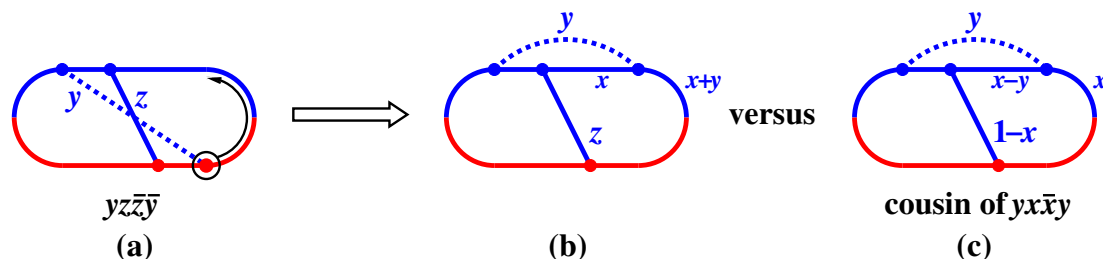
**Figure 11**. (a–b) The back-end transformation of the $x \leftrightarrow z$ permutation of $yx\bar{x}\bar{y}$ compared to (c) the $x \to 1-x$ cousin of the Class I virtual diagram $yx\bar{x}y$.

integrate over loop variables (in this case $y$). So we want to add (a) with (c), not (a) with (b). Unlike (a) and (b), the differential rates $d\Gamma/dx\,dy$ associated with (a) and (c) are not exactly the negative of each other. However, this is inessential because the momentum fractions of lines in (b) and (c) match up in the $y \to 0$ limit: the differences are suppressed by relative factors of $y$. As argued earlier in a different context, a correction of relative order $y$ to (2.1) will not affect IR logarithms. So the lighter-blue ($\alpha'$) entries will have the same cancellation of IR logarithms as the darker-blue ($\alpha$) entries.

The diagrams corresponding to the darker-pink rectangles ($\beta$) of table 1 are shown in figure 12. Here the real and virtual diagrams are related by a *front*-end transformation [18, 20], which graphically corresponds to sliding the earliest-time (left-most) vertex around the front of the diagram. Like the back-end transformation, the front-end transformation introduces an overall minus sign. However, it *also* involves a relabeling of momentum fractions as[23]

$$(x, y, E) \longrightarrow \left( \frac{x}{1-y}, \frac{-y}{1-y}, (1-y)E \right), \tag{3.3}$$

in the case of figure 12. Now note that in the $y \to 0$ limit of interest to extracting IR logs, this transformation simplifies to

$$(x, y, E) \longrightarrow (x, -y, E) \tag{3.4}$$

up to corrections that, for each, are suppressed by an additional factor of $y$. So, *except* for $y \to -y$, the front-end related diagrams in figure 12 should cancel each other, similar to what happened for the back-end transformations in the $\alpha'$ group discussed previously.

Discussing the effect of $y \to -y$ on the cancellation of front-end related diagrams is subtle. To make front-end transformations like (3.3) successfully relate diagrams, one must be very careful [18, 20] to figure out, in formulas for diagrams, which instances of longitudinal momentum fractions like $y$ should be written as $|y|$ and which as simply $y$. We will not attempt to justify or re-derive it here. The $y$ in the denominator of the IR log term

$$\frac{\#\ln y + \#}{y} \tag{3.5}$$

---

[23]See in particular section 4.2 of ref. [18] and section 2.2 of ref. [20] (but note that our figure 12 here already implements the step $x \leftrightarrow y$ discussed for figures 9 and 10 of ref. [20]).
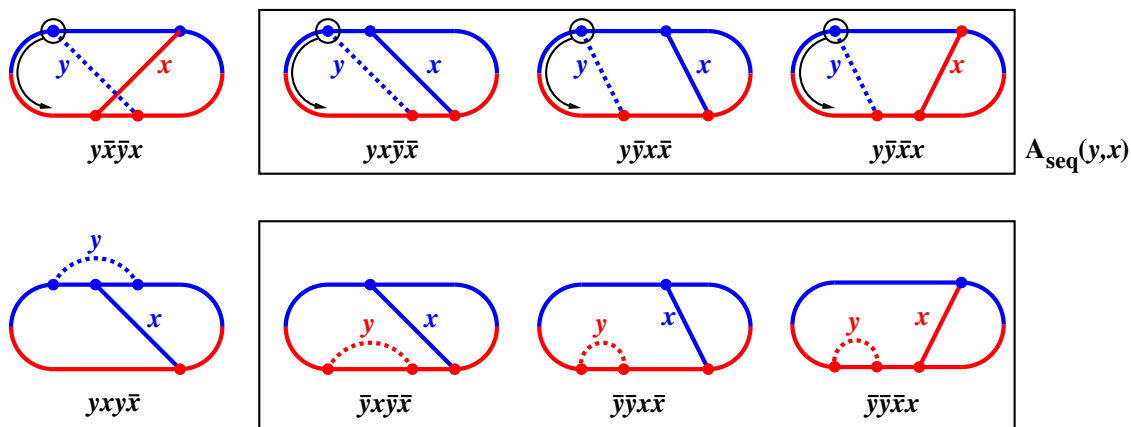
**Figure 12**. Diagrams corresponding to the darker-pink rectangles ($\beta$) in table 1. The $g{\to}ggg$ diagrams (top row) are related by front-end transformation to the virtual $g{\to}gg$ diagrams of the bottom row.

from (2.1) turns out to be a $|y|$.[24] That leaves the possibility that $y \to -y$ could take $\ln y$ to $\ln(-y)$ in (3.5). Since a front-end transformation also negates the diagram, that means that the sum of a pair of front-end related diagrams could have a non-zero result proportional to

$$\frac{\ln y}{y} - \frac{\ln(-y)}{y} = \pm \frac{i\pi}{y} \,. \tag{3.6}$$

The details are complicated. In general, we find both $\ln y$ and $\ln|y|$ terms in our small-$y$ expansions of diagrams. As an example, we carry out this analysis for $\mathcal{A}_{\text{seq}}(y,x)$ in appendix E, and show how the IR single log of $\mathcal{A}_{\text{seq}}(y,x)$ does not cancel that of its front-end transformation but instead leaves behind a left-over $i\pi$ term like (3.6). However, we have not taken the time to do the same analytically for the other front-end related pair of diagrams also marked $\beta$ (darker pink) in table 1: $2\operatorname{Re}(y\bar{x}\bar{y}x) + 2\operatorname{Re}(yxy\bar{x})$. Instead, we have just extracted the small-$y$ behavior of that sum numerically and find that the IR log exactly cancels that of the $\mathcal{A}_{\text{seq}}(y,x)$ pair. That is, altogether, the IR logs from the four diagrams in the dark-pink rectangles ($\beta$) cancel each other. Regrettably, we do not know a simpler way to argue that the left-over terms (3.6) must cancel among these diagrams.

Finally, the IR logs from the lighter-pink rectangles ($\beta'$) cancel each other similarly.

### 3.3 Diagrams with 4-gluon or instantaneous vertices

In our discussion of non-ABC diagrams above, we have left out diagrams that contain 4-gluon vertices [17], examples of which are shown in figures 13(a) and (b). As mentioned earlier, our analysis of diagrams makes use of Light-Cone Perturbation Theory. In LCPT, there are non-local, effective 4-gluon interactions that are instantaneous in light-cone time. We have left out diagrams that contain these interactions as well, an example of which is

---

[24]The $1/|y|$ factor comes from the small-$y$ behavior of the $g{\to}gg$ DGLAP splitting function $P(y)$ associated with the $y$ emission. To implement front-end transformations, DGLAP splitting functions should involve the absolute values of the particle momentum fractions, as is implemented in ref. [20] eqs. (A.5) and (A.23). See footnote 35 or ref. [20].
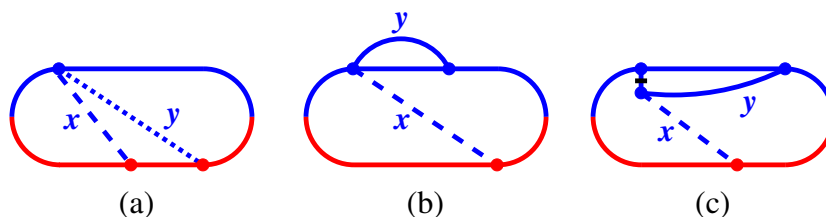
**Figure 13**. Examples of diagrams that involve 4-gluon or LCPT instantaneous vertices, which have been left out of our discussion.

shown in figure 13(c). (See ref. [18] for examples of the analysis of such diagrams, for generic $y$, in the case of large-$N_f$ QED.) There is no reason to suspect that diagrams involving 4-gluon or LCPT instantaneous vertices would contribute to (net) logarithms, and we find that they do not [22].

# 4 The A3 diagram

## 4.1 Scales and form

We start with a calculation of the IR logs associated with the A3 diagram (including adding its complex conjugate). This corresponds to the $y \to 0$ limit of $2\,\mathrm{Re}(xy\bar{y}\bar{x})$. Throughout this paper, we do not assume that $x$ is small, and we will treat $x$ and $1-x$ as order $y^0$. We will also not bother, in parametric formulas, to show the constant, dimensionful factor $\sqrt{E/\hat{q}}$ associated with formation times. So, the time interval (1.1a) that gives rise to double logs will be summarized as simply

$$y \ll \Delta t \ll \sqrt{y}. \tag{4.1}$$

For given values of $x$ and $y$, ref. [20] gives formulas for the various diagrams in terms of one-dimensional integrals of the form

$$\mathrm{diagram}(x,y) = \int_0^\infty d(\Delta t)\, f(x,y,\Delta t), \tag{4.2}$$

where $f$ is a quite complicated algebraic function specific to each diagram. (We'll give more details as needed.) There is a complication, however. The integral above has a UV divergence associated with $\Delta t \to 0$. The regulated divergences give rise to what are called "pole terms" in refs. [14–16, 20]. To handle the UV divergence separately, we split (4.2) into

$$\mathrm{diagram}(x,y) = \lim_{a \to 0} \left[ \int_0^a d(\Delta t)\, f(x,y,\Delta t) + \int_a^\infty d(\Delta t)\, f(x,y,\Delta t) \right] \tag{4.3}$$

and regulate the first integral with dimensional regularization.

We should mention that in the treatment of divergent integrals for generic $y$ in ref. [20], we needed to evaluate the second integral numerically. That motivated further reorganization of the second integral to improve numerical accuracy by removing its sensitivity to the tiny
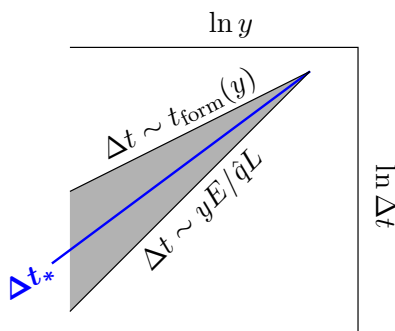
**Figure 14**. A choice of intermediate scale $\Delta t_*(y)$ splitting the (shaded) double log region of figure 1. Remember that we (parametrically) define $L = t_{\rm form}(x)$ in our application.

cut-off $a$. That numerics-motivated reorganization is unnecessary here because our goal is to derive *analytic* results for the small-$y$ expansion.[25]

To calculate IR single logs, imagine choosing a dividing time $(\Delta t)_*$ somewhere in the parametric range (4.1),[26] and further divide (4.3) into pieces

$$\text{diagram}(x,y) = \lim_{a\to 0}\left[\int_0^a d(\Delta t)\, f(x,y,\Delta t) + \int_a^{(\Delta t)_*} d(\Delta t)\, f(x,y,\Delta t)\right]$$
$$+ \int_{(\Delta t)_*}^{\infty} d(\Delta t)\, f(x,y,\Delta t). \tag{4.4}$$

For small $y$, we then make a $\Delta t \ll \sqrt{y}$ approximation to the $\Delta t$ integral over the interval $[a,(\Delta t)_*]$ in (4.4) and a $\Delta t \gg y$ approximation to the integral over $[(\Delta t)_*,\infty]$. That is, we split the calculation of double and single logs by dividing the double log region into two, as divided pictorially by the blue line in figure 14.

Later, our small-$y$ expansions of these integrals will turn out to be more compact if we formally restrict the choice of the dividing time $(\Delta t)_*$ to the narrower range

$$y^{2/3} \ll (\Delta t)_* \ll y^{1/2}. \tag{4.5}$$

So $(\Delta t)_* \sim y^{7/12}$, for example. Note that there are no unusual fractional powers of $y$ in our final results (2.11) for small-$y$ expansions; the choice (4.5) is just a convenience for managing expansions of intermediate results before the eventual cancellation of $(\Delta t)_*$ dependence in the combination (4.4).

The "interesting" part of the $[a,(\Delta t)_*]$ and $[(\Delta t)_*,\infty]$ integrals in (4.4) will be the behavior of the integrands at $\Delta t \sim y$ and $\Delta t \sim \sqrt{y}$, respectively. So, we will loosely refer

---

[25]The further reorganization is explained in section 4.3.2 of ref. [18] and appendix D.1 of ref. [20]. Since that is unnecessary here, we will not include the corresponding "$\mathcal{D}_2$" subtractions in our formulas for diagrams. Similarly, what we call our "pole pieces" in this paper do not have those $\mathcal{D}_2$ subtractions added back in. We should clarify that, even for numerics, no such $\mathcal{D}_2$ subtractions are needed for some *combinations* of diagrams such as eq. (A.12) of ref. [20], which combines the A3 diagram with other $g{\to}ggg$ crossed diagrams. For that combination, the un-subtracted integral is insensitive to arbitrarily small $a$ [14, 16].

[26]A similar strategy was used in ref. [13]. (But their analysis, which was in the context of transverse momentum broadening, did not need to confront the UV divergences that we have for individual ABC diagrams. So they did not need any dividing scale analogous to our $a$.)

to these two integrals as the "$\Delta t \sim y$" and "$\Delta t \sim \sqrt{y}$" contributions, even though it is actually the entire range (4.1) that generates the double log.

Our strategy in this paper will be to take as our starting point the general formulas [20] for diagrams, which do not assume small $y$, and from them analytically extract the $y\to 0$ expansion (2.1). The analysis will be similar to the analysis of ref. [20] appendix E.4 of IR power-law divergences, which corresponds to the $O(y^{-3/2})$ terms in the small-$y$ expansion (2.1). But now we must push the analysis to higher order in the expansion to find the IR log (order $y^{-1}$) terms as well.

It will aid our discussion to write out explicitly the highest-level structure of the integrands $f$ in terms of the same notation used in ref. [20]. Specifically, (4.2) for the A3 diagram (including its complex conjugate) is

$$\left[\frac{d\Gamma}{dx\,dy}\right]_{\text{A3}} = \int_0^\infty d(\Delta t)\, 2\,\text{Re}\, C(-1, y, z, x, \alpha, \beta, \gamma, \Delta t), \tag{4.6}$$

with

$$C = D - \lim_{\hat{q}\to 0} D. \tag{4.7}$$

Eq. (4.7) represents subtracting out the result the diagram would have in vacuum, which is merely a trick for simplifying calculations.[27] The symbols $(\alpha, \beta, \gamma)$ above are functions of $x$ and $y$ and represent various combinations of helicity-dependent DGLAP splitting functions; their detailed formulas are not important for now. The other arguments $(-1, y, z, x)$ of $C$ are the longitudinal momentum fractions of the four high-energy gluon lines in the A3 diagram of figure 7 during the time $\Delta t$ spanned by the $y$ emission.

We will not write out the detailed generic-$y$ formulas for $D$, $\alpha$, $\beta$, and $\gamma$ here. Readers may find them in appendix A of ref. [20], and we will use them in various appendices. However, here in the main text, it will be useful to know that $\gamma$ dominates over $\alpha$ and $\beta$ in the small-$y$ limit, where

$$\gamma = \frac{2\,P(x)}{C_{\text{A}} x^2 (1-x)^3 y^3}\left[1 + O(y)\right]. \tag{4.8}$$

[Some of our intermediate calculations will be sensitive to the relative $O(y)$ corrections in (4.8), but ultimately we will not need an explicit formula for those corrections.]

## 4.2  $\Delta t \sim y$ contribution to A3 diagram

Unfortunately, an annoying complication arises in the small-$y$ expansion. Though the A3 diagram overall has the small-$y$ expansion (2.1), which starts with $O(y^{-3/2})$, the $\Delta t \sim y$ integration in (4.4) produces a spurious $y^{-2}$ divergence which is *canceled* by a similar $y^{-2}$ divergence of the pole term in (4.4). Because of this, in order to extract the $y^{-1}$ behavior of IR logs, we must expand the $\Delta t \sim y$ integral, and so its integrand, to higher relative order in $y$ than hoped. This complication was previously encountered in the calculation of IR power-law divergences in ref. [20] appendix E.4.

---

[27]See the discussion in section 5.4 in ref. [14]. Note that our calculations are for splitting of on-shell high-energy partons in the medium. In consequence, the total rate for splitting in the vacuum must be zero.
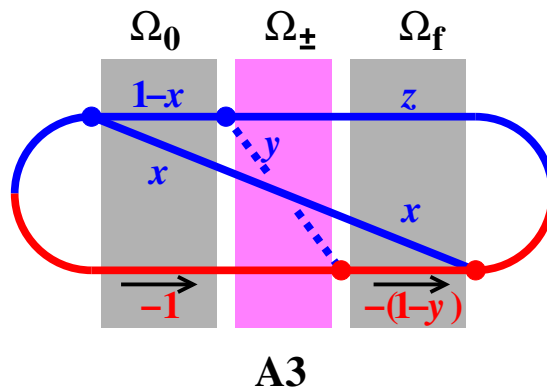
**Figure 15**. The A3 diagram with shading denoting the initial 3-particle evolution (left), the 4-particle evolution (middle), and the final 3-particle evolution (right). Our names $\Omega$ for the corresponding complex harmonic oscillator frequencies are marked atop each region.

We originally planned to use a symbolic algebra program to Taylor expand the integrand $f(x, y, \Delta t)$ in powers of $y \sim \Delta t$. That is awkward because of the very complicated formula for $f = 2 \operatorname{Re} C$ and issues of branch cuts, and because automated expansions tend to produce long, complicated results that are hard to organize and simplify. In the end, we decided to do expansions by hand.

The steps leading to the small-$y$ expansion of the $\Delta t$-integrand of the A3 diagram for $\Delta t \sim y$ are summarized in appendix C.1. In the specific case of the A3 diagram, we obtain

$$
\begin{aligned}
D \simeq -\frac{C_{\mathrm{A}}^2 \alpha_{\mathrm{s}}^2}{8\pi^2 (\Delta t)^2} (xyz)^2 (1-x)(1-y)\gamma \\
\times \left\{ \left( 1 + \xi - 2s\xi\tau^2 \right) \ln\left( \frac{xy}{(1-x)(1-y)}(1+\tau) \right) + \frac{1}{1+\tau} \right. \\
\left. + \xi\left[ -\frac{2\tau}{1+\tau} - \frac{(1+s)\tau^3}{(1+\tau)^2} \right] \right\},
\end{aligned} \tag{4.9}
$$

where we have found it convenient to define the variables

$$
s \equiv \frac{x^2}{12(1-x+x^2)}, \qquad \xi \equiv \frac{xy}{2z}, \qquad \tau \equiv \frac{i(\Omega_0 + \Omega_{\mathrm{f}})\Delta t}{2\xi}. \tag{4.10}
$$

$\Omega_0$ and $\Omega_{\mathrm{f}}$ are the complex harmonic oscillator frequencies associated with the initial and final 3-particle evolution, as indicated by the gray areas in figure 15. They are given by (2.4) and its generalization to other momentum fractions:

$$
\Omega_0 = \Omega_{-1,x,1-x}, \quad \Omega_{\mathrm{f}} = \Omega_{-(1-y),x,z}, \tag{4.11}
$$

where

$$
\Omega_{\zeta_1, \zeta_2, \zeta_3} = \sqrt{-\frac{i\hat{q}_{\mathrm{A}}}{2E}\left( \frac{1}{\zeta_1} + \frac{1}{\zeta_2} + \frac{1}{\zeta_3} \right)}. \tag{4.12}
$$

Note that $\xi$ in (4.10) is proportional to $y$ and so is small in the small-$y$ limit, but $s$ is order $y^0$. The rescaled time variable $\tau$ is order $y^0$ for the case $\Delta t \sim y$ we are currently

working on. The leading terms in (4.9) are written in red (or with a red-colored factor) and will give rise, after integration over $\Delta t$, to the spurious $y^{-2}$ divergence mentioned earlier. The other terms (without red) will give rise to $O(y^{-1})$ terms after integration over $\Delta t$ and so will contribute to IR logarithms.

We should explain a technical point at this juncture: why have we not fully expanded the small-$y$ dependence of (4.9)? Note, for instance, the overall factor $(1-y)$. If we wanted to, for example, we could have expanded

$$(1-y) \times \frac{1}{1+\tau} \simeq \frac{1}{1+\tau} - \frac{y}{1+\tau}\,, \tag{4.13}$$

in (4.10) in order to more clearly separate leading and sub-leading terms. It turns out that leaving (4.13) unexpanded not only makes the expression (4.9) more compact but will also later simplify handling sub-leading terms in the cancellation of the spurious leading divergence with the pole terms in (4.4). For similar reasons, it is advantageous to avoid expanding the overall factor of $\gamma = \gamma(x,y)$, as well as the factors of $1-y$ and $1+\tau$ in the argument of the logarithm in (4.9) [noting that the definition (4.10) of $\tau$ depends on $y$ through the definitions of $\xi$ and $\Omega_{\mathrm{f}}$ (and $z \equiv 1-x-y$)].

The next step is to extract the vacuum limit of (4.9) so that we can make the vacuum subtraction (4.7). Since harmonic oscillator frequencies $\Omega$ are proportional to $\sqrt{\hat{q}}$, the vacuum limit for fixed $\Delta t$ is the $\tau \to 0$ limit by virtue of the definitions (4.10). For A3, the vacuum-subtracted version $C$ of (4.9) is then

$$
\begin{aligned}
C \simeq {}& -\frac{C_{\mathrm{A}}^2 \alpha_{\mathrm{s}}^2}{8\pi^2}(xyz)^2(1-x)(1-y)\gamma \\
& \times \frac{1}{(\Delta t)^2}\left\{(1+\xi)\left[\ln(1+\tau) - \frac{\tau}{1+\tau}\right] - 2s\xi\tau^2\ln(2\xi(1+\tau)) + \xi\left[-\frac{\tau}{1+\tau} - \frac{(1+s)\tau^3}{(1+\tau)^2}\right]\right\},
\end{aligned}
\tag{4.14}
$$

where we've reorganized terms a bit. We've also used

$$\frac{xy}{(1-x)(1-y)} = 2\xi\left[1 + O(y)\right] \tag{4.15}$$

to simplify the argument of the (sub-leading) $s\xi\tau^2\ln(\cdots)$ term.

Next, we need to integrate $\Delta t$ over $[a,(\Delta t)_*]$, as in the relevant term of (4.4). Changing integration variables from $\Delta t$ to $\tau$ gives

$$
\begin{aligned}
\int_a^{(\Delta t)_*} & d(\Delta t)\, 2\operatorname{Re} C \simeq \\
& -\frac{C_{\mathrm{A}}^2 \alpha_{\mathrm{s}}^2}{8\pi^2}(xyz)^2(1-x)(1-y)\gamma \operatorname{Re}\left[i(\Omega_0 + \Omega_{\mathrm{f}})\int_{\tau_a}^{\tau_*} d\tau \left\{(\tfrac{1}{\xi}+1)\left[\frac{\ln(1+\tau)}{\tau^2} - \frac{1}{\tau(1+\tau)}\right]\right.\right. \\
& \left.\left. - 2s\ln(2\xi(1+\tau)) - \frac{1}{\tau(1+\tau)} - \frac{(1+s)\tau}{(1+\tau)^2}\right\}\right].
\end{aligned}
\tag{4.16}
$$

From (4.5) and (4.10), the rescaled dividing time $\tau_*$ is large ($\tau_* \gg 1$) and in the range

$$y^{-1/3} \ll \tau_* \ll y^{-1/2}. \tag{4.17}$$

The rescaled UV cut-off $\tau_a$ should be treated as arbitrarily small.

The indefinite version $\int d\tau \{\cdots\}$ of the integral gives

$$\mathfrak{c}(\tau) \equiv -(\tfrac{1}{\xi}+1)\frac{\ln(1+\tau)}{\tau} - 2s\tau\ln(2\xi(1+\tau)) + 2s\tau - \ln\tau - 3s\ln(1+\tau) - \frac{1+s}{1+\tau}. \quad (4.18)$$

Then (4.16) becomes

$$\int_a^{(\Delta t)_*} d(\Delta t)\, 2\,\mathrm{Re}\,C \simeq -\frac{C_{\mathrm{A}}^2\alpha_{\mathrm{s}}^2}{8\pi^2}(xyz)^2(1-x)(1-y)\gamma$$
$$\times \mathrm{Re}\Big[i(\Omega_0+\Omega_{\mathrm{f}})\{\tfrac{1}{\xi}+2+s+\ln\big(\tfrac{i\Omega_0 a}{\xi}\big)+\mathfrak{c}(\tau_*)\}\Big], \quad (4.19)$$

where, expanding for large $\tau_*$ with (4.17),

$$\mathfrak{c}(\tau_*) \simeq -\frac{1}{\xi}\left(\frac{\ln\tau_*}{\tau_*}+\frac{1}{\tau_*^2}\right) - 2s\tau_*\ln(2\xi\tau_*) + 2s\tau_* - (1+3s)\ln\tau_* - 2s \quad (4.20)$$

up to corrections parametrically smaller than 1. Those corrections are too small to affect IR logarithms because the overall factors multiplying $\mathfrak{c}(\tau_*)$ are of order $y^2\gamma = O(y^{-1})$, so that any further suppression corresponds to IR-convergent additions to the small-$y$ expansion (2.1).

The red $1/\xi$ term in (4.19) gives a contribution of order $y^2\gamma/\xi = O(y^{-2})$ to (4.19). This is the spurious $y^{-2}$ divergence mentioned earlier.

## 4.3 UV piece of the A3 diagram

The dimensionally-regulated UV contribution to A3 in (4.4) can be assembled from formulas in ref. [20]. In appendix C.2, we display the generic-$y$ formula for this contribution and then expand in $y$. The result, through next-to-leading order in $y$, is

$$\left[\frac{d\Gamma}{dx\,dy}\right]_{\mathrm{A3}}^{(\Delta t<a)} \equiv 2\,\mathrm{Re}\left[\frac{d\Gamma}{dx\,dy}\right]_{xy\bar{y}\bar{x}}^{(\Delta t<a)}$$
$$\simeq \frac{C_{\mathrm{A}}^2\alpha_{\mathrm{s}}^2}{8\pi^2}(xyz)^2(1-x)(1-y)\gamma\,\mathrm{Re}\Big[(i\Omega_0+i\Omega_{\mathrm{f}})$$
$$\times\left\{\frac{1}{\xi}+\frac{2}{\epsilon}+\ln\big(\frac{\mu^4 a}{i\Omega_0 E^2}\big)+1+\ln(2\pi^2)-\ln(e^{-i\pi}xyz)\right\}\Big]. \quad (4.21)$$

We again find it convenient to leave some elements unexpanded, such as $\gamma$ and $\Omega_{\mathrm{f}}$.

If we add (4.21) to (4.19), the spurious $y^{-2}$ divergences (the red terms) cancel. With them out of the way, one may then use the *leading* approximation (4.8) to $\gamma$. The result for the total $\Delta t < (\Delta t)_*$ contribution to A3 is then

$$\left[\frac{d\Gamma}{dx\,dy}\right]_{\mathrm{A3}}^{(\Delta t<a)} + \int_a^{(\Delta t)_*} d(\Delta t)\, 2\,\mathrm{Re}\,C$$
$$\simeq \frac{C_{\mathrm{A}}\alpha_{\mathrm{s}}^2 P(x)}{2\pi^2 y}\,\mathrm{Re}\left[i\Omega_0\left\{2\Big[\frac{1}{\epsilon}+\ln\big(\frac{\pi\mu^2}{\Omega_0 E}\big)\Big]-1+s-2\ln(1-x)-\kappa(\tau_*)\right\}\right], \quad (4.22)$$

where we find it convenient to isolate the $\tau_*$-dependent terms of (4.20) as

$$\kappa(\tau_*) \equiv -\frac{1}{\xi}\left(\frac{\ln\tau_*}{\tau_*}+\frac{1}{\tau_*^2}\right) - 2s\tau_*\ln(2\xi\tau_*) + 2s\tau_* - (1+3s)\ln\tau_*. \quad (4.23)$$

Note that the dependence on $a$ has canceled in (4.22), as it must.

## 4.4 $\Delta t \sim \sqrt{y}$ contribution to A3 diagram

Turn now to the last term in (4.4). We repeat the procedure of section 4.2, but now with time scale $\Delta t \sim \sqrt{y}$ instead of $\Delta t \sim y$. Like before, we need a corresponding small-$y$ approximation of the integrand $2\operatorname{Re}C$. We again start with the function $D$ of (4.7). Details of the expansion are summarized in appendix C.3, with result

$$D \simeq -\frac{C_A \alpha_s^2 P(x)}{4\pi^2 y}\left[(\Omega_y \csc_y)^2 \ln S + \frac{\xi \Omega_y^3 \Delta t}{2S}\csc_y(\csc_y + \cot_y)^2\right], \qquad (4.24)$$

where

$$S \simeq {\color{red}2i\Omega_0\,\Delta t} + (2+3s)(\Omega_0\,\Delta t)^2 + \xi\Omega_y(\csc_y + \cot_y)\Delta t \qquad (4.25)$$

and we introduce the short-hand notation

$$\operatorname{trig}_y \equiv \operatorname{trig}(\Omega_y\,\Delta t). \qquad (4.26)$$

The red term in (4.25) indicates the leading-order behavior, which in this case will generate a $y^{-3/2}$ power-law divergence like in (2.1), not a $y^{-2}$ divergence like in section 4.2.[28]

A caution is needed: it may be tempting to immediately expand the $\ln S$ of (4.24) using (4.25). The caution is that we need to subtract out the vacuum result for $D$ in (4.7), but the red term in (4.25) *vanishes* in vacuum (where $\hat{q}$ and so $\Omega_0$ are zero). That means that the small-$y$ expansion of $S$ looks different in vacuum:

$$\lim_{\hat{q}\to 0} S \simeq 2\xi. \qquad (4.27)$$

The vacuum subtracted version of $D$ is then

$$C \simeq -\frac{C_A \alpha_s^2 P(x)}{4\pi^2 y}\left\{(\Omega_y \csc_y)^2 \ln S - \frac{i\xi\Omega_y^3}{4\Omega_0}\csc_y(\csc_y + \cot_y)^2 - \frac{\ln(2\xi)}{(\Delta t)^2} - \frac{1}{(\Delta t)^2}\right\}. \qquad (4.28)$$

Only now is it safe to expand the logarithm as

$$\ln S \simeq {\color{red}\ln(2i\Omega_0\,\Delta t)} - i(1 + \tfrac{3}{2}s)\Omega_0\,\Delta t - \frac{i\xi}{2\Omega_0}\Omega_y(\csc_y + \cot_y). \qquad (4.29)$$

To integrate over $\Delta t$, it is convenient to switch integration variables to

$$\tilde{\tau} \equiv i\Omega_y\,\Delta t. \qquad (4.30)$$

Using

$$\xi\Omega_y^2 = 6s\Omega_0^2 + O(y) \qquad (4.31)$$

[taken from (2.9) and (4.10)] to simplify parts of the expression, we find

$$\int_{(\Delta t)_*}^\infty d(\Delta t)\, 2\operatorname{Re}C \simeq$$
$$-\frac{C_A \alpha_s^2 P(x)}{2\pi^2 y}\operatorname{Re}\int_{\tilde{\tau}_*}^\infty d\tilde{\tau}\left\{{\color{red}i\Omega_y}\left[\frac{1}{\operatorname{sh}^2\tilde{\tau}}\ln\left(\frac{2\Omega_0\tilde{\tau}}{\Omega_y}\right) - \frac{[\ln(2\xi)+1]}{\tilde{\tau}^2}\right]\right.$$
$$\left. - i\Omega_0\left[\frac{(1+\tfrac{3}{2}s)\tilde{\tau}}{\operatorname{sh}^2\tilde{\tau}} - \frac{\tfrac{3}{2}s(1+\operatorname{ch}\tilde{\tau})(3+\operatorname{ch}\tilde{\tau})}{\operatorname{sh}^3\tilde{\tau}}\right]\right\}. \qquad (4.32)$$

---

[28]Because of this, one may dispense with the exact definition of $\xi$ from (4.10) and just take $\xi \simeq xy/2(1-x)$ here.

The "interesting" region $\Delta t \sim \sqrt{y}$ of integration corresponds to $\tilde{\tau} \sim 1$, and the lower cut-off $\tilde{\tau}_*$ on the integration is parametrically small ($\tilde{\tau}_* \ll 1$) by virtue of (2.9) and (4.5). The integrals of the terms in (4.32) are then much simpler because we only need their small-$\tau_*$ expansion.

To integrate, we find it convenient to first re-organize the terms multiplying red $i\Omega_y$ in (4.32) as

$$\frac{1}{\operatorname{sh}^2 \tilde{\tau}} \ln\left(\frac{2\Omega_0 \tilde{\tau}}{\Omega_y}\right) - \frac{\ln(2\xi)}{\tilde{\tau}^2} = \frac{1}{\tilde{\tau}^2} \ln\left(\frac{\Omega_0 \tilde{\tau}}{\xi \Omega_y}\right) + \left(\frac{1}{\operatorname{sh}^2 \tilde{\tau}} - \frac{1}{\tilde{\tau}^2}\right) \ln\left(\frac{2\Omega_0 \tilde{\tau}}{\Omega_y}\right). \tag{4.33}$$

Almost all of the $\tilde{\tau}$ integrals have results in terms of elementary functions, and one may then expand the result in powers of $\tilde{\tau}_* \ll 1$. The one integral that is slightly more complicated is[29]

$$\int_{\tilde{\tau}_*}^{\infty} d\tilde{\tau} \left(\frac{1}{\operatorname{sh}^2 \tilde{\tau}} - \frac{1}{\tilde{\tau}^2}\right) \ln(c\tilde{\tau}) = -\ln(c\pi) + \gamma_{\mathrm{E}} + \tfrac{1}{3}\tilde{\tau}_*(\ln(c\tilde{\tau}_*) - 1) + O(\tilde{\tau}_*^3 \ln \tau_*). \tag{4.34}$$

The integration in (4.32) yields

$$\int_{(\Delta t)_*}^{\infty} d(\Delta t)\, 2\operatorname{Re} C(\Delta t) \simeq$$
$$\frac{C_A \alpha_s^2 P(x)}{2\pi^2 y} \operatorname{Re}\left[i\Omega_y \left\{\ln\left(\frac{2\pi\Omega_0}{\Omega_y}\right) - \gamma_{\mathrm{E}}\right\}\right.$$
$$\left. + i\Omega_0 \left\{1 - \ln 2 + 2s - (1+3s)\ln\left(\frac{\xi\Omega_y}{\Omega_0}\right) + \kappa(\tau_*)\right\}\right], \tag{4.35}$$

where $\kappa(\tau_*)$ is again (4.23). Though it was convenient to set up the original integral (4.35) in terms of the small parameter $\tilde{\tau}_*$, it's nonetheless convenient to have written the final result (4.35) in terms of the $\tau_*$ instead, converting between them using their definitions (4.10) and (4.30). This way, we will be able to easily see the cancellation of the splitting-time dependence $\kappa(\tau_*)$ when summing all contributions to A3.

## 4.5  A3 result

The total result (4.4) for the small-$y$ expansion of A3 is the sum of (4.22) and (4.35):

$$\left[\frac{d\Gamma}{dx\,dy}\right]_{\mathrm{A3}} \simeq \frac{C_A \alpha_s^2 P(x)}{2\pi^2 y} \operatorname{Re}\left[i\Omega_y \left\{\ln\left(\tfrac{2\pi\Omega_0}{\Omega_y}\right) - \gamma_{\mathrm{E}}\right\}\right.$$
$$+ i\Omega_0\left\{2\left[\tfrac{1}{\epsilon} + \ln\left(\tfrac{\pi\mu^2}{\Omega_0 E}\right)\right] - (1+3s)\ln\left(\tfrac{\xi\Omega_y}{\Omega_0}\right)\right.$$
$$\left.\left. - 2\ln(1-x) - \ln 2 + 3s\right\}\right]. \tag{4.36}$$

Using the definitions (4.10) and some algebra, this result demonstrates the A3 case ($p, q = 1, 3$) of the more general formula (2.11a) presented earlier.

---

[29]To derive (4.34), first write $\int_{\tilde{\tau}_*}^{\infty} = \int_0^{\infty} - \int_0^{\tilde{\tau}_*}$. Then do the $\int_0^{\infty}$ integral exactly. It is given by eq. (E.18) of ref. [20], which is derived in the corresponding paragraph of appendix B of ref. [20]. For the $\int_0^{\tilde{\tau}_*}$ integral, expand the integrand in powers of small $\tilde{\tau} \le \tilde{\tau}_* \ll 1$ and integrate that expansion term by term to the desired order.
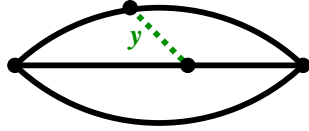
**Figure 16**. If colors (red vs. blue) are not shown, and if the momentum fractions associated with the underlying $g \to gg$ process (black lines above) are not shown, then all of the ABC diagrams can be drawn in the same form, shown above.

## 5 Other $p \neq q$ ABC diagrams

Return now to the depiction in figure 6 of the ABC diagrams. Ignoring the color differences between red and blue lines, and the label "$x$", all the diagrams look the same in the case $p \neq q$: they can all be drawn in the form of figure 16. So one might guess that the results for these diagrams are all related by permutations of the momentum fractions (2.7) of the three lines of the underlying, hard $g \to gg$ splitting process. The one fly in the ointment is that, as mentioned in section 2.2, there *are* differences between blue (amplitude) and red (conjugate amplitude) lines, arising from complex phases. As in the discussion of section 3.2, these phases can give rise to "$i\pi$" terms in our interference diagrams which, when multiplied by other phases, give rise to "$\pi$" terms when one takes $2\operatorname{Re}(\cdots)$ to add in the interference diagram's complex conjugate. Starting from our result for A3, written in the form of the $p, q = 1, 3$ case of (2.11a), one might *guess* that the $p \neq q$ ABC diagrams as a group give

$$
\begin{aligned}
\left[\frac{d\Gamma}{dx\,dy}\right]_{pq} \simeq \frac{C_A \alpha_s^2 P(x)}{2\pi^2 y} \operatorname{Re}\Big[ & i\Omega_y \Big\{ -\ln\big(\tfrac{\Omega_y}{2\pi\Omega_0}\big) - \gamma_E + \pi \times \text{?}_{pq} \Big\} \\
& + i\Omega_0 \Big\{ 2\Big[\tfrac{1}{\epsilon} + \ln\big(\tfrac{\pi\mu^2}{\Omega_0 E}\big)\Big] - \big(1 + \tfrac{\mathfrak{r}_r^2}{2(\mathfrak{r}_1^2 + \mathfrak{r}_2^2 + \mathfrak{r}_3^2)}\big) \Big[ \ln\big(\tfrac{|\mathfrak{r}_p \mathfrak{r}_q \mathfrak{r}_r| y\Omega_y}{\Omega_0}\big) + \pi \times \text{?}_{pq} \Big] \\
& \hspace{4cm} + \tfrac{\mathfrak{r}_r^2}{2(\mathfrak{r}_1^2 + \mathfrak{r}_2^2 + \mathfrak{r}_3^2)} \big[ 1 - \ln 2 + 2\ln(2|\mathfrak{r}_p \mathfrak{r}_q|) \big] \Big\} \Big] \quad (5.1)
\end{aligned}
$$

for some $(p, q)$-dependent values of the question marks "$\text{?}_{pq}$" above. In our guess, we have only included such $\pi$ terms in the case of logarithms whose arguments depend on $y$, since it is the color of the $y$ line that can change between different ABC diagrams.

The goal of this paper is to simply find the formula for the single logs, in the most efficient way we can manage. Rather than derive (5.1) and carefully analyze every branch cut and complex phase, the most efficient method for us was to simply take (5.1) as an ansatz and then use numerical extraction of the $y \to 0$ limits of generic-$y$ formulas [20] to determine the question marks, which we expect to be simple fractions. Doing that produces and verifies our final results (2.11a).[30]

---

[30]The $\pi$ terms associated with the power-law divergences [the red $i\Omega_y$ terms in (5.1)] were previously extracted in appendix E of ref. [20]. Some (A3,B3,C1,C2) were extracted analytically, but the derivation was only shown for the case A3. Other $\pi$ terms (A2,B1) were determined by numerics. (See in particular table 1 of ref. [20], where bolded entries indicate an analytic derivation.) With the formulas for the power-law divergences then in hand, one may subtract all of (5.1) except for the $i\Omega_0 \pi \times \text{?}_{pq}$ from the generic-$y$ numerical result for each diagram, and then numerically determine that remaining $i\Omega_0 \pi \times \text{?}_{pq}$ term for small $y$. (We went down to $y \sim 10^{-10}$ for these numerical extractions, which requires using very-high precision arithmetic.)

$$\text{B3} = \text{A3}|_{x \to 1-x}$$
$$\text{C1} = \text{bkEnd}[\text{frEnd}(\text{A3})]^*$$
$$\text{C2} = \text{C1}|_{x \to 1-x}$$
$$\text{A2} = \text{B1}|_{x \to 1-x}$$

**Table 2**. A sequence of relations to relate other $p{\neq}q$ ABC diagrams to A3 and B1.
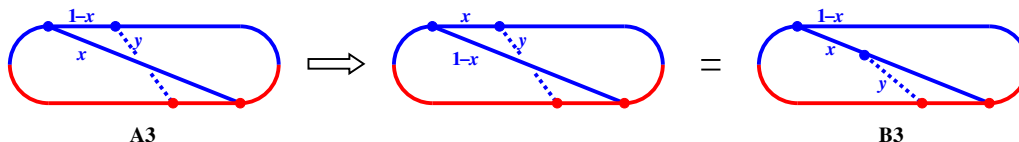


**Figure 17**. Obtaining the B3 diagram from the A3 diagram by $x \to 1-x$.

Most of the $p{\neq}q$ ABC diagrams are related to each other (even for $y$ not small) through combinations of front- and back-end transformations and/or changing $x \to 1-x$. These relations are shown in table 2. They provide another way to understand the symmetry of (5.1) and could in principle be used to analytically derive most of the $i\pi$ terms if one were willing to carefully repeat the extraction of the small-$y$ limit of A3 in a way consistent with front-end transformation, keeping track of all the relevant phases and branch cuts.

The simplest relations are the $x \to 1-x$ relations in the table. Consider B3 as an example. If one changes $x \to 1-x$ in the A3 diagram, the result is just a different way of drawing the B3 diagram, as shown in figure 17. This permutes $(\mathfrak{x}_1, \mathfrak{x}_2, \mathfrak{x}_3) \equiv (1-x, x, -1)$ to $(\mathfrak{x}_2, \mathfrak{x}_1, \mathfrak{x}_3)$, which exactly matches (2.11a) for the cases of A3 and B3.

A more subtle example is the C1 diagram. This can be obtained from A3 by doing both a front-end and back-end transformation and also complex conjugation (which exchanges blue and red), as shown in figure 18. [The complex conjugation isn't important since the results we quote in (2.11a) take $2\,\text{Re}(\cdots)$ of the diagrams shown, in order to include the complex conjugate diagrams.] Here we are front-end transforming the $x$ emission vertex, unlike the front-end transformation of the $y$ vertex discussed in the context of (3.3). The corresponding transformation is [20]

$$(x, y, E) \longrightarrow \left( \frac{-x}{1-x}, \frac{y}{1-x}, (1-x)\, E \right). \tag{5.2}$$

This takes longitudinal momenta

$$((1{-}x)E, xE, -E) \to \left( E, -xE, -(1{-}x)E \right) \tag{5.3}$$

and so, up to signs, corresponds to a permutation of the momenta of the underlying, hard $g{\to}gg$ process. This is how, in this way of looking at things, the symmetry (except for $i\pi$ terms) of (2.11a) comes about.

One could relate *all* of the ABC diagrams using such transformations if it were possible to add to table 2 a rule for B1 in terms of any other $p{\neq}q$ ABC diagram. Just looking at the momentum fractions of lines in the relevant diagrams, it's possible that something
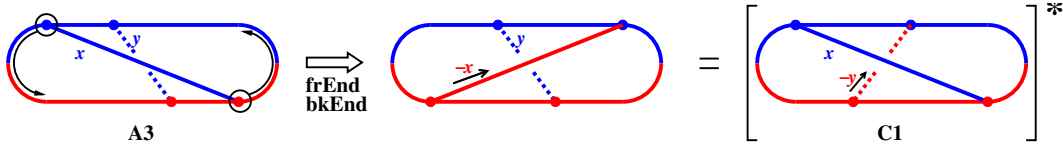
**Figure 18**. Obtaining the C1 diagram from the A3 diagram by front- and back-end transformation and complex conjugation.

like $B1 = \mathrm{bkEnd}[\mathrm{frEnd}(B3)]|^*_{y\to -y}$ might work. But we have not made any study of the validity of this type of transformation (which includes the extra step $y \to -y$); so we leave it aside.

# 6 The A1 diagram

## 6.1 Scales and form

Analyzing the $y\to 0$ expansion of the A1 diagram, which involves a gluon self-energy loop in the amplitude, has both similarities and differences with the previous analysis of the A3 diagram.

One difference is that there is nothing special about the scale $\Delta t \sim y$. Instead, we return to the decomposition

$$\mathrm{diagram}(x,y) = \lim_{a\to 0}\left[\int_0^a d(\Delta t)\, f(x,y,\Delta t) + \int_a^\infty d(\Delta t)\, f(x,y,\Delta t)\right] \qquad (6.1)$$

of (4.3), where the $\Delta t$ integral is split into just a regularized UV contribution ($\Delta t < a$) and everything else. The only interesting physics scale for this diagram is $\Delta t \sim t_{\mathrm{form}}(y)$, which in our parlance is $t \sim y^{1/2}$.

The other difference is that the generic-$y$ formula for the A1 diagram [20], calculated in the large-$N_c$ limit, has contributions from *two* different large-$N_c$ color routings, depicted in figure 19.[31] This is in contrast to the A3 diagram (figure 20), which has only one possible large-$N_c$ color routing.

The sum of the two color routings is written in the generic-$y$ formulation of ref. [20] as

$$2\,\mathrm{Re}\left[\frac{d\Gamma}{dx\,dy}\right]_{xyy\bar{x}} = \tfrac{1}{2}\big[A_{\mathrm{new}}(x,y) + A_{\mathrm{new}}(x,z)\big], \qquad (6.2)$$

where the explicit factor of $\frac{1}{2}$ represents the symmetry factor for the amplitude loop of the A1 diagram (the blue gluon self-energy loop in figure 19). Eq. (6.2) is the appropriate normalization if one intends to integrate over *all* values of the loop momentum fraction $y$, which for the A1 diagram would be $\int_0^{1-x} dy$. However, in our discussion, we have used the letter $y$ to always represent the *softest* gluon. So, we should instead think of the loop integral as running only over *half* the values, as $\int_0^{(1-x)/2} dy$ [with only $y\to 0$ now corresponding to a virtual gluon becoming soft], and so we compensate by normalizing our "differential rate"

---

[31]For a brief discussion of specifics concerning the A1 diagram $xyy\bar{x}$, see appendix D.4 of ref. [20].
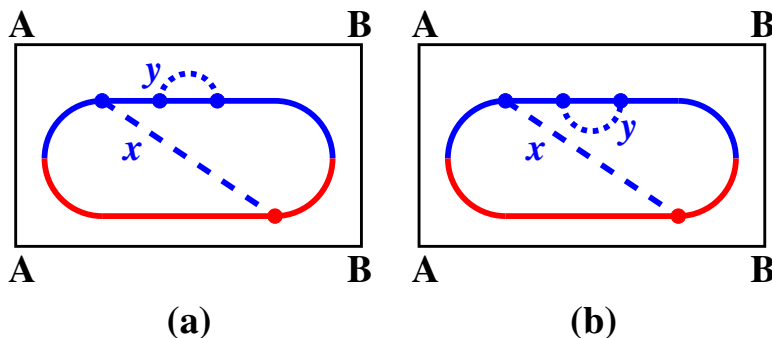
**Figure 19**. The two large-$N_c$ color routings of the A1 diagram, analogous to the treatment of the $xy\bar{x}\bar{y}$ diagram in section 2.2.1 of ref. [15]. Here we imagine drawing our time-ordered large-$N_c$ diagrams on a cylinder, as in ref. [15]: the top edge AB of the each rectangle should be identified with the bottom edge AB. In the large-$N_c$ limit, medium interactions (not drawn) are correlated between each pair of high-energy particle lines that are neighbors as one circles the cylinder.
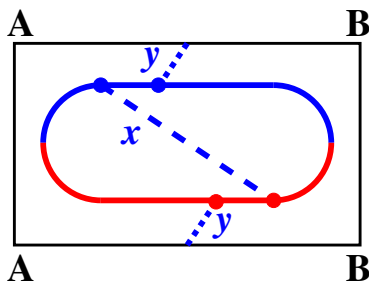


**Figure 20**. The A3 diagram drawn on a cylinder, as in section 4.3 of ref. [14].

in this paper as

$$\left[\frac{d\Gamma}{dx\,dy}\right]_{\mathrm{A1}} \equiv 2\,\mathrm{Re}\left[\frac{d\Gamma}{dx\,dy}\right]_{xyy\bar{x}} \equiv A_{\mathrm{new}}(x,y) + A_{\mathrm{new}}(x,z) \tag{6.3}$$

instead of (6.2).

In what follows, we will first focus on color routing (a) of figure 19 and the calculation of the small-$y$ limit of $A_{\mathrm{new}}(x,y)$. We'll later write the answer in a general form that will allow us to obtain the small-$y$ limit of the other color routing $A_{\mathrm{new}}(x,z) = A_{\mathrm{new}}(x,1{-}x{-}y)$ by a permutation symmetry.

Following the treatment in [18, 20], we will *not* use the trick of subtracting out the vacuum piece for the A1 diagram.[32] The analog of the A3 diagram's (4.6) then has the form

$$A_{\mathrm{new}}(x,y) = \int_0^\infty d(\Delta t)\, 2\,\mathrm{Re}\,\widetilde{D}_{\mathrm{new}}(-1,y,z,x,\bar{\alpha},\bar{\beta},\bar{\gamma},\Delta t), \tag{6.4}$$

---

[32]Similar to the discussion in footnote 27, the total vacuum piece for single splitting $g{\to}gg$ must vanish, in the context of this calculation. That doesn't necessarily mean that the vacuum piece need vanish for each, individual *time-ordered* diagram, such as A1, that contributes to $g{\to}gg$. But it does vanish, even for individual diagrams, in dimensional regularization, since there is then no scale in vacuum that can make up the dimensions of the answer. So there is no harm in subtracting vacuum pieces for some diagrams and not for others, as convenient, provided one also calculates the "pole terms" (from the integral over $\Delta t < a$) correspondingly.

which should be split up, following (6.1), into pieces

$$A_{\text{new}}(x,y) = A_{\text{new}}^{(\Delta t < a)}(x,y) + \int_a^\infty d(\Delta t)\, 2\,\text{Re}\,\widetilde{D}_{\text{new}}(-1,y,z,x,\bar{\alpha},\bar{\beta},\bar{\gamma},\Delta t).\qquad(6.5)$$

The formulas for the relevant combinations $(\bar{\alpha},\bar{\beta},\bar{\gamma})$ of helicity-dependent DGLAP splitting functions are given in appendix A of ref. [20]. In the small-$y$ limit, $\bar{\alpha}$ dominates over $\bar{\beta}$ and $\bar{\gamma}$ with

$$\bar{\alpha} = \frac{2\,P(x)}{C_{\text{A}}x^2(1-x)^4 y^3}\left[1 + O(y)\right],\qquad(6.6)$$

analogous to the case of (4.8) for the A3 diagram.

There is one modification of our $\widetilde{D}_{\text{new}}$ here compared to the $D_{\text{new}}$ of ref. [20]. Unlike refs. [18, 20], we will be doing the integral in the last term of (6.1) analytically rather than numerically, and so we will not have to make additional subtractions to that integral to make it better behaved for numerical integration. This means leaving out what were called "$\mathcal{D}_2$" subtractions that were implemented in refs. [18, 20].[33] Leaving out those additional subtractions will slightly simplify the small-$y$ analysis that we want to do here.

## 6.2 $\Delta t \sim \sqrt{y}$ contribution to A1 routing (a)

We first need an expansion in $\Delta t \sim \sqrt{y}$ for the $\Delta t$-integrand, similar to (4.24). Details are given in appendix D.1, with result, now for the A1 diagram,

$$\widetilde{D}_{\text{new}} \simeq \frac{C_{\text{A}}\alpha_{\text{s}}^2 P(x)}{4\pi^2 y}\left(\Omega_y \csc_y\right)^2\left[\ln S_{\text{new}} - \frac{\xi\Omega_y}{4i\Omega_0}\frac{(\csc_y - \cot_y)^2}{\csc_y}\right],\qquad(6.7)$$

where

$$S_{\text{new}} \simeq 2i\Omega_0\,\Delta t + (2+3s)(\Omega_0\,\Delta t)^2 + \xi\Omega_y(-\csc_y + \cot_y)\Delta t.\qquad(6.8)$$

The only difference between $S_{\text{new}}$ above and the $S$ of (4.25) is the minus sign on $\csc_y$ in the last term. $s$ is the same as in (4.10). $\xi$ is also the same, but its leading-order expression $\xi \simeq xy/2(1-x)$ will be adequate in the current context.

Expanding $\ln S_{\text{new}}$ in $y$, switching integration variables to the $\tilde{\tau}$ of (4.30), and again using (4.31), the $[a,\infty]$ integral of (6.1) is

$$\int_a^\infty d(\Delta t)\, 2\,\text{Re}\,\widetilde{D}_{\text{new}}(\Delta t) \simeq$$
$$\frac{C_{\text{A}}\alpha_{\text{s}}^2 P(x)}{2\pi^2 y}\,\text{Re}\int_{\tilde{\tau}_a}^\infty d\tilde{\tau}\left\{i\Omega_y\left[\frac{1}{\text{sh}^2\tilde{\tau}}\ln\left(\frac{2\Omega_0\tilde{\tau}}{\Omega_y}\right)\right] - i\Omega_0\left[\frac{(1+\frac{3}{2}s)\tilde{\tau}}{\text{sh}^2\tilde{\tau}} + \frac{\frac{3}{2}s(1-\text{ch}\,\tilde{\tau})(3-\text{ch}\,\tilde{\tau})}{\text{sh}^3\tilde{\tau}}\right]\right\},$$
$$(6.9)$$

---

[33]The $\mathcal{D}_2$ subtractions are explained in section 4.3.2 of ref. [18] and appendix D of ref. [20]. Our omission of them corresponds to leaving out the last term in eq. (A.64) of ref. [20] and modifying pole terms accordingly. In particular, our $A_{\text{new}}^{(\Delta t < a)}$ in (6.5) above is a modified version of the $A_{\text{new}}^{\text{pole}}$ in eqs. (A.62) and (A.66) of ref. [20], so that $A_{\text{new}}(x,y)$ will remain the same.

where $\tilde{\tau}_a = i\Omega_y a$ is arbitrarily small. Performing the integration as in section 4.4, again using (4.33) and (4.34),

$$\int_a^\infty d(\Delta t)\, 2\,\mathrm{Re}\,\widetilde{D}_{\mathrm{new}} \simeq \frac{C_A \alpha_s^2 P(x)}{2\pi^2 y}\,\mathrm{Re}\left[\frac{\ln(2i\Omega_0 a)+1}{a} + i\Omega_y\left\{-\ln\left(\frac{2\pi\Omega_0}{\Omega_y}\right)+\gamma_E\right\}\right.$$
$$\left. + i\Omega_0\left\{\ln(i\Omega_0 a)+\ln\left(\frac{2\Omega_y}{\Omega_0}\right)-1+3s(\ln 2-1)\right\}\right],$$
(6.10)

ignoring corrections that vanish as $a \to 0$.

### 6.3 UV piece and total A1 routing (a)

The dimensionally-regulated contribution corresponding to the $A_{\mathrm{new}}^{(\Delta t < a)}$ term in (6.5) can be assembled from formulas in refs. [18, 20]. In appendix D.2, we discuss the generic-$y$ formula and then expand in $y$. The result is

$$A_{\mathrm{new}}^{(\Delta t < a)} \simeq \frac{C_A \alpha_s^2 P(x)}{2\pi^2 y}\,\mathrm{Re}\left[-\frac{\ln(2i\Omega_0 a)+1}{a} + i\Omega_0\left\{-2\left(\frac{1}{\epsilon}+\ln\left(\frac{\pi\mu^2}{E\Omega_0}\right)\right)+\ln(xy(1-x))\right.\right.$$
$$\left.\left. - \ln(i\Omega_0 a) - \ln 2 + 1\right\}\right]. \quad (6.11)$$

Adding this to (6.10), the dependence on the UV separation scale $a$ cancels, as it must. We are left with

$$A_{\mathrm{new}}(x,y) \simeq \frac{C_A \alpha_s^2 P(x)}{2\pi^2 y}\,\mathrm{Re}\left[i\Omega_y\left\{\ln\left(\frac{\Omega_y}{2\pi\Omega_0}\right)+\gamma_E\right\}\right. \qquad (6.12)$$
$$\left. + i\Omega_0\left\{-2\left(\frac{1}{\epsilon}+\ln\left(\frac{\pi\mu^2}{E\Omega_0}\right)\right)+\ln(xy(1-x))+\ln\left(\frac{\Omega_y}{\Omega_0}\right)+3s(\ln 2-1)\right\}\right].$$

### 6.4 The other color routing

Using the longitudinal momentum fractions $(\mathfrak{x}_1,\mathfrak{x}_2,\mathfrak{x}_3) \equiv (1-x, x, -1)$ of the underlying hard single-splitting process, we can algebraically manipulate (6.12) into a form similar to (2.11b):

$$A_{\mathrm{new}}(x,y) \simeq -\frac{C_A \alpha_s^2 P(x)}{2\pi^2 y}\,\mathrm{Re}\left[i\Omega_y\left\{-\ln\left(\frac{\Omega_y}{2\pi\Omega_0}\right)-\gamma_E\right\}\right.$$
$$\left. + i\Omega_0\left\{2\left[\frac{1}{\epsilon}+\ln\left(\frac{\pi\mu^2}{\Omega_0 E}\right)\right]-\ln\left(\frac{|\mathfrak{x}_1\mathfrak{x}_2\mathfrak{x}_3|y\Omega_y}{\Omega_0}\right)+\frac{\mathfrak{x}_2^2}{2(\mathfrak{x}_1^2+\mathfrak{x}_2^2+\mathfrak{x}_3^2)}(1-\ln 2)\right\}\right]. \quad (6.13)$$

Now note that in the color routing for this result, figure 19(a), the soft $y$ gluon's neighbors going around the cylinder are $\mathfrak{x}_1 = 1-x$ (the line that the $y$ gluon leaves and reconnects to) and $\mathfrak{x}_3 = -1$. And note that the $(\mathfrak{x}_1,\mathfrak{x}_2,\mathfrak{x}_3)$ appear symmetrically in (6.13) *except* for the $\mathfrak{x}_2^2$ factor in the last term.

Compare that to the other color routing, figure 19(b), which corresponds to the $A_{\text{new}}(x,z)$ in (6.3). Now the soft $y$ gluon's neighbors going around the cylinder are $\mathfrak{r}_1 = 1-x$ (the line that the $y$ gluon leaves and reconnects to) and $\mathfrak{r}_2 = x$. So we may expect that the result is the same as (6.13) except with that $\mathfrak{r}_2^2$ factor replaced by $\mathfrak{r}_3^2$:

$$A_{\text{new}}(x,z) \simeq -\frac{C_A \alpha_s^2 P(x)}{2\pi^2 y} \operatorname{Re}\left[ i\Omega_y \left\{ -\ln\left(\frac{\Omega_y}{2\pi\Omega_0}\right) - \gamma_E \right\} \right.$$
$$\left. + i\Omega_0 \left\{ 2\left[\frac{1}{\epsilon} + \ln\left(\frac{\pi\mu^2}{\Omega_0 E}\right)\right] - \ln\left(\frac{|\mathfrak{r}_1\mathfrak{r}_2\mathfrak{r}_3|y\Omega_y}{\Omega_0}\right) + \frac{\mathfrak{r}_3^2}{2(\mathfrak{r}_1^2+\mathfrak{r}_2^2+\mathfrak{r}_3^2)}(1 - \ln 2) \right\} \right]. \quad (6.14)$$

We have checked (both analytically and numerically) that this is correct.

Adding together the two color routings (6.13) and (6.14) as in (6.3) gives our final result for the small-$y$ limit of the A1 diagram, which is the $p{=}1$ case of (2.11b).

# 7   Other $p{=}q$ ABC diagrams

The B2 diagram is simply the A1 diagram with $x \to 1-x$, and so corresponds to the $p{=}2$ case of (2.11b). The C3 diagram can be related to the A1 diagram by front- and back-end transformation:

$$\text{C3} = \text{bkEnd}[\text{frEnd}(\text{A1})]^*, \quad (7.1)$$

and the front-end transformations may introduce $i\pi$ terms, as previously discussed in section 5. Again, rather than carefully keep track of all the branch cuts necessary to implement front-end transformations in our small-$y$ expansions, we have determined the $i\pi$ terms by generalizing the A1 result to

$$\left[\frac{d\Gamma}{dx\,dy}\right]_{pp} \simeq -2 \times \frac{C_A \alpha_s^2 P(x)}{2\pi^2 y} \operatorname{Re}\left[ i\Omega_y \left\{ -\ln\left(\frac{\Omega_y}{2\pi\Omega_0}\right) - \gamma_E + \pi \times \textbf{?}_{pp} \right\} \right.$$
$$+ i\Omega_0 \left\{ 2\left[\frac{1}{\epsilon} + \ln\left(\frac{\pi\mu^2}{\Omega_0 E}\right)\right] - \left[\ln\left(\frac{|\mathfrak{r}_1\mathfrak{r}_2\mathfrak{r}_3|y\Omega_y}{\Omega_0}\right) + \pi \times \textbf{?}_{pp}\right] \right.$$
$$\left. \left. + \frac{\mathfrak{r}_q^2+\mathfrak{r}_r^2}{4(\mathfrak{r}_1^2+\mathfrak{r}_2^2+\mathfrak{r}_3^2)}(1 - \ln 2) \right\} \right] \quad (7.2)$$

and then using numerical extraction of the $y{\to}0$ limit from the generic-$y$ formulas of ref. [20] to determine the question marks. Our final result is (2.11b).

# 8   Conclusion

Our results were already summarized earlier in sections 1 and 2.2. Our primary result is the expression (1.8) for the sub-leading, single IR logarithm arising from soft radiative corrections to an underlying, hard, gluon splitting process $g{\to}gg$. We remind readers that this result was calculated for an idealized situation, with many caveats described in sections 1.1 and 1.2, not least of which was the assumption that the size of the medium is large compared to relevant formation times.

## Acknowledgments

## A Correction to treatment of front-end virtual sequential diagrams in ref. [20]

In this appendix, we fix an error concerning $i\pi$ terms in the result for the pole piece $\mathcal{A}_{\text{seq}}^{\text{pole}}(x,y)$ of sequential diagrams in the original published version of eq. (A.37) of ref. [20]. The problem only manifests when one front-end transforms the $g{\to}ggg$ sequential diagrams to get results for front-end virtual sequential diagrams, as in eq. (A.60) of ref. [20]. The problem has to do with getting signs and phases correct, which we never presented an explicit derivation of in ref. [20]. Here, we go through the derivation.

The sequential diagrams are given by the bottom row of figure 8 (plus their complex conjugates), and $\mathcal{A}_{\text{seq}}(x,y)$ represents one particular color-routing of those diagrams, as described in ref. [15]. The pole piece of those diagrams was computed in ref. [16], where the possibility of front-end transformations was not considered.

In the process of generalizing ref. [16] to (now correctly) handle signs and phases for front-end transformations, we will *also* incorporate some inconsequential corrections [18] to the formulas in the original published version of ref. [16], with explanation of those particular corrections left to footnotes. The footnoted corrections are inconsequential because they mildly affect intermediate equations but not the final result for $\mathcal{A}_{\text{seq}}^{\text{pole}}(x,y)$.

The total pole piece $\mathcal{A}_{\text{seq}}^{\text{pole}}(x,y)$ is finite, but intermediate steps are carried out, following ref. [16], with the aid of dimensional regularization with $d \equiv d_\perp = 2-\epsilon$ transverse spatial dimensions.

### A.1 $xy\bar{x}\bar{y}$ diagram

A formula for one of the color routings (called $xy\bar{x}\bar{y}_2$) of the $xy\bar{x}\bar{y}$ diagram shown in figure 8 was given in eq. (5.14) of ref. [16] as[34]

$$\left[\frac{d\Gamma}{dx\,dy}\right]_{xy\bar{x}\bar{y}_2} \simeq \left(\frac{\mu}{E}\right)^{2\epsilon} \frac{C_A^2 \alpha_s^2 M_i M_f^{\text{seq}}}{2^{\frac{d}{2}+2} d\pi^d E^d} \frac{\Gamma^2(\frac{d+2}{4})}{\Gamma(\frac{d}{2})\sin(\frac{\pi d}{4})} \left(i\hat{x}_1\hat{x}_2\hat{x}_3\hat{x}_4\Omega_i\,\text{sgn}\,M_i\right)^{d/2}$$

$$\times (d\bar{\alpha} + \bar{\beta} + \bar{\gamma})\int \frac{d(\Delta t)}{(\Delta t)^{d/2}} + \{i \leftrightarrow f^{\text{seq}}\}, \tag{A.1}$$

where, for example, $M_i \equiv M_{E,x} \equiv x(1-x)E$ and $M_f^{\text{seq}} = yz(1-x)E$. Both of these $M$'s are positive for the $xy\bar{x}\bar{y}$ diagram, and so the $\text{sgn}\,M$ factors in (A.1) were replaced by $+1$ in the rest of the discussion of $xy\bar{x}\bar{y}$ in ref. [16]. However, front-end transformations can

---

[34]Eq. (A.1) has one of our ultimately-inconsequential corrections: the inclusion of the overall factor $(\mu/E)^{2\epsilon}$, where $\mu$ is the renormalization scale, as discussed in ref. [18]. See in particular the discussion surrounding eq. (F.31) of ref. [18].

negate $M_i$ and so, in the application to virtual diagrams, we need to keep those factors of $\operatorname{sgn} M$.[35] Following through the subsequent development, and using[36]

$$\bar{\alpha} + \tfrac{1}{d}\bar{\beta} + \tfrac{1}{d}\bar{\gamma} = \frac{P(x)}{C_A x^2 (1-x)^2} \, \frac{P(\frac{y}{1-x})}{C_A (1-x) y^2 (1-x-y)^2} \,, \tag{A.2}$$

eq. (5.18) of ref. [16] then generalizes to

$$2 \operatorname{Re}\left[\frac{d\Gamma}{dx\,dy}\right]_{xy\bar{x}\bar{y}}^{(\Delta t < a)} \simeq \frac{\alpha_s^2 \mu^{2\epsilon} P(x) P(\mathfrak{y})}{4\pi^2 (1-x)} \, \frac{d}{2} \, \mathrm{B}(\tfrac{1}{2}+\tfrac{d}{4}, -\tfrac{d}{4}) \left(\int_0^a \frac{d(\Delta t)}{(\Delta t)^{d/2}}\right)$$

$$\times \operatorname{Re}\left[\left(\frac{M_{(1-x)E,\mathfrak{y}}}{2\pi i} \, \frac{(|M|\Omega)_{E,x}}{2\pi}\right)^{\frac{d}{2}-1} i(\Omega \operatorname{sgn} M)_{E,x}\right.$$

$$\left. + \left(\frac{M_{E,x}}{2\pi i} \, \frac{(|M|\Omega)_{(1-x)E,\mathfrak{y}}}{2\pi}\right)^{\frac{d}{2}-1} i(\Omega \operatorname{sgn} M)_{(1-x)E,\mathfrak{y}}\right], \tag{A.3}$$

where $\mathfrak{y} \equiv y/(1-x)$. For front-end transformations, the important distinction here relative to ref. [16] is the appearance of $\operatorname{sgn} M$ factors above in $\Omega \operatorname{sgn} M$ and $|M|\Omega = M\Omega \operatorname{sgn} M$.

## A.2 $x\bar{x}y\bar{y} + x\bar{x}\bar{y}y$ diagrams

Eq. (5.1) of ref. [16] analyzed the pole piece of the last two diagrams of figure 8 (plus their complex conjugates) and found the corresponding rate

$$\left[\Delta \frac{d\Gamma}{dx\,dy}\right]_{\substack{x\bar{x}y\bar{y}+x\bar{x}\bar{y}y \\ +\bar{x}x\bar{y}y+\bar{x}xy\bar{y}}} = -\frac{1}{1-x} \int_0^\infty d(\Delta t_x) \int_0^\infty d(\Delta t_y) \, \tfrac{1}{2}(\Delta t_x + \Delta t_y)$$

$$\times \operatorname{Re}\left[\frac{d\Gamma}{dx\,d(\Delta t_x)}\right]_{E,x} \operatorname{Re}\left[\frac{d\Gamma}{d\mathfrak{y}\,d(\Delta t_y)}\right]_{(1-x)E,\mathfrak{y}}, \tag{A.4}$$

where[37]

$$\left[\frac{d\Gamma}{dx\,d(\Delta t)}\right]_{E,x} \equiv \left(\frac{\mu}{E}\right)^\epsilon \frac{\alpha_s P(x)}{x^2 (1-x)^2 E^d} \boldsymbol{\nabla}_{\boldsymbol{B}^{\bar{\mathrm{x}}}} \cdot \boldsymbol{\nabla}_{\boldsymbol{B}^{\mathrm{x}}} \langle \boldsymbol{B}^{\bar{\mathrm{x}}}, \Delta t | \boldsymbol{B}^{\mathrm{x}}, 0\rangle_{E,x}\Big|_{\boldsymbol{B}^{\bar{\mathrm{x}}}=\boldsymbol{B}^{\mathrm{x}}=0}$$

$$= -\left(\frac{\mu}{E}\right)^\epsilon \frac{\alpha_s P(x)}{x^2 (1-x)^2 E^d} \left(\frac{M\Omega \csc(\Omega \Delta t)}{2\pi i}\right)^{d/2} i d M\Omega \csc(\Omega \Delta t) \tag{A.5}$$

and the last equality comes from ref. [16] eqs. (3.4–3.5). The formulas for $M$'s and $\Omega$'s are such that the phase of $\Omega$ is $e^{-i\pi/4}$ when $M > 0$ and $e^{+i\pi/4}$ when $M < 0$. Given this, the results for one type of integral we need is

$$\frac{d\Gamma}{dx} = \operatorname{Re}\int_0^\infty d(\Delta t) \left[\frac{d\Gamma}{dx\,d(\Delta t)}\right]_{E,x}$$

$$= \operatorname{Re}\left[-\left(\frac{\mu}{E}\right)^\epsilon \frac{\alpha_s P(x)}{x^2 (1-x)^2 E^d} \frac{i d M}{2} \left(\frac{|M|\Omega}{2\pi}\right)^{d/2} \mathrm{B}(\tfrac{1}{2}+\tfrac{d}{4}, -\tfrac{d}{4})\right], \tag{A.6}$$

---

[35] We must also use appropriate absolute value signs in the formulas for the DGLAP splitting functions $P(x)$ and DGLAP combinations $(\bar{\alpha}, \bar{\beta}, \bar{\gamma})$, as in ref. [20] eqs. (A.5) and (A.46).

[36] Eq. (A.2) is the corrected version of ref. [16] (5.17). See ref. [20] (C.11) and the related discussion of ref. [18] (F.32). This completes our starting points for the "inconsequential corrections" which do not affect the original result of ref. [16] for $\mathcal{A}_{\mathrm{seq}}^{\mathrm{pole}}$.

[37] Eq. (A.5) is also updated along the same lines as footnote 34.

which generalizes ref. [16] eq. (5.4). The other type of integral we need, specifically for the integral over $0 < \Delta t < a$, is the same as ref. [16] eq. (5.5b):

$$\operatorname{Re} \int_0^a d(\Delta t)\, \Delta t \left[\frac{d\Gamma}{dx\, d(\Delta t)}\right]_{E,x} = -\left(\frac{\mu}{E}\right)^\epsilon \frac{d\alpha_{\rm s} P(x)}{2\pi E^{d-2}} \operatorname{Re}\left[\left(\frac{M}{2\pi i}\right)^{\frac{d}{2}-1} \int_0^a \frac{d(\Delta t)}{(\Delta t)^{d/2}}\right], \quad \text{(A.7)}$$

where $a$ is a tiny cut-off used to isolate the UV-divergent pole terms. Combining (A.4), (A.6), and (A.7) gives the following generalization of ref. [16] eq. (5.6):

$$\begin{aligned}
\left[\Delta \frac{d\Gamma}{dx\, dy}\right]_{\substack{x\bar{x}y\bar{y}+x\bar{x}\bar{y}y \\ +\bar{x}xy\bar{y}+\bar{x}xy\bar{y}}}^{(\Delta t<a)} = &-\frac{\alpha_{\rm s}^2 \mu^{2\epsilon} P(x)\, P(\mathfrak{y})}{4\pi^2(1-x)} \left(\frac{d}{2}\right)^2 {\rm B}(\tfrac{1}{2}+\tfrac{d}{4}, -\tfrac{d}{4}) \left(\int_0^a \frac{d(\Delta t)}{(\Delta t)^{d/2}}\right) \\
&\times \left\{ \operatorname{Re}\left[\left(\frac{M}{2\pi i}\right)^{\frac{d}{2}-1}\right]_{(1-x)E,\mathfrak{y}} \operatorname{Re}\left[\left(\frac{|M|\Omega}{2\pi}\right)^{\frac{d}{2}-1} i\Omega\, {\rm sgn}\, M\right]_{E,x} \right. \\
&\left. + \operatorname{Re}\left[\left(\frac{M}{2\pi i}\right)^{\frac{d}{2}-1}\right]_{E,x} \operatorname{Re}\left[\left(\frac{|M|\Omega}{2\pi}\right)^{\frac{d}{2}-1} i\Omega\, {\rm sgn}\, M\right]_{(1-x)E,\mathfrak{y}} \right\}.
\end{aligned}$$
(A.8)

## A.3  Total

Adding together (A.3) and (A.8) gives

$$\begin{aligned}
2\operatorname{Re}\left[\Delta \frac{d\Gamma}{dx\, dy}\right]_{x\bar{x}y\bar{y}+x\bar{x}\bar{y}y+xy\bar{x}\bar{y}}^{(\Delta t<a)} \simeq &\frac{\alpha_{\rm s}^2 \mu^{2\epsilon} P(x)\, P(\mathfrak{y})}{4\pi^2(1-x)} \left(\frac{d}{2}\right)^2 {\rm B}(\tfrac{1}{2}+\tfrac{d}{4}, -\tfrac{d}{4}) \int_0^a \frac{d(\Delta t)}{(\Delta t)^{d/2}} \\
&\times \left[\mathcal{Q} + \{E, x \leftrightarrow (1-x)E, \mathfrak{y}\}\right],
\end{aligned}$$
(A.9a)

where

$$\begin{aligned}
\mathcal{Q} \equiv &\frac{2}{d} \operatorname{Re}\left[\left(\frac{M_{(1-x)E,\mathfrak{y}}}{2\pi i} \frac{(|M|\Omega)_{E,x}}{2\pi}\right)^{\frac{d}{2}-1} i(\Omega\, {\rm sgn}\, M)_{E,x}\right] \\
&- \operatorname{Re}\left[\left(\frac{M}{2\pi i}\right)^{\frac{d}{2}-1}\right]_{(1-x)E,\mathfrak{y}} \operatorname{Re}\left[\left(\frac{|M|\Omega}{2\pi}\right)^{\frac{d}{2}-1} i\Omega\, {\rm sgn}\, M\right]_{E,x}.
\end{aligned}$$
(A.9b)

$\mathcal{Q}$ vanishes for $d=2$, and so $\mathcal{Q} = O(\epsilon)$. This means that we only need to keep the $O(1/\epsilon)$ piece of the prefactors in (A.9a):

$$2\operatorname{Re}\left[\Delta \frac{d\Gamma}{dx\, dy}\right]_{x\bar{x}y\bar{y}+x\bar{x}\bar{y}y+xy\bar{x}\bar{y}}^{(\Delta t<a)} = -\frac{\alpha_{\rm s}^2 P(x)\, P(\mathfrak{y})}{\pi^2(1-x)\epsilon}\left[\mathcal{Q} + \{E, x \leftrightarrow (1-x)E, \mathfrak{y}\}\right]. \quad \text{(A.10)}$$

Expanding (A.9b) to first order in $\epsilon$ gives

$$\begin{aligned}
\mathcal{Q} &= \frac{\epsilon}{2}\left\{\operatorname{Re}[i(\Omega\, {\rm sgn}\, M)_{E,x}] - \operatorname{Re}\left[i(\Omega\, {\rm sgn}\, M)_{E,x} \ln\left(\frac{{\rm sgn}\, M_{(1-x)E,\mathfrak{y}}}{i}\right)\right]\right\} \\
&= \frac{\epsilon}{2}\left\{\operatorname{Re}[i(\Omega\, {\rm sgn}\, M)_{E,x}] - \frac{\pi}{2}\operatorname{Re}[(\Omega\, {\rm sgn}\, M)_{E,x}]\, {\rm sgn}\, M_{(1-x)E,\mathfrak{y}}\right\}.
\end{aligned}$$
(A.11)

Using (A.11) in (A.10) gives our generalization of ref. [16] eq. (5.20). $\mathcal{A}_{\text{seq}}^{\text{pole}}$ is half of the above. Our generalization of ref. [16] eq. (7.4), and correspondingly our correction to ref. [20] eq. (A.37), is then

$$\mathcal{A}_{\text{seq}}^{\text{pole}} = -\frac{\alpha_s^2 \, P(x) \, P(\mathfrak{y})}{4\pi^2(1-x)} \operatorname{Re}\Big[i(\Omega \operatorname{sgn} M)_{E,x}(1 + \tfrac{i\pi}{2} \operatorname{sgn} M_{(1-x)E,\mathfrak{y}})$$
$$+ i(\Omega \operatorname{sgn} M)_{(1-x)E,\mathfrak{y}}(1 + \tfrac{i\pi}{2} \operatorname{sgn} M_{E,x})\Big]. \quad \text{(A.12)}$$

This correction is responsible for the $4\pi$ shift of figure 5 of this paper relative to figure 20 of ref. [20].

We note in passing that, because the complex phase of $\Omega$ is $e^{-(i\pi/4)\operatorname{sgn} M}$,

$$\operatorname{Re}(\Omega) = \operatorname{Re}(i\Omega \operatorname{sgn} M). \quad \text{(A.13)}$$

Using this, (A.13) may also be written in the alternate form

$$\mathcal{A}_{\text{seq}}^{\text{pole}} = -\frac{\alpha_s^2 \, P(x) \, P(\mathfrak{y})}{4\pi^2(1-x)} \operatorname{Re}\big[i(\Omega \operatorname{sgn} M)_{E,x} + i(\Omega \operatorname{sgn} M)_{(1-x)E,\mathfrak{y}}\big]$$
$$\times \big(1 - \tfrac{\pi}{2} \operatorname{sgn} M_{E,x} \operatorname{sgn} M_{(1-x)E,\mathfrak{y}}\big). \quad \text{(A.14)}$$

## B  Organization of IR divergences compared to ref. [20]

In this appendix, we will refer to table 1 of this paper, which describes certain cancellations among IR single and double logarithms, as the "log table." We will refer to table 1 of ref. [20], which described cancellations among IR *power-law* divergences, as the "power-law table." The purpose of this appendix is to describe the similarities and differences of the organization of these two tables.

The power-law table gives, for example, $y{\to}0$, $x{\to}0$ and $z{\to}0$ limits of the single diagram $2\operatorname{Re}(yx\bar{x}\bar{y})$. The log table, in contrast, always refers to the softest gluon as $y$ and so instead lists the $y{\to}0$ limit of the six diagrams corresponding to the permutations of the daughters $(x,y,z)$ of $2\operatorname{Re}(yx\bar{x}\bar{y})$. The $y{\to}0$ limit of $2\operatorname{Re}(yx\bar{x}\bar{y})$ in the power-law table corresponds here to the average of the $(x,y)$ and $(z,y)$ columns in the $2\operatorname{Re}(yx\bar{x}\bar{y})$ row of our log table; the $z{\to}0$ limit in the power-law table corresponds to the average of the $(x,z)$ and $(z,x)$ columns; and the $x{\to}0$ limit corresponds to the average of the $(y,x)$ and $(y,z)$ columns. We needed half as many columns in ref. [20] because, in the language of the current paper (where $y$ is always the softest gluon), the power-law divergences of each individual diagram have a symmetry under $x \to 1{-}x$ that the log divergences do not.

For a slightly different example, consider the Class I virtual diagram $2\operatorname{Re}(yx\bar{x}y)$. Now, the $y{\to}0$ limit of the power-law table corresponds to the average of the $(x,y)$ and $(1{-}x,y)$ columns of the log table; and the $z{\to}0$ limit to the average of the $(x,z)$ and $(1{-}x,x{-}y)$ columns. For $2\operatorname{Re}(yx\bar{x}y)$, we do not list anything in the log table corresponding to the $x{\to}0$ column of the power-law table. That's because even for power-law divergences, the $x{\to}0$ behavior of virtual diagrams was not relevant to checking the cancellation of IR divergences among diagrams, for the reasons explained in ref. [20].[38]

---

[38]Specially, see section 3 and appendix E.2 of ref. [20].

As a final example, consider the Class II virtual diagram $2\,\mathrm{Re}(x\bar{y}\bar{y}x)$. Since this is a virtual diagram, the $x{\to}0$ column of the power-law table is irrelevant, as mentioned above. Because it is specifically a Class II diagram (as defined in ref. [20]), the $z{\to}0$ limit is also irrelevant because there are no IR divergences in this limit: no line of the diagram becomes soft in the limit $z{\to}0$. So only the $y{\to}0$ column of the power-law diagram is relevant, and this corresponds to the average of the $(x,y)$ and $(1{-}x,y)$ columns of the log table.

We should clarify the meaning of the double-size boxes for A1, B2, and C3 in our log table. Each of these diagrams has two large-$N_\mathrm{c}$ color orderings. Consider A1, for example. If one focuses on a particular large-$N_\mathrm{c}$ color ordering, then the $(x,y)$ and $(x,z) = (x,1{-}x{-}y)$ entries for A1 in table 1 represent different soft-gluon limits. If one instead thinks of the full A1, summing both color routings, then the two entries are the same and should not be double counted.

## C  Small-$y$ behavior of A3 diagram integrand

For the A3 diagram, the generic-$y$ formula for the $D$ of (4.7) is [14]

$$
D(x_1,x_2,x_3,x_4,\alpha,\beta,\gamma,\Delta t) = \frac{C_\mathrm{A}^2\alpha_\mathrm{s}^2 M_\mathrm{i}M_\mathrm{f}}{32\pi^4 E^2}\,(-x_1 x_2 x_3 x_4)\Omega_+\Omega_-\csc(\Omega_+\Delta t)\csc(\Omega_-\Delta t)
$$
$$
\times\Big\{(\beta Y_\mathrm{y}Y_\mathrm{\bar{y}} + \alpha\overline{Y}_\mathrm{y\bar{y}}Y_\mathrm{y\bar{y}})I_0 + (\alpha+\beta+2\gamma)Z_\mathrm{y\bar{y}}I_1
$$
$$
+ [(\alpha+\gamma)Y_\mathrm{y}Y_\mathrm{\bar{y}} + (\beta+\gamma)\overline{Y}_\mathrm{y\bar{y}}Y_\mathrm{y\bar{y}}]I_2 - (\alpha+\beta+\gamma)(\overline{Y}_\mathrm{y\bar{y}}Y_\mathrm{\bar{y}}I_3 + Y_\mathrm{y}Y_\mathrm{y\bar{y}}I_4)\Big\}. \quad \text{(C.1)}
$$

A summary containing this formula and expressions for its various elements may be found in Appendices A.2.1–A.2.2 of ref. [20]. Of those, it will be useful to have at hand

$$
I_0 = \frac{4\pi^2}{(X_\mathrm{y}X_\mathrm{\bar{y}} - X_\mathrm{y\bar{y}}^2)}\,, \qquad I_1 = -\frac{2\pi^2}{X_\mathrm{y\bar{y}}}\ln\left(\frac{X_\mathrm{y}X_\mathrm{\bar{y}} - X_\mathrm{y\bar{y}}^2}{X_\mathrm{y}X_\mathrm{\bar{y}}}\right), \qquad \text{(C.2a)}
$$

$$
I_2 = I_0 - \frac{I_1}{X_\mathrm{y\bar{y}}}\,, \qquad I_3 = \frac{X_\mathrm{y\bar{y}}I_0}{X_\mathrm{\bar{y}}}\,, \qquad I_4 = \frac{X_\mathrm{y\bar{y}}I_0}{X_\mathrm{y}} \qquad \text{(C.2b)}
$$

and

$$
\begin{pmatrix} X_\mathrm{y} & Y_\mathrm{y} \\ Y_\mathrm{y} & Z_\mathrm{y} \end{pmatrix} \equiv \begin{pmatrix} |M_0|\Omega_0 & 0 \\ 0 & 0 \end{pmatrix} - ia_\mathrm{y}^{-1\top}\begin{pmatrix} \Omega_+\cot_+ & \\ & \Omega_-\cot_- \end{pmatrix}a_\mathrm{y}^{-1}, \qquad \text{(C.3a)}
$$

$$
\begin{pmatrix} X_\mathrm{\bar{y}} & Y_\mathrm{\bar{y}} \\ Y_\mathrm{\bar{y}} & Z_\mathrm{\bar{y}} \end{pmatrix} \equiv \begin{pmatrix} |M_\mathrm{f}|\Omega_\mathrm{f} & 0 \\ 0 & 0 \end{pmatrix} - ia_\mathrm{\bar{y}}^{-1\top}\begin{pmatrix} \Omega_+\cot_+ & \\ & \Omega_-\cot_- \end{pmatrix}a_\mathrm{\bar{y}}^{-1}, \qquad \text{(C.3b)}
$$

$$
\begin{pmatrix} X_\mathrm{y\bar{y}} & Y_\mathrm{y\bar{y}} \\ \overline{Y}_\mathrm{y\bar{y}} & Z_\mathrm{y\bar{y}} \end{pmatrix} \equiv -ia_\mathrm{y}^{-1\top}\begin{pmatrix} \Omega_+\csc_+ & \\ & \Omega_-\csc_- \end{pmatrix}a_\mathrm{\bar{y}}^{-1}, \qquad \text{(C.3c)}
$$

where

$$
\csc_\pm \equiv \csc(\Omega_\pm\Delta t), \qquad \cot_\pm \equiv \cot(\Omega_\pm\Delta t). \qquad \text{(C.4)}
$$

For the A3 diagram of interest here,

$$
M_0 = x(1{-}x)E, \qquad M_\mathrm{f} = xz(1{-}y)E. \qquad \text{(C.5)}
$$

Both are positive, and so we will drop the absolute value signs in (C.3).

From other formulas in appendices A.2.1–A.2.2 of ref. [20], one may extract the small-$y$ limits for the complex frequencies associated with 4-particle evolution:

$$\Omega_+ = \Omega_y[1 + O(y)], \tag{C.6a}$$

$$\Omega_- = (1 - 3s)^{1/2}\Omega_0 + O(y), \tag{C.6b}$$

where $\Omega_0$ and $s$ were defined previously in (2.4) and (4.10). One may similarly extract small-$y$ expansions of the matrices $a_{\mathrm{y}}$ and $a_{\bar{\mathrm{y}}}$ of normal mode vectors. We need their inverses in (C.3), whose expansions we find to be

$$a_{\bar{\mathrm{y}}}^{-1} = \begin{pmatrix} -\tfrac{1}{2}xy^{1/2} & y^{1/2} \\ -x^{1/2}(1-x)^{1/2}(1+uy) & -\tfrac{1}{2}x^{1/2}(1-x)^{-1/2}y \end{pmatrix} E^{1/2} + O(y^{3/2}), \tag{C.7a}$$

$$a_{\mathrm{y}}^{-1} = \begin{pmatrix} \tfrac{1}{2}xy^{1/2} & (1-x)y^{1/2} \\ -x^{1/2}(1-x)^{1/2}(1+vy) & \tfrac{1}{2}x^{1/2}(1-x)^{1/2}y \end{pmatrix} E^{1/2} + O(y^{3/2}). \tag{C.7b}$$

Above, $u = u(x)$ and $v = v(x)$ are some functions of $x$ which we did not bother to determine. Though $u$ and $v$ will appear in some intermediate formulas, each of their effects will cancel in final results.

## C.1 $\Delta t \sim y$

For $\Delta t \sim y$, we have $\Omega_\pm \Delta t \ll 1$ and so may use small-argument expansions for all of the trig functions in (C.3). The small-$y$ expansions we will need, at the order that we will need them, are

$$X_{\mathrm{y}} = -\frac{iM_0}{\Delta t} + M_0\Omega_0 + \frac{i}{3}M_0\Omega_0^2\Delta t + O(y^2), \tag{C.8a}$$

$$X_{\bar{\mathrm{y}}} = -\frac{iM_{\mathrm{f}}}{\Delta t} + M_{\mathrm{f}}\Omega_{\mathrm{f}} + \frac{i}{3}M_0\Omega_0^2\Delta t + O(y^2). \tag{C.8b}$$

$$X_{\mathrm{y}\bar{\mathrm{y}}} = -\frac{ixzE}{\Delta t} - \frac{i}{6}M_0\Big(\Omega_0^2 + \frac{i\hat{q}_{\mathrm{A}}x^2}{4M_0}\Big)\Delta t + O(y^2), \tag{C.8c}$$

$$Y_{\mathrm{y}} = \tfrac{1}{12}x(1-x)\hat{q}_{\mathrm{A}}\,\Delta t + O(y), \tag{C.8d}$$

$$Y_{\bar{\mathrm{y}}} = -\tfrac{1}{12}x\hat{q}_{\mathrm{A}}\,\Delta t + O(y), \tag{C.8e}$$

$$Y_{\mathrm{y}\bar{\mathrm{y}}} = -\frac{ixyE}{\Delta t} + O(y), \tag{C.8f}$$

$$\overline{Y}_{\mathrm{y}\bar{\mathrm{y}}} = +\frac{ixyzE}{\Delta t} + O(y), \tag{C.8g}$$

$$Z_{\mathrm{y}\bar{\mathrm{y}}} = -\frac{iyzE}{\Delta t} - \frac{\hat{q}_{\mathrm{A}}(1-x)}{12}\Delta t + O(y^2). \tag{C.8h}$$

In general, we need the final expansion of (C.1) to next-to-leading order (NLO) in $y$, because of the (ultimately canceling) spurious $y^{-2}$ divergence described in section 4.2. That requires NLO expressions for many of the $(X, Y, Z)$'s shown above. However, for the $X$'s, we need next-to-next-to-leading (NNLO) order in (C.8) because the leading-order terms cancel in the combination $X_{\mathrm{y}}X_{\bar{\mathrm{y}}} - X_{\mathrm{y}\bar{\mathrm{y}}}^2$. We will need $X_{\mathrm{y}}X_{\bar{\mathrm{y}}} - X_{\mathrm{y}\bar{\mathrm{y}}}^2$ for the NLO evaluation of the

$2\gamma Z_{y\bar{y}}I_1 + \gamma\overline{Y}_{y\bar{y}}Y_{y\bar{y}}I_2$ terms in (C.1), which are the terms that will contribute to the spurious $y^{-2}$ divergence. The NLO expansion is

$$X_y X_{\bar{y}} - X_{y\bar{y}}^2 = -\frac{M_0 M_f}{(\Delta t)^2}\left\{\left[\frac{xy}{(1-x)(1-y)} + i(\Omega_0+\Omega_f)\Delta t\right] - \left(2\Omega_0^2 + \frac{i\hat{q}_A x^2}{12M_0}\right)(\Delta t)^2 + O(y^3)\right\}. \tag{C.9}$$

This appears in $I_1$ in the combination

$$\frac{X_y X_{\bar{y}} - X_{y\bar{y}}^2}{X_y X_{\bar{y}}} = \frac{xy}{(1-x)(1-y)}\left[(1+\tau) - (1+s)\xi\tau^2 + O(y^2)\right], \tag{C.10}$$

where $s$, $\xi$, and $\tau$ are defined as in (4.10) and behave parametrically as

$$s \sim y^0, \qquad \xi \sim y, \tag{C.11}$$

and

$$\tau \sim y^0 \quad (\text{for } \Delta t \sim y). \tag{C.12}$$

From the explicit formulas for $(\alpha, \beta, \gamma)$ give in ref. [20] eq. (A.23), parametrically

$$\gamma \sim y^{-3}, \qquad \alpha \simeq -\beta \sim y^{-2}, \qquad \alpha+\beta \sim y^{-1}. \tag{C.13}$$

Combined with the above formulas, the terms

$$2\gamma Z_{y\bar{y}}I_1 \sim \gamma\overline{Y}_{y\bar{y}}Y_{y\bar{y}}I_2 \sim y^{-2} \qquad (\text{for } \Delta t \sim y) \tag{C.14}$$

of (C.1) contribute to $D$ starting at leading order in $y$, and

$$-\gamma\overline{Y}_{y\bar{y}}Y_{\bar{y}}I_3 \sim -\gamma Y_y Y_{y\bar{y}}I_4 \sim y^{-1} \qquad (\text{for } \Delta t \sim y) \tag{C.15}$$

contribute at NLO in $y$. The rest of the terms in (C.1) are parametrically smaller and do not contribute to IR logarithms.

Using the preceding expansions, we find contribution

$$D_{(1)} \simeq -\frac{C_A^2\alpha_s^2}{8\pi^2(\Delta t)^2}(xyz)^2(1-x)(1-y)\gamma$$
$$\times \left\{\left(1+\xi - 2s\xi\tau^2\right)\ln\left(\frac{xy}{(1-x)(1-y)}(1+\tau)\right) + \frac{1}{1+\tau}\right.$$
$$\left. + \xi\left[-\frac{2\tau}{1+\tau} - \frac{(1+3s)\tau^2}{1+\tau} + \frac{(1+s)\tau^2}{(1+\tau)^2}\right]\right\} \tag{C.16}$$

to $D$ from $2\gamma Z_{y\bar{y}}I_1 + \gamma\overline{Y}_{y\bar{y}}Y_{y\bar{y}}I_2$ and

$$D_{(2)} \simeq -\frac{C_A^2\alpha_s^2}{4\pi^2(\Delta t)^2}x^2y^2(1-x)^3\gamma\frac{s\xi\tau^2}{(1+\tau)} \tag{C.17}$$

from $-\gamma(\bar{Y}_{y\bar{y}}Y_{\bar{y}}I_3 + Y_y Y_{y\bar{y}}I_4)$. The sum of (C.16) and (C.17) gives our $\Delta t \sim y$ expansion of $D$ in (4.9).

## C.2 UV contribution

From eqs. (D.6–D.9) and (D.19) of ref. [20], the UV contribution from the A3 diagram is

$$\left[\frac{d\Gamma}{dx\,dy}\right]_{xy\bar{y}\bar{x}}^{(\Delta t < a)} = \frac{C_{\rm A}^2 \alpha_{\rm s}^2}{16\pi^2} \left[\frac{2}{\epsilon} + \ln\left(\frac{\mu^4 a}{E^2}\right) + 1 + \ln(2\pi^2)\right] \left[(i\Omega_0)^{d/2} + (i\Omega_{\rm f})^{d/2}\right]$$

$$\times\, xyz^2(1-x)^2(1-y)^2 \left[(\alpha+\beta) + \frac{(\alpha+\gamma)xy}{(1-x)(1-y)}\right]$$

$$-\frac{iC_{\rm A}^2\alpha_{\rm s}^2}{16\pi^2}(\Omega_0 + \Omega_{\rm f})xyz^2(1-x)^2(1-y)^2$$

$$\times \left\{\left[(\alpha+\beta) + \frac{(\alpha+\gamma)xy}{(1-x)(1-y)}\right]\ln(e^{-i\pi}xyz) - 2\gamma + \frac{2(\alpha+\gamma)xy}{(1-x)(1-y)}\right\}. \quad \text{(C.18)}$$

We are only interested in terms that contribute $O(1/y)$ or larger to (C.18), since those are the only terms that can generate single or double log behavior. Recalling the scaling (C.13) of $(\alpha, \beta, \gamma)$ with $y$, we find that only the terms proportional to $\gamma$ are large enough. Most of those terms are $O(\ln y/y)$ or $O(1/y)$, in which case one may make small $y$ approximations in prefactors, such as $(1-y)^2 \simeq 1$. The *only* term that's even bigger is the red $-2\gamma$ term in the last line of (C.18), which generates spurious $1/y^2$ behavior, for which NLO terms in $y$ are important. So we can use the small-$y$ approximation

$$\left[(i\Omega_0)^{d/2} + (i\Omega_{\rm f})^{d/2}\right] \simeq 2(i\Omega_0)^{d/2} = 2i\Omega_0\left[1 - \tfrac{\epsilon}{2}\ln(i\Omega_0) + O(\epsilon^2)\right]$$

$$\simeq (i\Omega_0 + i\Omega_{\rm f})\left[1 - \tfrac{\epsilon}{2}\ln(i\Omega_0) + O(\epsilon^2)\right] \quad \text{(C.19)}$$

in the *first* line of (C.18). (The last approximation in (C.19) will be convenient for combining with other terms.) Keeping all this in mind, we can rewrite (C.18) through NLO in $y$ as

$$\left[\frac{d\Gamma}{dx\,dy}\right]_{xy\bar{y}\bar{x}}^{(\Delta t < a)} = \frac{C_{\rm A}^2\alpha_{\rm s}^2}{16\pi^2}(xyz)^2(1-x)(1-y)\gamma(i\Omega_0 + i\Omega_{\rm f})$$

$$\times \left\{\left[\frac{2}{\epsilon} + \ln\left(\frac{\mu^4 a}{i\Omega_0 E^2}\right) + 1 + \ln\left(2\pi^2\right)\right]\right.$$

$$\left. - \left[\ln\left(e^{-i\pi}xyz\right) - \frac{2(1-x)(1-y)}{xy} + 2\right]\right\}. \quad \text{(C.20)}$$

Taking $2\,\mathrm{Re}(\cdots)$, and using

$$\frac{2(1-x)(1-y)}{xy} = \frac{2(z+xy)}{xy} = \frac{1}{\xi} + 2, \quad \text{(C.21)}$$

gives (4.21).

## C.3 $\Delta t \sim \sqrt{y}$

For $\Delta t \sim \sqrt{y}$, the power counting is a little different than in section C.1. We still have $\Omega_-\Delta t \ll 1$, but now $\Omega_+\Delta t \simeq \Omega_y\Delta t \sim 1$. So not all trig functions can be expanded. We will again need to evaluate $D$ to NLO in $y$, but this time NLO will be suppressed compared

to leading order by a factor of $\sqrt{y}$ rather than a factor of $y$. That means that we will be able to ignore corrections to $D$ that are suppressed by a full power of $y$. However, similar to section C.1, we will need to expand $X$'s to NNLO because of cancellation of the leading-order contributions in the combination $X_y X_{\bar{y}} - X_{y\bar{y}}^2$. The expansions of (C.3) we will need are

$$X_y = -i(1+2vy)M_0(\Omega\cot)_- + (M\Omega)_0 - \tfrac{i}{4}x^2yE(\Omega\cot)_y + O(y), \tag{C.22a}$$

$$X_{\bar{y}} = -i(1+2uy)M_0(\Omega\cot)_- + (M\Omega)_0 - \tfrac{i}{4}x^2yE(\Omega\cot)_y + O(y), \tag{C.22b}$$

$$X_{y\bar{y}} = -i(1+(u+v)y)M_0(\Omega\csc)_- + \tfrac{i}{4}x^2yE(\Omega\csc)_y + O(y^{3/2}), \tag{C.22c}$$

$$Y_y = -(1-x)Y_{\bar{y}}[1 + O(y)], \tag{C.22d}$$

$$Y_{\bar{y}} = \frac{ixyE}{2}\left[(\Omega\cot)_y - \frac{1}{\Delta t}\right] + O(y^{3/2}), \tag{C.22e}$$

$$Y_{y\bar{y}} = -\frac{ixyE}{2}\left[(\Omega\csc)_y + \frac{1}{\Delta t}\right] + O(y^{3/2}), \tag{C.22f}$$

$$\overline{Y}_{y\bar{y}} = -(1-x)Y_{y\bar{y}}[1 + O(y)], \tag{C.22g}$$

$$Z_{y\bar{y}} = -iy(1-x)E(\Omega\csc)_y + O(y^{3/2}), \tag{C.22h}$$

where

$$\csc_y \equiv \csc(\Omega_y\Delta t), \qquad \cot_y \equiv \cot(\Omega_y\Delta t). \tag{C.23}$$

Above, $\csc_-$ and $\csc_+$ should be expanded in the small argument $\Omega_-\Delta t = O(y^{1/2})$, but it's algebraically convenient to save that step until after one simplifies the combination $X_y X_{\bar{y}} - X_{y\bar{y}}^2$. That combination turns out to be

$$X_y X_{\bar{y}} - X_{y\bar{y}}^2 = M_0^2\left[-\frac{2i\Omega_0}{\Delta t} + \Omega_0^2 + \Omega_-^2 - \frac{xy}{2(1-x)\Delta t}\Omega_y(\csc_y + \cot_y)\right] + O(y^{1/2}), \tag{C.24}$$

and then $S \equiv (X_y X_{\bar{y}} - X_{y\bar{y}}^2)/X_y X_{\bar{y}}$ is given through NLO by the $S$ shown in (4.25). Note that the dependence on the $u$ and $v$ of (C.7) affected the NNLO contributions to the $X$'s in (C.22), but their effects have canceled in the NLO result for $X_y X_{\bar{y}} - X_{y\bar{y}}^2$ above, which is why they do not affect our calculation.

Combining (C.13) with the above formulas, the term

$$2\gamma Z_{y\bar{y}} I_1 \sim y^{-2} \qquad \text{(for } \Delta t \sim \sqrt{y}) \tag{C.25}$$

of (C.1) contributes to $D$ starting at leading order in $y$, and

$$\gamma \overline{Y}_{y\bar{y}} Y_{y\bar{y}} I_2 \sim \gamma Y_y Y_{\bar{y}} I_2 \sim -\gamma \overline{Y}_{y\bar{y}} Y_{\bar{y}} I_3 \sim -\gamma Y_y Y_{y\bar{y}} I_4 \sim y^{-3/2} \qquad \text{(for } \Delta t \sim y) \tag{C.26}$$

contribute at NLO in $y$. The rest of the terms in (C.1) are parametrically smaller and do not contribute to IR logarithms.[39] Using the preceding expansions, we find contribution

$$D_{(A)} \simeq -\frac{C_A\alpha_s^2 P(x)}{4\pi^2 y}(\Omega\csc)_y^2 \ln S \tag{C.27}$$

---

[39]Remember that $D$ also contains prefactors in (C.1) and is integrated over $\Delta t$ to get a rate $d\Gamma/dx\,dy$. Because of this, (C.25) contributes $O(y^{-3/2})$ to the rate [which at leading order gives a power-law IR divergence], and (C.26) contributes $O(y^{-1})$ [which at leading order contributes IR logarithms].

to $D$ from $2\gamma Z_{y\bar{y}} I_1$ and

$$D_{(B)} \simeq -\frac{C_A \alpha_s^2 P(x)}{4\pi^2 y} \frac{\xi \Omega_y^3 \Delta t}{2S} \csc_y (\csc_y + \cot_y)^2 \qquad (\text{C.28})$$

from $\gamma(\overline{Y}_{y\bar{y}} Y_{y\bar{y}} I_2 + Y_y Y_{\bar{y}} I_2 - \overline{Y}_{y\bar{y}} Y_{\bar{y}} I_3 - Y_y Y_{y\bar{y}} I_4)$. The sum of (C.27) and (C.28) gives our $\Delta t \sim \sqrt{y}$ expansion of $D$ in (4.24).

## D  Small-$y$ behavior of A1 diagram integrand

### D.1  $\Delta t \sim \sqrt{y}$

The extraction of the small-$y$ behavior for $\Delta t \sim \sqrt{y}$ for the A1 diagram is very similar to that for the A3 diagram in section C.3. The function

$$
\begin{aligned}
\widetilde{D}_{\text{new}}&(x_1, x_2, x_3, x_4, \bar{\alpha}, \bar{\beta}, \bar{\gamma}, \Delta t) = \\
&-\frac{C_A^2 \alpha_s^2 M_i^2}{32\pi^4 E^2} (-x_1 x_2 x_3 x_4) \Omega_+ \Omega_- \csc(\Omega_+ \Delta t) \csc(\Omega_- \Delta t) \\
&\qquad\qquad \times \Big\{ (\bar{\beta} Y_y^{\text{new}} Y_y^{\text{new}} + \bar{\gamma} \overline{Y}_{yy'}^{\text{new}} Y_{yy'}^{\text{new}}) I_0^{\text{new}} + (2\bar{\alpha} + \bar{\beta} + \bar{\gamma}) Z_{yy'}^{\text{new}} I_1^{\text{new}} \\
&\qquad\qquad\qquad + \big[ (\bar{\alpha} + \bar{\gamma}) Y_y^{\text{new}} Y_y^{\text{new}} + (\bar{\alpha} + \bar{\beta}) \overline{Y}_{yy'}^{\text{new}} Y_{yy'}^{\text{new}} \big] I_2^{\text{new}} \\
&\qquad\qquad\qquad - (\bar{\alpha} + \bar{\beta} + \bar{\gamma}) (\overline{Y}_{yy'}^{\text{new}} Y_y^{\text{new}} I_3^{\text{new}} + Y_y^{\text{new}} Y_{yy'}^{\text{new}} I_4^{\text{new}}) \Big\} \quad (\text{D.1})
\end{aligned}
$$

is taken from eq. (A.64) of ref. [20] *except* that the $\mathcal{D}_2^{(\mathbb{I})}$ term is excluded, as we have discussed in the main text. Above and below,

$$\begin{pmatrix} X_{y'}^{\text{new}} & Y_{y'}^{\text{new}} \\ Y_{y'}^{\text{new}} & Z_{y'}^{\text{new}} \end{pmatrix} \equiv \begin{pmatrix} X_y^{\text{new}} & Y_y^{\text{new}} \\ Y_y^{\text{new}} & Z_y^{\text{new}} \end{pmatrix} \equiv \text{ the } \begin{pmatrix} X_y & Y_y \\ Y_y & Z_y \end{pmatrix} \text{ of eq. (C.3a)}, \qquad (\text{D.2a})$$

$$\begin{pmatrix} X_{yy'}^{\text{new}} & Y_{yy'}^{\text{new}} \\ \overline{Y}_{yy'}^{\text{new}} & Z_{yy'}^{\text{new}} \end{pmatrix} \equiv -i a_y^{-1\top} \begin{pmatrix} \Omega_+ \csc_+ & \\ & \Omega_- \csc_- \end{pmatrix} a_y^{-1}. \qquad (\text{D.2b})$$

The relevant expansions are

$$X_{y'}^{\text{new}} = X_y^{\text{new}} = -i(1 + 2vy) M_0 (\Omega \cot)_- + (M\Omega)_0 - \tfrac{i}{4} x^2 y E (\Omega \cot)_y + O(y), \qquad (\text{D.3a})$$

$$X_{yy'}^{\text{new}} = -i(1 + 2vy) M_0 (\Omega \csc)_- - \tfrac{i}{4} x^2 y E (\Omega \csc)_+ + O(y), \qquad (\text{D.3b})$$

$$Y_{y'}^{\text{new}} = Y_y^{\text{new}} = -\frac{ixy(1-x)E}{2} \left[ (\Omega \cot)_y - \frac{1}{\Delta t} \right] + O(y^{3/2}), \qquad (\text{D.3c})$$

$$\overline{Y}_{yy'}^{\text{new}} = Y_{yy'}^{\text{new}} = -\frac{ixy(1-x)E}{2} \left[ (\Omega \csc)_y - \frac{1}{\Delta t} \right] + O(y^{3/2}), \qquad (\text{D.3d})$$

$$Z_{yy'}^{\text{new}} = -iy(1-x)^2 E (\Omega \csc)_y + O(y^{3/2}), \qquad (\text{D.3e})$$

and thence

$$(X_y X_{y'} - X_{yy'}^2)^{\text{new}} = M_0^2 \left[ -\frac{2i\Omega_0}{\Delta t} + \Omega_0^2 + \Omega_-^2 - \frac{xy}{2(1-x)\Delta t} \Omega_y (-\csc_y + \cot_y) \right] + O(y^{1/2}) \quad (\text{D.4})$$

and the $S_{\text{new}} \equiv \left[ (X_y X_{y'} - X_{yy'}^2)/X_y X_{y'} \right]^{\text{new}}$ given by (6.8).

For small $y$, eq. (A.46) of ref. [20] for $(\bar{\alpha}, \bar{\beta}, \bar{\gamma})$ has parametric behavior

$$\bar{\alpha} \sim y^{-3}, \qquad \bar{\beta} \simeq -\bar{\gamma} \sim y^{-2}, \qquad \bar{\beta}+\bar{\gamma} \sim y^{-1}. \tag{D.5}$$

The dominant contribution to (D.1) is then

$$\widetilde{D}_{(\mathrm{A})}^{\mathrm{new}} \simeq \frac{C_{\mathrm{A}}\alpha_{\mathrm{s}}^2\, P(x)}{4\pi^2 y}\, (\Omega\csc)_y^2 \ln S_{\mathrm{new}}, \tag{D.6}$$

from $2\bar{\alpha}(Z_{\mathrm{yy'}}I_1)^{\mathrm{new}}$ and, contributing to NLO terms,

$$\widetilde{D}_{(\mathrm{B})}^{\mathrm{new}} \simeq -\frac{C_{\mathrm{A}}\alpha_{\mathrm{s}}^2\, P(x)}{4\pi^2 y}\, \frac{\xi\Omega_y^3\Delta t}{2S_{\mathrm{new}}}\csc_y(\csc_y - \cot_y)^2 \tag{D.7}$$

from $\bar{\alpha}(\overline{Y}_{\mathrm{yy'}}Y_{\mathrm{yy'}}I_2 + Y_{\mathrm{y}}Y_{\mathrm{y'}}I_2 - \overline{Y}_{\mathrm{yy'}}Y_{\mathrm{y'}}I_3 - Y_{\mathrm{y}}Y_{\mathrm{yy'}}I_4)^{\mathrm{new}}$. The sum of (D.6) and (D.7) gives our $\Delta t \sim \sqrt{y}$ expansion of $\widetilde{D}_{\mathrm{new}}$ in (6.7).

## D.2 UV contribution

Eq. (A.66) of ref. [20] gives the pole piece of $A_{\mathrm{new}}(x,y)$ as[40]

$$A_{\mathrm{new}}^{\mathrm{pole}}(x,y) = \frac{\alpha_{\mathrm{s}}^2}{2\pi^2}\, \frac{P(x)\, P(\frac{y}{1-x})}{1-x}\, \mathrm{Re}\Big\{i\Omega_0\Big[-\Big(\tfrac{1}{\epsilon} + \ln(\tfrac{\pi\mu^2}{E\Omega_0})\Big) + \tfrac{1}{2}\ln(xyz)\Big]\Big\}. \tag{D.8}$$

But this[41]

$$A_{\mathrm{new}}^{\mathrm{pole}}(x,y) \propto \lim_{\text{``}a\to 0\text{''}} 2\,\mathrm{Re}\left\{\left[\frac{d\Gamma}{dx\,dy}\right]_{xyy\bar{x}_2}^{(\Delta t<a)} + \left[\frac{d\Gamma}{dx,dy}\right]_{xyy\bar{x}_2}^{(\mathcal{D}_2)}\right\} \tag{D.9}$$

contains a $\mathcal{D}_2$ addition which we do not want here, because we did not make the corresponding $\mathcal{D}_2$ subtraction in (D.1). Instead, we just want the piece

$$2\,\mathrm{Re}\left[\frac{d\Gamma}{dx\,dy}\right]_{xyy\bar{x}_2}^{(\Delta t<a)}. \tag{D.10}$$

To remove the $\mathcal{D}_2$ contribution from (D.8), take note of eqs. (4.31) and (F.37) of [18]:

$$\mathbb{I} = 2\pi^2(i\Omega_0)^{d-1}\Big[-\Big(\frac{2}{\epsilon} - \gamma_{\mathrm{E}} + \ln(4\pi)\Big) - \frac{\ln(2i\Omega_0 a) + 1}{i\Omega_0 a} - \ln(i\Omega_0 a) + 3\ln(2\pi)\Big], \tag{D.11}$$

$$\int_a^\infty d(\Delta t)\, \mathcal{D}_2^{(\mathbb{I})}(\Delta t) = 2\pi^2\Big(\frac{\ln(2i\Omega_0 a) + 1}{a} + i\Omega_0\big[\ln(2i\Omega_0 a) - 1\big]\Big), \tag{D.12}$$

which combine to give

$$\mathbb{I} + \int_a^\infty d(\Delta t)\, \mathcal{D}_2^{(\mathbb{I})}(\Delta t) = 2\pi^2(i\Omega_0)^{d-1}\Big[-\Big(\frac{2}{\epsilon} - \gamma_{\mathrm{E}} + \ln(4\pi)\Big) + \ln 2 - 1 + 3\ln(2\pi)\Big]. \tag{D.13}$$

---

[40]We've specialized here to the case sgn $M > 0$. That is, we are focused on the A1 diagram and not concerned here with front-end transformations.

[41]For (D.9), see the discussion of appendix D.4 of ref. [20]. We've used the proportionality sign $\propto$ here just to avoid dwelling on the factor of 2 difference between $d\Gamma/dx\,dy$ and $A_{\mathrm{new}}$ in (6.3), having to do with which is defined to contain the amplitude loop symmetry factor of $\frac{1}{2}$. This detail will not matter for the method we will use to remove the $\mathcal{D}_2$ contribution from (D.8).

By comparing (D.11) to (D.13), we see that we can recover the result (D.11) *without* the $\mathcal{D}_2$ addition by taking

$$\frac{1}{\epsilon} \longrightarrow \frac{1}{\epsilon} + \frac{1}{2}\left(\frac{\ln(2i\Omega_0 a)+1}{i\Omega_0 a} + \ln(i\Omega_0 a) + \ln 2 - 1\right) \tag{D.14}$$

in the result (D.13) *with* the $\mathcal{D}_2$ addition.

Making the substitution (D.14) into the formula (D.8) for $A_{\rm new}^{\rm pole}$ then gives us the piece of $A_{\rm new}^{\rm pole}$ that does not involve $\mathcal{D}_2$:

$$\frac{\alpha_{\rm s}^2}{2\pi^2} \frac{P(x)\,P(\frac{y}{1-x})}{1-x} \,{\rm Re}\left\{ i\Omega_0\left[-\left(\tfrac{1}{\epsilon} + \ln(\tfrac{\pi\mu^2}{E\Omega_0})\right) + \tfrac{1}{2}\ln(xyz) \right.\right.$$
$$\left.\left. - \frac{1}{2}\left(\frac{\ln(2i\Omega_0 a)+1}{i\Omega_0 a} + \ln(i\Omega_0 a) + \ln 2 - 1\right)\right]\right\}. \tag{D.15}$$

Taking the small-$y$ limit and reorganizing gives (6.11).

# E  Small-$y$ behavior of $\mathcal{A}_{\rm seq}(y,x)$

In this appendix, we investigate the small-$y$ expansion of $\mathcal{A}_{\rm seq}(y,x)$ and its front-end transformation, which appear as two of the four entries in the dark pink ($\beta$) section of table 1. We want analytic formulas for the small-$y$ expansion of $\mathcal{A}_{\rm seq}(y,x)$ that will work for both positive and negative values of $y$.

## E.1  $A_{\rm seq}(y,x)$ vs. $A_{\rm seq}(x,y)$

Most formulas concerning $\mathcal{A}_{\rm seq}$ in earlier papers [15, 16, 20] are written for $\mathcal{A}_{\rm seq}(x,y)$ rather than $\mathcal{A}_{\rm seq}(y,x)$. Furthermore, $\mathcal{A}_{\rm seq}(x,y)$ has the same longitudinal momentum fractions $(x_1,x_2,x_3,x_4) = (-1,y,z,x)$ for 4-particle evolution as both the A1 and A3 diagrams discussed earlier in this paper. Because it is quicker and easier to re-use previous formulas, it will be more convenient to study the small-$y$ behavior of $\mathcal{A}_{\rm seq}(x,y)$ instead of $\mathcal{A}_{\rm seq}(y,x)$. Fortunately, we have checked with numerics that the small-$y$ expansions of the two are equal to each other up to and including $O(y^{-1})$ — that is, they produce the same IR power-law divergences and IR logarithms. So, for the sake of simplicity, in this appendix we will study the small-$y$ expansion analytically for $\mathcal{A}_{\rm seq}(x,y)$ (for both positive and negative values of $y$) instead of directly for the $\mathcal{A}_{\rm seq}(y,x)$ appearing in table 1.

## E.2  Setup for $A_{\rm seq}(x,y)$

Unlike our analysis of the A1 and A3 diagrams in this paper, we will carefully keep track of the signs needed in our analysis of $\mathcal{A}_{\rm seq}(x,y)$ to handle either sign of $y$.

The basic formulas for $\mathcal{A}_{\rm seq}(x,y)$ are summarized in eqs. (A.32–A.36) of ref. [20], which are

$$\mathcal{A}_{\rm seq}(x,y) = \mathcal{A}_{\rm seq}^{\rm pole}(x,y) + \int_0^\infty d(\Delta t)\left[2\,{\rm Re}\big(B_{\rm seq}(x,y,\Delta t)\big) + F_{\rm seq}(x,y,\Delta t)\right], \tag{E.1}$$

$$B_{\rm seq}(x,y,\Delta t) = C_{\rm seq}(-1,y,z,x,\bar{\alpha},\bar{\beta},\bar{\gamma},\Delta t), \tag{E.2}$$

$$C_{\rm seq} = D_{\rm seq} - \lim_{\hat{q}\to 0} D_{\rm seq}, \tag{E.3}$$

$$
\begin{aligned}
D_{\text{seq}}(x_1,&x_2,x_3,x_4,\bar{\alpha},\bar{\beta},\bar{\gamma},\Delta t) = \\
&\frac{C_A^2\alpha_s^2 M_i M_f^{\text{seq}}}{32\pi^4 E^2}(-x_1 x_2 x_3 x_4)\Omega_+\Omega_-\csc(\Omega_+\Delta t)\csc(\Omega_-\Delta t) \\
&\times\Big\{(\bar{\beta}Y_y^{\text{seq}}Y_{\bar{x}}^{\text{seq}}+\bar{\alpha}\overline{Y}_{y\bar{x}}^{\text{seq}}Y_{y\bar{x}}^{\text{seq}})I_0^{\text{seq}}+(\bar{\alpha}+\bar{\beta}+2\bar{\gamma})Z_{y\bar{x}}^{\text{seq}}I_1^{\text{seq}} \\
&\quad+[(\bar{\alpha}+\bar{\gamma})Y_y^{\text{seq}}Y_{\bar{x}}^{\text{seq}}+(\bar{\beta}+\bar{\gamma})\overline{Y}_{y\bar{x}}^{\text{seq}}Y_{y\bar{x}}^{\text{seq}}]I_2^{\text{seq}} \\
&\quad-(\bar{\alpha}+\bar{\beta}+\bar{\gamma})(\overline{Y}_{y\bar{x}}^{\text{seq}}Y_{\bar{x}}^{\text{seq}}I_3^{\text{seq}}+Y_y^{\text{seq}}Y_{y\bar{x}}^{\text{seq}}I_4^{\text{seq}})\Big\},
\end{aligned} \tag{E.4}
$$

$$
\begin{aligned}
F_{\text{seq}}(x,y,\Delta t) = \frac{\alpha_s^2 P(x)P(\mathfrak{y})}{4\pi^2(1-x)}\Big[&\text{Re}\big(i(\Omega\,\text{sgn}\,M)_{E,x}\big)\,\text{Re}\big(\Delta t\,\Omega_{(1-x)E,\mathfrak{y}}^2\csc^2(\Omega_{(1-x)E,\mathfrak{y}}\Delta t)\big) \\
&+\text{Re}\big(i(\Omega\,\text{sgn}\,M)_{(1-x)E,\mathfrak{y}}\big)\,\text{Re}\big(\Delta t\,\Omega_{E,x}^2\csc^2(\Omega_{E,x}\Delta t)\big)\Big], \quad \text{(E.5)}
\end{aligned}
$$

where

$$
M_f^{\text{seq}} = yz(1-x)E. \tag{E.6}
$$

For $\mathcal{A}^{\text{pole}}$, we want to use the corrected formula given by eq. (A.14) of this paper instead of the formula in ref. [20]. Other formulas of interest from appendix A.2.3 of ref. [20] are

$$
\begin{pmatrix} X_y^{\text{seq}} & Y_y^{\text{seq}} \\ Y_y^{\text{seq}} & Z_y^{\text{seq}} \end{pmatrix} \equiv \text{the } \begin{pmatrix} X_y & Y_y \\ Y_y & Z_y \end{pmatrix} \text{ of eq. (C.3a)}, \tag{E.7a}
$$

$$
\begin{pmatrix} X_{\bar{x}}^{\text{seq}} & Y_{\bar{x}}^{\text{seq}} \\ Y_{\bar{x}}^{\text{seq}} & Z_{\bar{x}}^{\text{seq}} \end{pmatrix} \equiv \begin{pmatrix} |M_f^{\text{seq}}|\Omega_f^{\text{seq}} & 0 \\ 0 & 0 \end{pmatrix} - i(a_{\bar{x}}^{\text{seq}})^{-1\top}\begin{pmatrix} \Omega_+\cot_+ & \\ & \Omega_-\cot_- \end{pmatrix}(a_{\bar{x}}^{\text{seq}})^{-1}, \tag{E.7b}
$$

$$
\begin{pmatrix} X_{y\bar{x}}^{\text{seq}} & Y_{y\bar{x}}^{\text{seq}} \\ \overline{Y}_{y\bar{x}}^{\text{seq}} & Z_{y\bar{x}}^{\text{seq}} \end{pmatrix} \equiv -ia_y^{-1\top}\begin{pmatrix} \Omega_+\csc_+ & \\ & \Omega_-\csc_- \end{pmatrix}(a_{\bar{x}}^{\text{seq}})^{-1}, \tag{E.7c}
$$

where

$$
a_{\bar{x}}^{\text{seq}} \equiv \begin{pmatrix} 0 & 1 \\ 1 & 0 \end{pmatrix} a_y. \tag{E.8}
$$

Above, $a_{\bar{y}}$ is the same matrix that appeared in our analysis of the A3 diagram in appendix C.

For small $y$, it turns out that $\Delta t \times 2\,\text{Re}\,B_{\text{seq}}(x,y,\Delta t)$ transitions at $\Delta t \sim \sqrt{y}$ between a constant value for $\Delta t \ll \sqrt{y}$ and zero for $\Delta t \gg \sqrt{y}$. For our purposes, we may therefore adequately approximate the behavior of $\Delta t \times 2\,\text{Re}\,B_{\text{seq}}$ for all $\Delta t$ by finding its small-$y$ approximation for $\Delta t \sim \sqrt{y}$. It turns out that $\Delta t \times F_{\text{seq}}(x,y,\Delta t)$ does something similar at $\Delta t \sim y^0$, and so we may adequately approximate its behavior for all $\Delta t$ by finding its small-$y$ approximation for $\Delta t \sim y^0$. Once we have those approximations, we will integrate the sum $2\,\text{Re}\,B_{\text{seq}}(x,y,\Delta t)+F_{\text{seq}}(x,y,\Delta t)$ over $\Delta t$ [which is equivalent to integrating $\Delta t \times 2\,\text{Re}\,B_{\text{seq}}(x,y,\Delta t)+\Delta t \times F_{\text{seq}}(x,y,\Delta t)$ over $\ln(\Delta t)$] as in (E.1).

### E.3 $B_{\text{seq}}$ for $\Delta t \sim \sqrt{y}$

Using (C.7) and (E.8), we find that the expansions we need of (E.7) for $\Delta t \sim \sqrt{y}$ are

$$
X_y^{\text{seq}} = -i\frac{M_0}{\Delta t}+(M\Omega)_0+O(y^{1/2}), \tag{E.9a}
$$

$$X_{\bar{\mathrm{x}}}^{\mathrm{seq}} = Z_{\mathrm{y}\bar{\mathrm{x}}}^{\mathrm{seq}} = (M\Omega)_{\mathrm{f}}^{\mathrm{seq}}(\operatorname{sgn} y - i\cot_y) + O(y^{3/2}), \tag{E.9b}$$

$$Y_{\mathrm{y}\bar{\mathrm{x}}}^{\mathrm{seq}} = -\frac{iM_0}{\Delta t} + O(y^{1/2}), \tag{E.9c}$$

$$\overline{Y}_{\mathrm{y}\bar{\mathrm{y}}}^{\mathrm{seq}} = -iM_{\mathrm{f}}^{\mathrm{seq}}(\Omega\csc)_y + O(y^{3/2}), \tag{E.9d}$$

and the parametric result that

$$X_{\mathrm{y}\bar{\mathrm{x}}}^{\mathrm{seq}} \sim Y_{\mathrm{y}}^{\mathrm{seq}} \sim Y_{\bar{\mathrm{x}}}^{\mathrm{seq}} \sim y^{1/2}. \tag{E.9e}$$

Above, we have taken $M_0 = x(1-x)E$ to be positive, but $y$ and so $M_{\mathrm{f}}^{\mathrm{seq}} = y(1-x)(1-x-y)$ may have either sign. Note in particular that $|M_{\mathrm{f}}^{\mathrm{seq}}| = M_{\mathrm{f}}^{\mathrm{seq}}\operatorname{sgn} y$. Unlike the analysis of the A1 and A3 diagrams, we do *not* need expansions of the $X$'s to NNLO in order to get a NLO result for $(X_{\mathrm{y}}X_{\bar{\mathrm{x}}} - X_{\mathrm{y}\bar{\mathrm{x}}}^2)^{\mathrm{seq}}$ because here the leading-order behavior of the $X$'s does not cancel in the combination.

Using the scaling (D.5) of $(\bar{\alpha}, \bar{\beta}, \bar{\gamma})$, the only term of (E.4) that contributes up to NLO in $\sqrt{y}$ is the $\bar{\alpha}\overline{Y}_{\mathrm{y}\bar{\mathrm{x}}}Y_{\mathrm{y}\bar{\mathrm{x}}}I_0$ term. Because we want to allow for front-end transformations, we need to use the version of $\bar{\alpha}$ in eq. (A.46) of ref. [20] that is consistent with front-end transformations, which involves appropriate absolute value signs. The small-$y$ limit is

$$\bar{\alpha} = \frac{2\,P(x)}{C_{\mathrm{A}}x^2(1-x)^4|y|^3}\left[1 + O(y)\right], \tag{E.10}$$

instead of the less-general (6.6) that we used for the A1 diagram (where $y$ was positive). We then find

$$D_{\mathrm{seq}} \simeq \frac{C_{\mathrm{A}}\alpha_{\mathrm{s}}^2\,P(x)}{4\pi^2|y|\,\Delta t}\,(1 - i\Omega_0\,\Delta t)\,\Omega_y(\cot_y - i\operatorname{sgn} y). \tag{E.11}$$

Subtracting the vacuum limit $\hat{q} \to 0$ then gives

$$B_{\mathrm{seq}} = C_{\mathrm{seq}} \simeq \frac{C_{\mathrm{A}}\alpha_{\mathrm{s}}^2\,P(x)}{4\pi^2|y|\,\Delta t}\left[(1 - i\Omega_0\,\Delta t)\,\Omega_y(\cot_y - i\operatorname{sgn} y) - \frac{1}{\Delta t}\right]. \tag{E.12}$$

### E.4 Assembling $\mathcal{A}_{\mathrm{seq}}(x, y)$

As mentioned earlier, the behavior of $F_{\mathrm{seq}}(x, y, \Delta t)$ is non-trivial only at $\Delta t \sim y^0$. So expand (E.5) for small $y$ at $\Delta t \sim y^0$. The gluon splitting function $P(\xi)$ also has an absolute value sign in its definition in eq. (A.5) of ref. [20], in order to facilitate front-end transformations. Accounting for this, the expansion of $F_{\mathrm{seq}}$ is

$$F_{\mathrm{seq}} \simeq \frac{C_{\mathrm{A}}\alpha_{\mathrm{s}}^2\,P(x)}{2\pi^2|y|}\left[\operatorname{Re}(i\Omega_y\operatorname{sgn} y)\operatorname{Re}\left(\Delta t\,(\Omega\csc)_0^2\right) + \operatorname{Re}(i\Omega_0)\operatorname{Re}\left(\Delta t\,(\Omega\csc)_y^2\right)\right] \tag{E.13}$$

through NLO.

The small-$y$ expansion of the pole term (A.14) is

$$\mathcal{A}_{\mathrm{seq}}^{\mathrm{pole}} \simeq -\frac{C_{\mathrm{A}}\alpha_{\mathrm{s}}^2\,P(x)}{2\pi^2|y|}\operatorname{Re}\left[i\Omega_y\operatorname{sgn} y + i\Omega_0\right]\left(1 - \tfrac{\pi}{2}\operatorname{sgn} y\right). \tag{E.14}$$

Combining (E.12), (E.13) and (E.14), the small-$y$ expansion of (E.1) is

$$
\begin{aligned}
\mathcal{A}_{\mathrm{seq}}(x,y) \simeq \frac{C_{\mathrm{A}}\alpha_{\mathrm{s}}^2\,P(x)}{2\pi^2|y|}\Bigg\{ & -\operatorname{Re}(i\Omega_y\operatorname{sgn}y + i\Omega_0)(1-\tfrac{\pi}{2}\operatorname{sgn}y) \\
& + \int_0^\infty d(\Delta t)\,\bigg[\operatorname{Re}\left(\frac{\Omega_y(\cot_y - i\operatorname{sgn}y)}{\Delta t}\right) - \frac{1}{(\Delta t)^2} \\
& \qquad\qquad + \operatorname{Re}(i\Omega_y\operatorname{sgn}y)\operatorname{Re}\left(\Delta t\,(\Omega\csc)_0^2\right) \\
& \qquad - \operatorname{Re}(i\Omega_0\Omega_y(\cot_y - i\operatorname{sgn}_y)) + \operatorname{Re}(i\Omega_0)\operatorname{Re}(\Delta t\,(\Omega\csc)_y^2)\bigg]\Bigg\}.
\end{aligned}
\tag{E.15}
$$

The $\Delta t$ integral of individual terms in the integrand above would be divergent due to their $\Delta t \to 0$ or $\Delta t \to \infty$ behavior. But the combination of terms in the integrand conspires so that the total integral is convergent.

## E.5  Integration

The integral may be performed using the same techniques as appendix B of ref. [20]. First, add an unnecessary regulator: multiply the integrand by $(\Delta t)^\epsilon$, with the understanding that we will take $\epsilon \to 0$ at the end of the calculation. If we treat this regulator with the same logic as dimensional regularization (i.e. calculate integrals for values of $\epsilon$ where they converge and then analytically continue to $\epsilon \to 0$), we may the split up the integral into regulated integrals of the individual terms in the integrand and tackle those integrals one at a time.

### E.5.1  Leading-order terms

For instance, defining[42]

$$
\tilde{\tau} \equiv i(\Omega_y\operatorname{sgn}y)\Delta t,
\tag{E.16}
$$

we may write

$$
\begin{aligned}
\int_0^\infty d(\Delta t)\,(\Delta t)^\epsilon\,\frac{\Omega_y(\cot_y - i\operatorname{sgn}y)}{\Delta t} &= (i\Omega_y\operatorname{sgn}y)^{1-\epsilon}\int_0^\infty d\tilde{\tau}\,\tilde{\tau}^{-1+\epsilon}\,(\coth\tilde{\tau} - 1) \\
&= (i\Omega_y\operatorname{sgn}y)^{1-\epsilon}\int_0^\infty d\tilde{\tau}\,\tilde{\tau}^{-1+\epsilon}\,2\sum_{n=1}^\infty e^{-2n\tilde{\tau}} = (2i\Omega_y\operatorname{sgn}y)^{1-\epsilon}\,\Gamma(\epsilon)\,\zeta(\epsilon) \\
&= i\Omega_y\operatorname{sgn}y\left[-\frac{1}{\epsilon} + \ln\left(\frac{i\Omega_y\operatorname{sgn}y}{\pi}\right) + \gamma_{\mathrm{E}} + O(\epsilon)\right].
\end{aligned}
\tag{E.17}
$$

By logic similar to dimensional regularization, integrals of powers like $1/(\Delta t)^2$ give zero. For the next integral, switch to $\sigma \equiv i\Omega_0\,\Delta t$ and use the integral from eq. (B.13) of ref. [20]:

$$
\int_0^\infty d(\Delta t)\,(\Delta t)^\epsilon\,\Delta t\,(\Omega\csc)_0^2 = (i\Omega_0)^{-\epsilon}\int_0^\infty d\sigma\,\frac{\sigma^{1+\epsilon}}{\operatorname{sh}^2\sigma} = \frac{1}{\epsilon} - \ln(2i\Omega_0) + 1 + O(\epsilon).
\tag{E.18}
$$

---

[42]Recall that the complex phase of $\Omega_y$ is $e^{-i(\pi/4)\operatorname{sgn}y}$. The $\operatorname{sgn}y$ is needed in the definition of $\tilde{\tau}$ in (E.16) so that, in the first step of (E.17), one does not deform the contour through a region where the integrand blows up as $|\Delta t| \to \infty$.

Combining these integration results gives the convergent integral of the leading (red) terms in (E.15):

$$
\int_0^\infty d(\Delta t) \left[ \mathrm{Re}\left( \frac{\Omega_y(\cot_y - i\,\mathrm{sgn}\,y)}{\Delta t} \right) - \frac{1}{(\Delta t)^2} + \mathrm{Re}(i\Omega_y\,\mathrm{sgn}\,y)\,\mathrm{Re}\left( \Delta t\,(\Omega\csc)_0^2 \right) \right]
$$
$$
= \mathrm{Re}(i\Omega_y\,\mathrm{sgn}\,y\,\ln(i\Omega_y\,\mathrm{sgn}\,y)) + \mathrm{Re}(i\Omega_y\,\mathrm{sgn}\,y)\,\mathrm{Re}\left[ -\ln(i\Omega_0) - \ln(2\pi) + \gamma_{\mathrm{E}} + 1 \right]. \quad \text{(E.19)}
$$

### E.5.2 NLO terms

Similarly, the integrals we need for the NLO (black) terms in (E.15) are

$$
\int_0^\infty d(\Delta t)\,(\Delta t)^\epsilon\,\Omega_y(\cot_y - i\,\mathrm{sgn}_y) = (2i\Omega_y\,\mathrm{sgn}\,y)^{-\epsilon}\,\Gamma(1+\epsilon)\,\zeta(1+\epsilon)
$$
$$
= \frac{1}{\epsilon} - \ln(2i\Omega_y\,\mathrm{sgn}\,y) + O(\epsilon), \quad \text{(E.20)}
$$
$$
\int_0^\infty d(\Delta t)\,(\Delta t)^\epsilon\,\Delta t\,(\Omega\csc)_y^2 = \frac{1}{\epsilon} - \ln(2i\Omega_y\,\mathrm{sgn}\,y) + 1 + O(\epsilon), \quad \text{(E.21)}
$$

which gives

$$
\int_0^\infty d(\Delta t) \left[ -\mathrm{Re}(i\Omega_0\Omega_y(\cot_y - i\,\mathrm{sgn}_y)) + \mathrm{Re}(i\Omega_0)\,\mathrm{Re}(\Delta t\,(\Omega\csc)_y^2) \right]
$$
$$
= \mathrm{Re}(i\Omega_0\ln(i\Omega_y\,\mathrm{sgn}\,y)) + \mathrm{Re}(i\Omega_0)\,\mathrm{Re}(-\ln(i\Omega_y\,\mathrm{sgn}\,y) + 1). \quad \text{(E.22)}
$$

### E.6 Final expansion and implications

Now use (E.19) and (E.22) in (E.15) to get the small-$y$ expansion of $\mathcal{A}_{\mathrm{seq}}(x,y)$. We can isolate the relative phases of the $y > 0$ and $y < 0$ case by using the fact that the complex phase of $\Omega_y$ is $e^{-i(\pi/4)\,\mathrm{sgn}\,y}$ to write the final result in the form

$$
\mathcal{A}_{\mathrm{seq}}(x,y) \simeq \frac{C_{\mathrm{A}}\alpha_{\mathrm{s}}^2 P(x)}{2\pi^2|y|} \left\{ \mathrm{Re}\left( i\Omega_{|y|} \right) \left[ \ln\left( \frac{|\Omega_y|}{2\pi|\Omega_0|} \right) + \gamma_{\mathrm{E}} - \frac{\pi}{4} + \frac{\pi}{2}\,\mathrm{sgn}\,y \right] + \mathrm{Re}\left( i\Omega_0 \right) \frac{\pi}{4}\,\mathrm{sgn}\,y \right\}. \quad \text{(E.23)}
$$

The discussion surrounding eqs. (3.3)–(3.6) in the main text qualitatively explained the imperfect cancellation, in the small-$y$ limit, of the $\mathcal{A}_{\mathrm{seq}}(y,x)$ diagrams with the virtual diagrams given by the front-end transformation of $\mathcal{A}_{\mathrm{seq}}(y,x)$. In the small-$y$ limit (up to and including the order relevant for IR logarithms), that front-end transformation involves an overall minus sign for the diagrams and the negation of $y$ as in (3.4). So the sum of the original and front-end transformed diagrams gives

$$
\mathcal{A}_{\mathrm{seq}}(y,x) + \mathrm{frEnd}[\mathcal{A}_{\mathrm{seq}}(y,x)] \simeq \mathcal{A}_{\mathrm{seq}}(y,x) - \mathcal{A}_{\mathrm{seq}}(-y,x), \quad \text{(E.24)}
$$

where now $y > 0$. As discussed at the start of this appendix, $\mathcal{A}_{\mathrm{seq}}(y,x)$ has the same small-$y$ behavior as $\mathcal{A}_{\mathrm{seq}}(x,y)$. The explicit formula (E.23) for the latter then gives that the sum of diagrams (E.24) is equivalent to

$$
\mathcal{A}_{\mathrm{seq}}(x,y) - \mathcal{A}_{\mathrm{seq}}(x,-y) \simeq \frac{C_{\mathrm{A}}\alpha_{\mathrm{s}}^2 P(x)}{2\pi^2 y} \left\{ \mathrm{Re}(i\Omega_y)\pi + \mathrm{Re}(i\Omega_0)\frac{\pi}{2} \right\}. \quad \text{(E.25)}
$$

As discussed in the main text but now seen explicitly, everything has canceled *except* for $\pi$ terms that originated from logarithms of complex phases that were changed in some way by $y \to -y$. From numerics, we know that these $\pi$ terms cancel only when the larger set of diagrams depicted by the dark pink ($\beta$) regions of table 1 are added together.

### E.7 Implication for $\bar{s}(x)$ and $c(x)$ in figure 5

In arriving at (E.25), we used the corrected version (A.14) of $\mathcal{A}_{\text{seq}}^{\text{pole}}$. If we had instead used the original, uncorrected version for eq. (A.37) of ref. [20], we would have obtained

$$[\mathcal{A}_{\text{seq}}(x,y) - \mathcal{A}_{\text{seq}}(x,-y)]^{\text{wrong}} \simeq \frac{C_A \alpha_s^2 P(x)}{2\pi^2 y}\left\{\text{Re}(i\Omega_y)\pi - \text{Re}(i\Omega_0)\frac{3\pi}{2}\right\}. \qquad \text{(E.26)}$$

Taking the difference of (E.25) and (E.26), the effect of the change on the total small-$y$ rate (including all diagrams and not just ABC diagrams) is

$$\left[\frac{d\Gamma}{dx\,dy}\right] - \left[\frac{d\Gamma}{dx\,dy}\right]^{\text{wrong}} \simeq \frac{C_A \alpha_s^2 P(x)}{\pi y}\text{Re}(i\Omega_0) = \frac{C_A \alpha_s}{y}\left[\frac{d\Gamma}{dx}\right]_{\text{LO}}. \qquad \text{(E.27)}$$

Comparison to (2.2), ignoring the subscript ABC there, yields

$$\bar{s}(x) = [\bar{s}(x)]^{\text{wrong}} - 4\pi. \qquad \text{(E.28)}$$

This is the origin of the $4\pi$ downward shift of our figure 5 compared to the earlier figure 20 of ref. [20].

## References

[1] L.D. Landau and I. Pomeranchuk, *Limits of applicability of the theory of bremsstrahlung electrons and pair production at high-energies*, *Dokl. Akad. Nauk Ser. Fiz.* **92** (1953) 535.

[2] L.D. Landau and I. Pomeranchuk, *Electron cascade process at very high energies*, *Dokl. Akad. Nauk Ser. Fiz.* **92** (1953) 735.

[3] A.B. Migdal, *Bremsstrahlung and pair production in condensed media at high-energies*, *Phys. Rev.* **103** (1956) 1811 [INSPIRE].

[4] L. Landau, *The Collected Papers of L.D. Landau*, Pergamon Press, New York, U.S.A. (1965).

[5] R. Baier, Y.L. Dokshitzer, A.H. Mueller, S. Peigne and D. Schiff, *The Landau-Pomeranchuk-Migdal effect in QED*, *Nucl. Phys. B* **478** (1996) 577 [hep-ph/9604327] [INSPIRE].

[6] R. Baier, Y.L. Dokshitzer, A.H. Mueller, S. Peigne and D. Schiff, *Radiative energy loss of high-energy quarks and gluons in a finite volume quark-gluon plasma*, *Nucl. Phys. B* **483** (1997) 291 [hep-ph/9607355] [INSPIRE].

[7] R. Baier, Y.L. Dokshitzer, A.H. Mueller, S. Peigne and D. Schiff, *Radiative energy loss and $p_T$ broadening of high-energy partons in nuclei*, *Nucl. Phys. B* **484** (1997) 265 [hep-ph/9608322] [INSPIRE].

[8] B.G. Zakharov, *Fully quantum treatment of the Landau-Pomeranchuk-Migdal effect in QED and QCD*, *JETP Lett.* **63** (1996) 952 [hep-ph/9607440] [INSPIRE].

[9] B.G. Zakharov, *Radiative energy loss of high-energy quarks in finite size nuclear matter and quark-gluon plasma*, *JETP Lett.* **65** (1997) 615 [hep-ph/9704255] [INSPIRE].

[10] J.-P. Blaizot and Y. Mehtar-Tani, *Renormalization of the jet-quenching parameter*, *Nucl. Phys. A* **929** (2014) 202 [arXiv:1403.2323] [INSPIRE].

[11] E. Iancu, *The non-linear evolution of jet quenching*, *JHEP* **10** (2014) 095 [arXiv:1403.1996] [INSPIRE].

[12] B. Wu, *Radiative energy loss and radiative $p_\perp$-broadening of high-energy partons in QCD matter*, *JHEP* **12** (2014) 081 [arXiv:1408.5459] [INSPIRE].

[13] T. Liou, A.H. Mueller and B. Wu, *Radiative $p_\perp$-broadening of high-energy quarks and gluons in QCD matter*, *Nucl. Phys. A* **916** (2013) 102 [arXiv:1304.7677] [INSPIRE].

[14] P. Arnold and S. Iqbal, *The LPM effect in sequential bremsstrahlung*, *JHEP* **04** (2015) 070 [*Erratum ibid.* **09** (2016) 072] [arXiv:1501.04964] [INSPIRE].

[15] P. Arnold, H.-C. Chang and S. Iqbal, *The LPM effect in sequential bremsstrahlung 2: factorization*, *JHEP* **09** (2016) 078 [arXiv:1605.07624] [INSPIRE].

[16] P. Arnold, H.-C. Chang and S. Iqbal, *The LPM effect in sequential bremsstrahlung: dimensional regularization*, *JHEP* **10** (2016) 100 [arXiv:1606.08853] [INSPIRE].

[17] P. Arnold, H.-C. Chang and S. Iqbal, *The LPM effect in sequential bremsstrahlung: 4-gluon vertices*, *JHEP* **10** (2016) 124 [arXiv:1608.05718] [INSPIRE].

[18] P. Arnold and S. Iqbal, *In-medium loop corrections and longitudinally polarized gauge bosons in high-energy showers*, *JHEP* **12** (2018) 120 [arXiv:1806.08796] [INSPIRE].

[19] P. Arnold, S. Iqbal and T. Rase, *Strong- vs. weak-coupling pictures of jet quenching: a dry run using QED*, *JHEP* **05** (2019) 004 [arXiv:1810.06578] [INSPIRE].

[20] P. Arnold, T. Gorda and S. Iqbal, *The LPM effect in sequential bremsstrahlung: nearly complete results for QCD*, *JHEP* **11** (2020) 053 [arXiv:2007.15018] [INSPIRE].

[21] P. Arnold, *Universality (beyond leading log) of soft radiative corrections to $\hat{q}$ in $p_\perp$ broadening and energy loss*, *JHEP* **03** (2022) 134 [arXiv:2111.05348] [INSPIRE].

[22] P. Arnold, T. Gorda and S. Iqbal, in preparation.